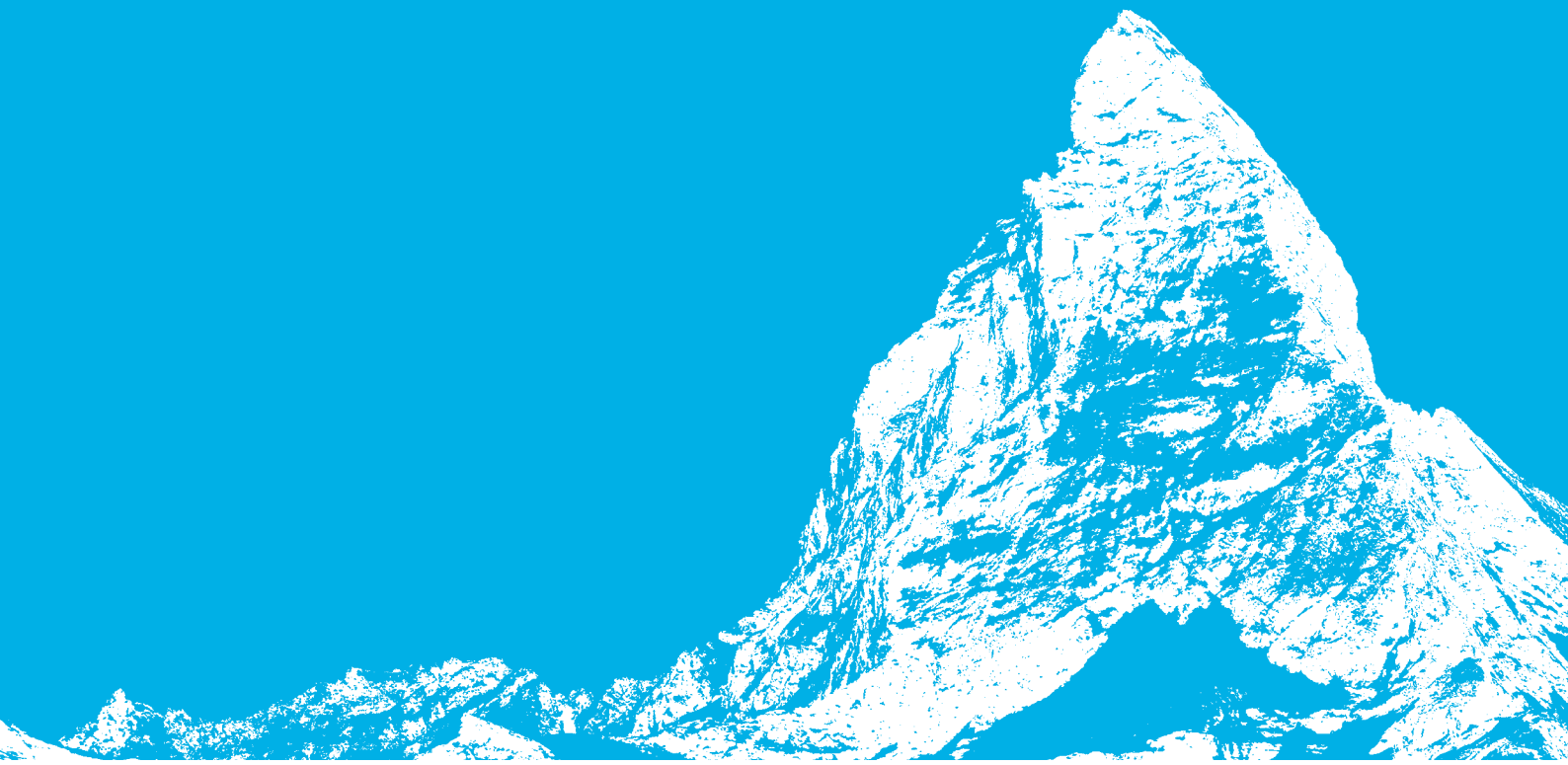

SCR'16 SWISS CONGRESS OF RADIOLOGY

MAY 19–21, 2016 | DAVOS

SCHWEIZERISCHER RADIOLOGIEKONGRESS
CONGRÈS SUISSE DE RADIOLOGIE

ONLINE ABSTRACT BOOK
of the Swiss Congress of Radiology

www.radiologiekongress.ch

TABLE OF CONTENTS

Dear Delegates and Visitors of the Swiss Congress of Radiology 2016,
Dear Colleagues!

The Swiss Society of Radiology (SGR-SSR), the Swiss Society of Nuclear Medicine (SGNM-SSMN) and the Swiss Association of Radiographers (SVMTRA-ASTRM) are delighted about the high quality and the great amount of abstracts which were submitted for presentation at the annual Swiss Congress of Radiology.

The continuous excellent work of all authors is highly appreciated as it makes the congress a very prestigious scientific meeting.

This "Online Abstract Book of the Swiss Congress of Radiology" is the 6th issue which is solely published online. It represents a cost efficient, durable and platform independent documentation of scientific abstracts, integration of the abstract data into both the Society's and Congress' web page as well as permanent accessibility all over the world.

The "Online Abstract Book of the Swiss Congress of Radiology" will permanently be accessible on both the Society's and Congress' web page at www.radiologiekongress.ch. It includes all the abstracts of the scientific talks and posters presented at the annual Swiss Congress of Radiology in Davos.

Proper citation of scientific abstracts is however important, especially in case of online-only web publications. The Swiss Society of Radiology thereof recommends the use of the following structure to cite abstracts from the "Online Abstract Book of the Swiss Congress of Radiology":

> "Author1 A, Author2 B, ..., Author last X. Title of the abstract (abstr.).
> Swiss Congress of Radiology 2016, Davos. Online Abstract Book, www.radiologiekongress.ch"

We look forward to welcoming you to the Swiss Congress of Radiology 2016 in Davos.

PD Dr. G. Andreisek, MBA
Member Scientific Committee SGR-SSR

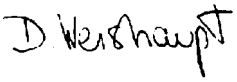

Prof. Dr. D. Weishaupt
President Scientific Committee SGR-SSR

SWISS CONGRESS OF RADIOLOGY 2016, DAVOS

Congress President

T. Jung, Zurich

SGR-SSR Executive Board

PRESIDENT
T. Jung, Zurich

PAST PRESIDENT
S. Duewell, Frauenfeld

TREASURER
T. Roeren, Aarau

ASSESSORS
H. Alkadhi, Zurich
C. Becker, Geneva
C. H. Benoit, Zurich
H. M. Hoogewoud, Fribourg
R. Kubik, Baden
D. Weishaupt, Zurich
U. Wolfensberger, Horgen

SGR-SSR Scientific Committee

PRESIDENT
D. Weishaupt, Zurich

MEMBERS
G. Andreisek, Zurich
M. Anooshiravani-Dumont, Geneva
M. Becker, Geneva
J. Bremerich, Basel
K. O. Loevblad, Geneva
Ch. Pfirrmann, Zurich
P. A. Poletti, Geneva
S. D. Qanadli, Lausanne
C. Reiner, Zurich
S. Schmidt, Lausanne
H. Thoeny, Bern

SGR-SSR Office

Schweizerische Gesellschaft für Radiologie –
Société Suisse de Radiologie (SGR-SSR)
Geschäftsstelle
c/o ecos Office
Bellerivestrasse 11
8008 Zurich
Phone +41 (0) 31 951 00 84
E-Mail info@sgr-ssr.ch
www.sgr-ssr.ch

Congress Management

c/o Education Congress Research GmbH
Wolfgang Duchek/Patricia Leeb/
Angelika Schwingshackl
Neutorgasse 9
1010 Vienna/Austria
Phone +43 1 5350599
Fax +43 1 5334064448
E-Mail info@radiologiekongress.ch
www.radiologiekongress.ch

SGR-SSR Abstract Reviewers

G. Andreisek, Zurich
M. Becker, Geneva
J. Bremerich, Basel
K. O. Loevblad, Geneva
P. Poletti, Geneva
C. Reiner, Zurich
S. Schmidt, Lausanne
H. Thoeny, Bern
D. Weishaupt, Zurich

SGR-SSR Poster Jury

T. Dietrich, St. Gallen
R. Duran, Lausanne
T. Frauenfelder, Zurich
V. Fretz, Winterthur
F. del Grande, Lugano
A. von Hessling, Lucerne
A. Hirschmann, Basel
P. Knuesel, Chur
A. Kaim, Aarau
T. de Perrot, Geneva
C. Reiner, Zurich
E. Tenisch, Lausanne
D. W. Tshering, Bern

SGNM-SSMN Abstract Reviewers

F. Forrer, St. Gallen
L. Giovanella, Bellinzona
P. Kaufmann, Zurich
P. Koch, Zurich
T Krause, Bern
S. Kneifel, Chur
E. Nitzsche, Aarau
J. Prior, Lausanne
O. Ratib, Geneva
R. Schibli, Villigen
K. Strobel, Lucerne
D. Wild, Basel
M. Wissmeyer, Geneva

SS101

Predictive Value of Low Dose and Dual-Energy CT for Successful Stone Disintegration in Shock Wave Lithotripsy: An in-vitro Study

S. Winklhofer, P. Stolzmann, C. Fankhauser, C. Poyet, P. Wolfsgruber, T. Sulser, H. Alkadhi, R. Largo; Zurich/CH

Purpose: Shock wave lithotripsy (SWL) represents a safe, effective, and frequently applied treatment option for urinary stone disease. Failure of stone disintegration may result in repeated treatments or alternative procedures. The ability to predict successful SWL will improve the selection of patients suitable for SWL. This study investigates single-energy computed tomography (SECT) and dual-energy computed tomography (DECT) to predict numbers of shock waves to stone disintegration in an in-vitro setting.
Methods and Materials: A total of 33 human urinary calculi (10 uric acid, 8 hydroxyapatite, 6 calcium oxalate monohydrate, 5 cysteine, 3 struvite, 1 brushite stones, mean size 6±3 mm) were scanned using a 128-slice DECT machine with single- (120kVp) and dual-energy settings (80/150, 100/150kVp) resulting in 6 different SECT and DECT data sets. Calculi were disintegrated using an electromagnetic lithotrypter over a 2-mm mesh until succesful disintegration.
Results: All stones were successfully disintegrated by applying a median of 72 shock waves (interquartile range 343). Regarding logistic regression analysis, CT numbers significantly ($p<0.01$) predicted fewer or more than median shock waves to successful disintegration and differed among data sets ($p<0.05$), both adjusted for stone composition ($p<0.001$) and size ($p<0.001$). Correlation coefficients ranged from rho=0.36 to 0.68 with best correlation for CT numbers and shock waves at 80 kVp ($p<0.001$).
Conclusion: Lower CT numbers are significantly associated with fewer shockwaves needed which is independent of stone composition and size. Optimal prediction of SWL success may be fascilated on the basis of low-dose CT data which is paralleled by a low radiation dose.

SS102

Assessment of Variation induced by Physiological Motion in Multi-Slice Renal Diffusion-Weighted Magnetic Resonance Imaging at 3T

I. Friedli, L. A. Crowe, S. de Seigneux, J.-P. Vallee; Geneva/CH

Purpose: Motion artifacts are a major source of error in Diffusion-Weighted Imaging (DWI) because the large diffusion gradients used make DWI more motion-sensitive than most other sequences. Despite the use of respiratory triggering schemes, random signal intensity (SI) dropout causes inter-slice SI variations. To reduce this inter-slices variability in Apparent Diffusion Coefficient (ADC), an algorithm to correct the SI of DWI in renal multi-slice acquisition images was developed.
Methods and Materials: Four volunteers were scanned with three single-shot SE-EPI DWI acquisitions (resolution 2x2x5mm^3, respiratory navigated (PACE)). After DWI image registration, a reconstructed set of images was rebuilt with the pixel providing the highest SI value of the 3 acquisitions to compensate SI dropout. SI of voxels in a ROI of the parenchyma was used to assess inter-slice variations with a Pearson standard deviation (PSD) expressed as the percentage of the mean SI in 4 consecutives slices.
Results: Uncorrected DWI images were impacted by SI dropout with inter-slices SI variations of 7.0% ± 1.2% [range: 2%-17%] against 4.2% ± 0.6% in corrected DWI. In 36/40 b-values analyzed, this artifact was significantly reduced in the corrected DWI compared to the 3 uncorrected images with a reduced inter-slice PSD ($p<0.001$). The reduction of DWI SI slice variation also reduced slice variation in ADC maps with 3.6% ± 1.2% in corrected images against 6.3% ± 0.6% in uncorrected images ($p=0.01$).
Conclusion: Motion induced SI dropout in navigated renal DWI is a significant drawback that can be corrected by our new algorithm based on the best information from 3 DWI slices.

SS103

Multiple Linear Regression for Predicting Fibrosis in the Kidney using T1 Mapping and 'RESOLVE' Diffusion-Weighted Magnetic Resonance Imaging (MRI)

I. Friedli, L. A. Crowe, L. Berchtold, S. Moll, K. Hadaya, T. de Perrot, P. Y. Martin, S. de Seigneux, J.-P. Vallee; Geneva/CH

Purpose: Renal interstitial fibrosis (IF) is currently evaluated by renal biopsy. T1 mapping and Diffusion Weighted Imaging (DWI) represent separate methods to assess IF. In this multi-parametric study, the sensitivity of both MRI sequences was first independently evaluated and, compared in a single statistic against IF.
Methods and Materials: The cortico-medullary differences ΔT1 and ΔADC (Apparent Diffusion Coefficient based on a readout-segmented DWI "RESOLVE") of 31 Chronic Kidney Disease (CKD) patients scheduled for biopsy were measured at 3T with a resolution of 2×2×5mm^3. Pearson's correlations with R^2 were performed to compare ΔT1 and ΔADC to the extent of IF, as well as $R^2_{adjusted}$ in a Multiple Linear Regression. R2 comparison was performed using Fisher Z-transform. Ten CKD were also chosen randomly and reproducibility calculated between two readers with Pearson's correlations and Intra-class Correlation Coefficient (ICC).
Results: Good quality images of the whole kidneys were obtained. An increase of ΔT1 and a decrease of ΔADC were measured with increasing IF. ΔADC outperformed ΔT1 to assess IF ($p=0.068$) ($R^2=0.68$, $p<0.001$ against $R^2=0.29$, $p<0.001$ when comparing ΔT1 and IF to ΔADC and IF). The correlation was improved by associating ΔT1 and ΔADC together ($R^2_{adjusted}=0.74$, $p<0.001$). Strong reproducibility of cortex, medulla and ΔADC was measured with ICCs, all>0.91 [95% CI:0.92-0.99] and the R^2-range=[0.96-0.97] between the two readers ($p<0.05$).
Conclusion: Even when ΔADC outperformed ΔT1 to assess IF, the combination of ΔADC and ΔT1 using multiple linear regression, improved the detection of renal IF. The methodology presented in this study could easily be extended to other fields of multi-parametric imaging.

SS104

Diffusion Tensor Imaging (DTI) as aPredictor of Prostate Cancer (PCa) Gleason Score: Quantitative Correlation

M. Kekelidze[1], J. Hohmann[2], T. Haas[2], G. Bongartz[2]; [1]Baden/CH, [2]Basel/CH

Purpose: To assess the association between PCa Gleason score and quantitative diffusion tensor imaging.
Methods and Materials: 31 PCa foci were prospectively analysed in 19 patients who underwent MRI prior to radical prostatectomy. 3T multiparametric-MRI included T1W-, T2W-, DW-, DTI (b-values=0/700, single-shot EPI and 20 gradient directions) and DCE-MRI using multi-channel pelvic phase-array coil. Quantitative values of fractional anisotropy (FA) and apparent diffusion coefficient (ADC) from DTI were correlated with PCa Gleason score from the prostatectomy specimens. Spearman rank analysis was applied for correlation.
Results: PCa showed increased FA vaue in 84% and decreased ADC in 81,8% of cases. Spearman analysis revealed a positive correlation between FA parameters and PCa Gleason score (r=0.784). The mean FA was significantly higher in PCa with Gleason score ≥ 4+4 compared to tumors with grade ≥3+3 (0,40±0,04 vs 0,25±0,02 respectively, p<0,001). Correlation between ADC and PCa Gleason score was inverse (r=-0.635) showing lower mean ADC (0,7±0,12 µm2/ms) in higher Gleason score (≥4+4) PCa and higher ADC (0,9±0,12 µm2/ms) in lower Gleason score ≥3+3 (p<0,001).
Conclusion: Fractional anisotropy in PCa shows positive correlation with Gleason score while ADC association is inverse. Combining FA and ADC parameters may predict tumor aggressiveness in PCa to enable differentiation of clinically significant cancer from indolent PCa.

SS105

Comparison of Image Quality and Patient Discomfort in Prostate MRI: Pelvic Phased Array Coil vs. Endorectal Coil

B. K. Barth[1], A. Cornelius[2], D. Nanz[1], D. Eberli[1], O. F. Donati[1]; [1]Zurich/CH, [2]Aarau/CH

Purpose: To compare image quality (IQ) and patient discomfort in prostate-MRI using a pelvic phased array (PPA) coil or an endorectal coil (ERC).
Methods and Materials: Ninety-eight patients (median age, 65.7; range 42.1-78.1) underwent prostate-MRI on a 3T scanner including T2w and DWI acquired with a PPA coil and an ERC within the same exam. Acquisition time was kept similar for both acquisitions. Two radiologists evaluated aspects of IQ on a 5-point Likert scale and classified image artifacts. All patients completed a questionnaire on discomfort/pain regarding the ERC using a visual analogue scale from 1-10.
Results: There was no significant difference in overall IQ for T2w images for both readers (reader 1, 3.27±0.91 and 3.07±0.84, p=0.057; reader 2, 3.70±0.75 and 3.77±0.81, p=0.555) for PPA coil and ERC, respectively. Overall IQ for DWI images was similar for reader 1 and better using the ERC for reader 2 (reader 1, 3.03±1.10 and 3.08±0.80 (p=0.67); reader 2 3.27±0.81 and 3.66±0.85 (p<0.05) for PPA coil and ERC). Susceptibility artifacts were frequent in more exams for ERC than for PPA coil acquisitions (109 vs. 75). Discomfort and pain experienced during insertion of the ERC was low altogether (VAS score, 3.5±2.1 for "discomfort" and 2.4±2.4 for "pain").
Conclusion: T2-weighted images may be acquired with comparable IQ using a PPA coil as compared to an ERC while DWI images showed better IQ using the ERC for one of two readers. The insertion of the ERC caused low to moderate discomfort and pain in patients.

SS106

Detecting High-Risk Prostate Cancer by Analysing the Histogram of ADC and IVIM Parameter Values

S. Barbieri, M. Brönnimann, S. Boxler, H. C. Thoeny; Bern/CH

Purpose: To differentiate prostate lesions with a primary Gleason grade (G_1)>=4 from those with G_1<=3 based on parameters (mean, skewness, and kurtosis) derived from the histogram of apparent diffusion coefficient (ADC) and intravoxel incoherent motion (IVIM: the diffusion coefficient D_t, the perfusion fraction F_p, and the pseudo-diffusion coefficient D_p) parameters. A secondary objective was to determine whether parameter values correlate with the lesions' Gleason score.
Methods and Materials: Diffusion-weighted magnetic resonance images (DW-MRI) of 66 patients with clinically significant prostate cancer were used to determine the histogram of ADC and IVIM parameter values associated with the patients' index lesion. Differences between G_1>=4 and G_1<=3 lesions were analyzed by two-sample t-tests. Further, we computed the area under the curve (AUC) of a classifier based on each variable and Pearson's correlation coefficient between each variable and the lesions' Gleason score.
Results: The mean of ADC and D_t, the skewness of F_p and D_p, and the kurtosis of F_p and D_p differed significantly (p<0.05) between lesions with high and with low G_1. The highest classification accuracy was achieved by the skewness of D_p (AUC=0.72) and the kurtosis of D_p (AUC=0.73). A moderate negative correlation was observed between the lesions' mean ADC (r=-0.43) and mean D_t (r=-0.30) values and the Gleason score. A moderate positive correlation was observed for the skewness (r=0.34) and kurtosis (r=0.36) of D_p.
Conclusion: Despite a moderate correlation between DW-MRI parameters and the aggressiveness of prostate cancer, the non-invasive diagnosis of individual patients by DW-MRI is not feasible yet.

SS107

Comparison of the New PIRADS 2.0 Criteria and a Simplified 3-tier Prostate Scoring System for Categorization of Prostate Lesions

M. Benz, G. Mueller, R. Sager, S.-R. Yang, A. L. Falkowski, M. Kekelidze, L. Bubendorf, G. Bongartz, T. Heye; Basel/CH

Purpose: To compare the new Prostate Imaging Reporting and Data System (PIRADS 2.0) and a clinically oriented, simplified, semi-quantitative 3-tier (ignore, follow, treat) prostate scoring system (PSS) for categorization of prostate lesions using multiparametric magnetic resonance (MR) imaging.
Methods and Materials: 48 patients (mean age, 62 yrs) who underwent T1- and T2-weighted, diffusion-weighted, and dynamic contrast enhanced multiparametric MR imaging of the prostate were included in this retrospective study. 38 patients underwent prostatectomy whereas 10 patients had at least 2 times negative prostate biopsy (negative control group). Two senior readers scored each lesion according to the PIRADS 2.0 criteria and PSS (peripheral zone: categories based on ADC-value ranges, tumor size ranges, and capsular contact/invasion were scored using a 3-tier scale, early arterial contrast enhancement was scored using a 2-tier scale; transitional zone: lesion capsule/morphology and tumor size were scored using a 3-tier scale, texture was scored using a 2-tier scale). PIRADS 2.0 and PSS scores were compared to the respective Gleason scores.
Results: Histopathologic analysis revealed no tumor/no clinically significant tumor (Gleason < 7) in 13 and significant cancer in 35 patients. The average AUC for PIRADS 2.0 and PSS was 0.69 and 0.74, respectively. The sensitivity, specificity and positive predictive for PIRADS 2.0 in diagnosing cancers with Gleason scores ≥7 was 0.83, 0.46 and 0.81, respectively, and 0.67, 0.77 and 0.89 for PSS, respectively.
Conclusion: PIRADS 2.0 classified more lesions as true positive whereas PSS outperformed PIRADS 2.0 with regards to true negative lesions.

SS108

Pre-Operative Uterine Volume Estimation: Transvaginal Ultrasound (TVUS) versus 3D MRI Volumetry.

D. A. Djema, V. Villard, A. Kalovidouri, C. D. Becker, M. Picarra, J. Dubuisson, D. Botsikas; Geneva/CH

Purpose: To compare the different methods of pre-operative uterine volume calculation based on transvaginal ultrasound (TVUS) and MRI in order to help the surgeon to select the optimal operative approach between abdominal, vaginal or laparoscopic hysterectomy
Methods and Materials: All women who underwent hysterectomy for a benign uterine pathology between January 2013 and June 2015 and who had a preoperative TVUS and a MRI were evaluated.
Uterine volumes were calculated by the means of TVUS and MRI measurements using prolate ellipsoid volume formula. 3D volumetry of the uterus on the basis of MRI images was also performed. Uterine weight measured on pathology was used as the standard of reference.
Results were compared with Friedman's test with Dunn's post-hoc analysis.
Results: Thirty-nine patients were evaluated in total. In 8 patients (mean uterine weight 679+/- 367g) ultrasound measurements were not possible, because of big size or position of the uterus. In the 31 remaining patients (mean uterine weight 320.2+/-350.4g, range 58-1650g) there was no statistically significant difference between the three methods of uterine volume calculation. There was a trend towards better correlation of MRI volumetric measurements (mean volume 332.3+/-372.8, p>0.999) compared to TVUS measurements (mean volume 297.6+/-326.4, p=0.6028)
Conclusion: Both TVUS and MRI are accurate modalities for pre-operative estimation of uterine volume. The best results are obtained by 3D volumetry based on MRI images. In patients in whom the big size or the position of the uterus does not allow ultrasound evaluation, MRI volumetry is the only reliable technique for prediction of uterine volume.

SS109

Sexual Anatomy Studied by MRI in Correlation with Sexual Function in Women with and without Genital Mutilation. Is It All about the Tip of the Iceberg?

M. Picarra, J. Abdulcadir, M. Bolmont, D. A. Djema, F. Bianchi-Demicheli, P. Petignat, M. Yaron, D. Botsikas; Geneva/CH

Purpose: Female genital mutilation (FGM) can involve the cutting of the clitoris, to eliminate sexual pleasure. The purpose of this study was to study if differences in the anatomy after FGM correlate with differences in sexual function, desire and body image.
Methods and Materials: Fifteen case women with FGM and 15 control women, matched by age and parity, were prospectively recruited to participate in this cross sectional study. All participants underwent pelvic MRI and completed validated questionnaires on desire (SDI; Sexual Desire Inventory), body image (QIC; Questionnaire d'Image Corporelle) and sexual function(FSFI; Female Sexual Function Index). Clitoral and bulbar size was measured in different image planes and volume of clitoris and bulbs was calculated based on these measurements.
Results: Women with FGM did not have significantly smaller clitoris glans width and body length but had a lower volume of the clitoris plus the bulbs. Women with FGM did not score lower on FSFI sub- scores for orgasm, desire and satisfaction or on the QIC, but reported more dyspaneuria. A larger total volume of clitoris and bulbs did not correlate with higher FSFI and SDI scores in women with FGM in contrast to uncut women.
Conclusion: MRI showed that women with FGM have sexual erectile tissues for sexual arousal, orgasm, and pleasure. The incorrect notion that women with FGM no longer have clitoris should be revised. In cases of sexual dysfunction, these women should be appropriately counseled and treated.

SS110

Performance of 18-F Choline PET/CT in Adenoma Detection in Hyperparathyroidism

K. Strobel, B. T. Nguyen, H. S. Grünig, S. Fischli, M. Pérez Lago, A. Zander, W. Müller; Luzern/CH

Purpose: To investigate the performance of 18F-Choline-PET/CT in the detection of parathyroid adenoma in hyperparathyroidism.
Methods and Materials: 18F-Choline-PET/CT of the neck/thorax was peformed in 19 patients (mean age 60.8 years, range 39-83) with hyperparathyroidism. 17 patients had previous ultrasound (US) and 15 patients conventional scintigraphy (CS). So far, 13 patients underwent surgery with parathyroid adenoma resection.
Results: US was positive in 10 of 17 (59%) patients, CR in 2 of 15 (13%) and PET/CT in 17 of 19 (89%) patients. In 13 operations 12 adenomas were successfully resected. In one case no adequate parathormone decline could be reached intraoperatively. In the 12 patients with successfully resected adenomas US had a sensitivity of 55% with one false positive, CS 11% (no false positive) and PET/CT a sensitivity of 83% with one false positive case.
Conclusion: The preliminary results indicate that 18F-Choline PET/CT is very accurate in the localisation of parathyroid adenomas and superior to conventional scintigraphy. In cases with negative or doubtful ultrasound 18F-Choline PET/CT might replace conventional scintigraphy in the future.

SS111

Localisation of Insulinoma: Comparison of Glucagon-like Peptide-1 Receptor (GLP1-R) SPECT/CT, PET/CT and MRI. Preliminary results of a prospective clinical study.

K. Antwi[1], M. Fani[1], T. Heye[1], G. Nicolas[1], E. M. Merkle[1], J. C. Reubi[2], M. P. D. B. Gloor[2], E. Christ[2], D. Wild[1]; [1]Basel/CH, [2]Bern/CH

Purpose: We aimed at prospectively comparing the sensitivity of GLP1-R PET/CT vs GLP1-R SPECT/CT vs standardized contrast enhanced 3T MRI in patients with endogenous hyperinsulinemic hypoglycemia. Preliminary results of an ongoing study are reported.
Methods and Materials: 23 of 32 consecutive patients with neuroglycopenic symptoms due to endogenous hyperinsulinemic hypoglycemia were enrolled (ClinicalTrials.gov, NCT02127541). A standardized contrast enhanced 3T MRI was performed. Afterwards the patients received a SPECT/CT at 4 and 72 hours after injection of ^{111}In-DOTA-exendin-4 and a PET/CT 2,5 hours after injection of ^{68}Ga-DOTA-exendin-4 in a randomized order. Reference standard was the histological diagnosis after surgery.
Results: 14 of 23 patients had negative previously performed conventional imaging (CT/MRI). In 3 patients ASVS was performed with inconclusive results. In 3 patients none of the performed imaging modalities were able to find any lesion; these patients were not operated until now. Five Patients are still awaiting surgery. 15 patients have been operated. In 14 patients histological diagnosis confirmed benign insulinoma, 1 patient had adult nesidioblastosis. In this interims analysis PET/CT showed a sensitivity of 100%, correctly identifying the insulinoma or nesidioblastosis in all 15 operated patients. Standardized 3T MRI and SPECT/CT showed a sensitivity of 78% and 67% respectively. PET/CT was the only modality which correctly identified the region of islet cell hyperplasia (nesidioblastosis) within the pancreas.
Conclusion: In our study GLP1-R PET/CT performs better as standardized MRI imaging and GLP1-R SPECT/CT at lower irradiation doses and less time consumption, compared to SPECT/CT. The capability of GLP-1-R PET/CT to localize adult nesidioblastosis needs further evaluation.

SS112

Value of Respiratory-Triggered, Periodically Rotated Overlapping Parallel T2-weithed Imaging in Evaluation of Pulmonary Nodules – Analysis with Tri-Modality PET/CT-MR

F. D. G. Barbosa[1], J. H. Geismar[2], G. Delso[1], M. Huellner[1], P. Stolzmann[1], P. Veit-Haibach[1]; [1]Zurich/CH, [2]Villigen/CH

Purpose: To prospectively evaluate the detection and conspicuity of pulmonary nodules in an oncological population using a trimodality PET/CT-MR protocol with respiratory-gatedT2-PROPELLER for possible integration into a simultaneous PET/MR protocol.
Methods and Materials: Overall, 149 patients referred for staging of malignancy were prospectively evaluated in this single-center study. Imaging was done using a tri-modality PET/CT-MR setup and was comprised of PET/CT and 3T-MR imaging with 3Ddual-echoGRE pulse sequence (Dixon) and an axial respiratory-gated T2-PROPELLER (T2-P). Images were assessed for presence, conspicuity, size and interpretation of the pulmonary parenchymal lesions. T2-P had significant higher conspicuity score of the lung nodules compared to T1-Dixon ($p<0.05$).
Results: Overall 299 pulmonary nodules detected in PET/CT. The overall detectability between the MR image sequences was significantly higher in T2-P (60%) compared to the other T1-Dixon sequences(16.1-37.8%). T2-P had a significantly higher detection rate among FDG-positive (92.4%) and also among confirmed malignant nodules (75.9%) compared to T1-Dixon. Nodules < 10mm had significantly lower detection rate by MR sequences compared to CT from PET/CT ($p<0.01$), however nodules >10mm T2-P had detection rate of 92.2% without significant difference compared to CT($p>0.05$). In a per-patient analysis there was no clinically significant change in interpretation of the nodules detected between T2-P and CT.
Conclusion: T2-P sequence has high sensitivity for the detectability of small pulmonary nodules (6-10mm) and had comparable detection rates in a patient-based analysis compared to CT. Clinical relevant assessment of pulmonary lung nodules can be done by T2-P in WB PET/MR staging of oncologic patients.

SS113

Diagnostic Accuracy of PET/MR in Comparison to PET/CT in Local Thoracic Staging of Malignant Pleural Mesothelioma

K. Martini, A. Meier, I. Schmitt-Opitz, W. Weder, P. Veit-Haibach, R. Stahel, T. Frauenfelder; Zurich/CH

Purpose: To investigate the diagnostic accuracy of PET/MR for local staging of malignant pleural mesothelioma (MPM) compared to PET/CT.
Methods and Materials: In a prospective clinical trial 22 consecutive patients (median age 66 years; range 40-76 years; 1 female, 21 male) with known MPM, who underwent PET/CT and PET/MR exams for either staging or re-staging/follow-up were evaluated. Imaging was conducted using a tri-modality PET/CT-MR set-up (Discovery PET/CT 690, 3T Discovery MR 750w, both GE Healthcare, Waukesha, WI, USA). Two independent readers evaluated images for T and N stage, confidence level (sure to unsure; 1-3) and subjective overall image quality (very good to non-diagnostic; 1-4). Inter-observer agreement of T and N stages (Cohen's kappa) and interclass correlation coefficient (ICC) between PET/CT vs. PET/MR was calculated.
Results: Inter observer agreement for evaluation of T and N stage in PET/CT images was excellent (k=0.871 and k= 0.869, respectively), whereas PET/MR imaging showed substantial agreement in T and N staging (k=0.744 and k= 0.749, respectively). The ICC of PET/CT vs. PET/MR was excellent for the evaluation of T as well as N stage (ICC=0.974 and ICC= 0.963, respectively). Diagnostic confidence was scored significantly higher in PET/MR compared to PET/CT (mean score = 1.16 and 1.48, respectively; $p<0.001$). Image quality was diagnostic for all image series.
Conclusion: Our findings suggest that diagnostic accuracy of PET/MR is comparable to PET/CT in T and N staging of MPM but has significant higher diagnostic confidence due to better soft tissue contrast of PET/MR compared to PET/CT.

SS114

Long-Term Prognostic Value of Cardiac Hybrid Imaging Integrating Nuclear Myocardial Perfusion Imaging with Coronary Computed Tomography Angiography

A. Pazhenkottil, R. Buechel, D. Benz, C. Gräni, F. Mikulicic, T. A. Fuchs, B. Hirt Moch, J. Stehli, O. Gaemperli, P. A. Kaufmann; Zurich/CH

Purpose: Cardiac hybrid imaging, obtained by image fusion of single-photon emission computed tomography (SPECT) myocardial perfusion imaging with coronary computed tomography angiography (CCTA), allows comprehensive assessment of coronary anatomy and myocardial perfusion for the diagnostic evaluation of coronary artery disease (CAD). However, there are no prognostic data on the long-term predictive value of cardiac hybrid imaging.
Methods and Materials: Patients (n=428) were classified into three groups according to the hybrid cardiac imaging findings: 1) stenosis by CCTA and matching reversible SPECT defect; 2) unmatched CCTA and SPECT finding; 3) normal finding by CCTA and SPECT. Endpoints were: all-cause death or nonfatal myocardial infarction (MI) (hard events) and a composite of major cardiac events (MACE: death, MI, unstable angina requiring hospitalisation, coronary revascularizations). Kaplan-Meier method identified survival free of MACE and Cox's proportional hazard regression determined independent predictors for cardiac events.
Results: Follow-up obtained in 414 patients (97%) revealed at a median follow-up period of 6.8 years a total of 160 MACE in 109 patients, including 45 deaths and 19 MI. The annual hard event rate was 7.0%, 3.7% and 1.2% for patients with matched, unmatched, and normal findings. The respective MACE rates were: 21.8%, 9.0%, and 2.4%. A corresponding matched hybrid image finding was associated with a significantly higher incidence of hard events and MACE (p<0.001) and proved to be an independent predictor for MACE.
Conclusion: Cardiac hybrid imaging allows long-term risk stratification in patients evaluated for CAD with a matched defect as strong predictor of MACE.

SS115

Early Response Monitoring with 18F-FDG PET/CT after Chemoradiotherapy with Cetuximab in Head and Neck Squamous Cell Carcinoma Patients (HNSCC)

F. D. G. Barbosa, G. Delso, M. Huellner, P. Stolzmann, P. Veit-Haibach; Zurich/CH

Purpose: To prospectively evaluate different time of response assessment by 18F-FDG PET/CT in head and neck Squamous Cell Carcinoma (HNSCC) patients after curative chemoradiotherapy.
Methods and Materials: Total of 50 patients with biopsy proven HNSCC were prospectively enrolled in this single-center study. All patients were treated equally with curative intent chemoradiotherapy (CRT) including Cetuximab(CTX). After that randomized into 2 different arms: with(armA) or without(armB) consolidation CTX from 2-14 weeks after the end of CRT. Patients performed 3 FDG-PET/CT's in stablished time period: pre-treatment(-PET/CT1), 1 week(PET/CT2) and 3 months(PET/CT3) after CRT. Images were assessed by neoplastic lesions evaluated qualitative and quantitatively (size, SUVmax, SUVmean, PETvolume) regarding image response in each scanner period and correlated to disease free survival, neoplastic recurrence/persistence within a minimum 18 months follow-up period. Multivariate Regression analysis was performed to assess independent predictors to progression free survival(PFS).
Results: Overall 50 primary lesions and 58 lymph node (LN) metastases were evaluated, with 64% of patients remained disease free, 22% had recurrence and 14% persistent disease. There was no significant difference in distribution of responders and non-responders at post-treatment (PET/CT2and3) time points (p>0.05) as well as compared with the reference clinical follow-up. Multivariate regression analysis demonstrated both SUVmax and diameter assessed at PET/CT3 represent independent predictor of progression free survival(PFS)
Conclusion: Early response(PET/CT2) can be assessed after CRT in HNSCC. PET/CT3 (differences in SUVmax and maximum lesion diameter) are independent predictors for PFS. PET/CT 2 cannot identify high risk patients for consolidation therapy but generally, imaging responders showed a significantly longer PFS compared to non-responders.

SS116

The potential of CT Morphological Criteria in Characterizing Small Sized (≤1cm) 18FDG Avid Lymph Nodes on PET/CT Imaging of Head and Neck Cancer

S. Malekzadeh, D. Duarte, V. Soubeyran, C. Duc, C. Constantin, M. E. Kamel; Sion/CH

Purpose: To investigate the diagnostic value of quantifying the morphological criteria of small ≤1cm FDG avid lymph nodes (LNs) in patients with head and neck cancer.
Methods and Materials: Twenty six patients were recruited. All FDG avid LNs that showed activity more than the background were identified. Quantitative morphological analysis of all small ≤1cm FDG avid LNs was performed. This analysis consisted of measuring their short (S) and long (L) axis diameters then a ratio (S/L) was created. To avoid any false measurement, both diameters were precisely defined after examining at least two different CT planes. All results were correlated with cytological or histological analysis.
Results: Thirty three small ≤1cm LNs met the selection criteria. Twenty (61%) were metastatic (SUVmax ranged from 2.2 to 23, mean 7.5 ±5.1), whereas 13 (39%) were benign (SUVmax ranged from 1.7 to 6.5, mean 3.5 ±1.4), *P*<0.01. The S/L axis ratio of metastatic LNs ranged from 0.72 to 1, mean 0.86 ±0.10. Corresponding values for benign LNs ranged from 0.45 to 0.70, mean 0.59 ±0.06, *P*<0.001. According to ROC analysis of S/L axis ratios, an >0.70 cutoff yielded the best tradeoff between sensitivity (95%) and specificity (100%) in detecting nodal metastases. Corresponding value for SUVmax was >5.2 for a sensitivity of 60% and a specificity of 92%.
Conclusion: Quantifying morphological criteria of small sized ≤1cm FDG avid LNs has the potential to ameliorate their characterization on PET/CT. A cut-off value of >0.70 for S/L axis ratio revealed very high sensitivity and ideal specificity in detecting nodal metastases.

SS117

Tumour Cachexia and Its Associated Activation of Brown Adipose Tissue

A. Becker, H. W. Nagel, I. A. Burger, C. Wolfrum; Zurich/CH

Purpose: Tumor induced anorexia and cachexia is a major therapeutic challenge in modern oncology, with an estimated 30% of deaths directly attributed to cachexia. Among other causes, excessive activation of brown adipose tissue (BAT) is being discussed.
Methods and Materials: In a retrospective study, 1060 consecutive scans of 1031 patients receiving a diagnostic ^{18}FDG-PET/CT from November 2014 to January 2015 were examined for the presence of active BAT. The BAT-activity and the tumor extent were classified according to a 3- and 4-tier system. The metabolic parameters (maximum activity, total volume and total glycolysis) of BAT and cancer tissue were measured on a PET/CT workstation.
Results: Metabolically active BAT was found in 53 patients (5.1%). Female, younger and/or leaner patients tended to have more BAT with higher activity, the incidence of cachexia (BMI<18.5) was higher in the BAT-positive cohort (n =10/18.9% vs. n=79/7.5%). Cachectic patients with active disease did not show more BAT activity. The majority of patients with active BAT did not have active tumor (n=34). For patients with both active BAT and tumor (n=19) a higher mean cancer metabolic activity correlated with higher BAT-activity. Furthermore, there was a significantly higher incidence of cachexy (n=7 or 36.8%) in this cohort.
Conclusion: Our data confirmed a link between BAT activation and cachexia. Many patients with active BAT did not have metabolically active tumor burden. However, for patients with both active BAT and tumor a linear correlation between BAT and tumor activity was demonstrated; these patients were also most likely to be cachectic.

SS118

Impact of TOF versus Non TOF PET Imaging for Choline PET/MR in Osseous Structures

U. J. Mühlematter, H. W. Nagel, F. D. G. Barbosa, G. Delso, E. Voert, P. Veit-Haibach, I. A. Burger; Zurich/CH

Purpose: The potential benefit of a direct combination of MRI with PET for prostate imaging seems obvious, since the superior soft tissue contrast should improve diagnostic accuracy. So fare, results were only comparable and not superior, mostly due to limitations of scatter and attenuation correction of the PET component in PET/MR systems. With the newer time-of-flight detectors this could at least in part be resolved.
Methods and Materials: 20 patients with prostate cancer undergoing a Choline PET/MR scan were prospectively enrolled. To assess the differences between TOF and non-TOF, all PET-images of the PET/MRI were reconstructed secondarily without TOF. The relative and absolute difference was assessed in 7 areas: temporal bone, C7, Th12, L5, femoral head, plevic bone, kidneys and within the ischioanal fossa. Comparison between TOF and non-TOF PET values was performed using concordance correlation coefficients (CCC).
Results: In all bony structures except the temporal bone non-TOF reconstructed images showed a significantly lower Cholin activity compared to the TOF images: Mean relative differences of maximal standardized uptake values (SUVmax) between TOF and non-TOF PET ranged from -23% for the temporal area to +48% for the femoral head. The CCC between TOF and non-TOF PET SUVmax values was 0.664, 0.722, 0.150, 0.439, 0.694, 0.729, 0.925, 0.595 for the C7, Th12, L5, femoral head, pelvic bone, kidneys and within the ischioanal fossa, respectively.
Conclusion: The results show that TOF reconstruction for Cholin PET/MR is especially important for the pelvic bony structures, since non-TOF image reconstruction will underestimate activity substantially.

SS119

A Dose Monitoring Software in Conventional X-Ray Imaging: Initial Experiences

C. Heilmaier, N. Zuber, D. Weishaupt; Zurich/CH

Purpose: A reasonable dose management is an important part of quality assurance in radiology. The purpose of the present study was to assess whether the implementation of a dose monitoring software is feasible in conventional X-ray imaging.
Methods and Materials: Dose data of 13 types of radiographies (=single image) and 14 studies (≥2 radiographies) was registered with a dose monitoring software, focusing on dose-area-product (DAP; mGycm^2) and entrance surface dose (ESD; mGy). The investigation was split in 2 periods of 5 months each. After period 1, acquisition parameters of the X-ray systems were reviewed and radiographers underwent a refresher training in radiation protection. Dose data of both periods was compared applying student *t*-tests.
Results: Dose data transfer was successfully accomplished in a total of 13,955 radiographies and 8,466 complete examinations in period 1 and 16,090 radiographies and 10,389 studies in period 2, respectively. Dose declined in all types of radiographies and studies in period 2 (mean DAP period 1: radiographies/complete examinations, 528/662 mGycm^2; mean DAP period 2: 386/602 mGycm2) with differences being statistically significant in 8 of 13 types of radiographies and 6 of 14 studies. Similar results were seen regarding the ESD (mean radiographies/complete examinations in period 1: 0.953/1.25 mGy; period 2: 0.744/1.17 mGy), in which dose significantly declined in period 2 in 6 of 13 radiographies and 5 of 14 studies.
Conclusion: Introduction of a dose monitoring software in conventional X-ray imaging is feasible and supports dose optimization.

SS120

Estimation of an Optimal Dose Protocol for Evaluation of the Lumbar Spine of Human Cadaveric Specimens in Upright Position with a Novel 3D X-Ray System

R. M. Benz[1], D. Harder[1], R. Menz[1], H.-W. Roser[1], F. Amsler[2], B. Stieltjes[1], A. Hirschmann[1]; [1]Basel/CH, [2]Biel-Benken/CH

Purpose: To estimate the optimal dose protocol of the lumbar spine in upright position using a novel 3-D X-ray system
Methods and Materials: Five formalin-fixed cadaveric specimens (BMI 22.2-34.8) were assessed in upright position using 3D tomography (Siemens Multitom Rax). Specimens were scanned at a detector surface dose (DSD) of 0.696 µGy and 160 projections with varying kV-levels (70/81/90/100/109/121kV). The optimal kV was chosen to additionally vary DSD (0.278/0.435/0.548/0.87/1.09µGy). Also, conventional CT of the specimens was acquired. Images were evaluated by two independent readers, rating: visibility of cortex/ endplates/ facet-joints/ neuroforamina/ nerve-roots/ trabeculae/ posterior alignment/ spinal canal/ cone-beam artifacts/ SNR (average measure intraclass correlation = 0.94). Additionally, radiation dose was measured with an anthropometric head phantom for all protocols on the X-ray system and the CT.
Results: In all specimens, the lowest technically possible kV (121 kV and 81kv, respectively) and highest technically possible DSD yielded the best image quality. For all anatomical structures, depiction was good in specimens with a BMI smaller than 30 and limited with a BMI above 30. Dose measurements are currently still under evaluation.
Conclusion: An optimal dose protocol for 3D-tomography of the lumbar spine in cadaveric specimen was estimated. These initial results indicate good depiction of anatomical structures in patients with a BMI<30. Further evaluation in vivo is underway and effort should be put into further optimizing protocols and patient dose.

SS121

The Initial Results of a Regional Swiss CT Dose Registry

A. Parakh, S. T. Schindera; Basel/CH

Purpose: To use the diagnostic reference levels (DRL) for CT obtained from a radiation tracking software (RTS) from a regional Swiss dose registry to benchmark at inter-institutional, national and international levels.
Methods and Materials: Dose-metric data from January 2014 to December 2015 was collected from eight CT scanners from five different institutions using a RTS (Radimetrics, Bayer Healthcare). Tracking of median and 75th percentile values for two $CTDI_{vol}$, DLP) for four common CT protocols (head, thorax, abdomen-pelvis, low-dose renal-colic) was done. The data of was compared amongst each other, to the national DRL (September 2010) and recently published dose-data from five University of California medical centres (October 2015).
Results: The four protocols amounted to 30,314 CT scans over two years. At the inter-institutional level, there was a four-fold difference between the median doses by two similar scanners at two different facilities for CT chest. At national level, published $CTDI_{vol}$ for CT head is 65 mGy. In the local registry only one institution exceeded this value (100 mGy), the range of the rest of the scanners was 34-64 mGy. In our study the DLP DRL values for thorax for all scanners was between 85-468 mGycm ie. lesser than that for US DRL (610 mGygm). Only two scanners (414 and 468 mGycm) exceeded the national DRL value of 400 mGycm as the range for the rest was 85-343 mGycm.
Conclusion: The lower dose-metric data values demonstrated in Swiss institutions could possibly reflect their adoption of dose-optimization techniques in clinical routine with most significant differences noted for CT thorax.

SS122

Lung Dose and Radiation-Induced Cancer Risk Assessment in Ultra-Low Dose Chest Computed Tomography (CT)

N. N. Saltybaeva, K. Martini, T. T. Frauenfelder, H. Alkadhi; Zurich/CH

Purpose: Lung cancer screening with CT has been recently recommended for decreasing lung cancer mortality. The radiation dose of CT, however, must be kept as low as reasonably achievable for reducing potential stochastic risks. The purpose of this study was to calculate individual patients' lung doses and to estimate cancer risks in ultra-low dose CT in comparison with a standard chest CT protocol.
Methods and Materials: This study included 52 adult patients (mean age 63±5years) undergoing chest CT on third-generation dual-source scanner. 27/52 patients (52%) had a standard non-enhanced chest CT protocol, 25 patients (48%) underwent ultra-low dose (ULD) CT at 100kVp with tin-filtration. 3D-dose distributions were obtained by using Monte Carlo simulations for each patient, taking into account their physical parameters and the individual CT protocol. Based on the dose distributions, patient-specific lung doses were calculated and relative cancer risk was estimated according to BEIRVII recommendations.
Results: Chest CT with an ULD protocol allowed for significant organ dose and cancer risk reductions ($p<0.001$). On average, lung dose was reduced from 8mGy to 0.3mGy while using ULD instead of the standard protocol, which is associated with lowering of the cancer risk from 9.5 to 0.4 per 100'000 cases. A strong correlation between lung dose and patient effective diameter with Pearson correlation coefficients of 0.7 and 0.8 for ULD and standard protocol, respectively, was found ($p<0.001$).
Conclusion: Use of the ULD protocol for chest CT allows for significant lung dose reduction and cancer risk reduction associated with ionizing radiation.

SS123

Repeated CT Scans in Trauma Transfers: A Retrospective Analysis of Indications and Radiation Dose Exposure

R. M. M. Hinzpeter, K. Sprengel, G. Wanner, H. Alkadhi; Zurich/CH

Purpose: CT repetition in polytrauma patients transferred from a regional hospital to a Level-I trauma-center is common, but reasons and indications are not yet well studied. This study sought to identify the frequency of repeated CT scans in polytrauma patients, to define indications, and to assess the radiation burden of repeated CT examinations.
Methods and Materials: This study included adult polytrauma patients (mean age 55 years) transferred to a trauma-center during one year. Indications for repeated CT were categorized into: inadequate data transfer, poor image quality, inadequate study, and follow-up of trauma injury known from previous CT. Radiation doses from repeated CT were calculated.
Results: Within the study period, 85/299 (28%) polytrauma patients were referred from a regional hospital to our trauma center, with the reasons: severe head injury (n=45,53%), other severe injuries (n=23,27%), repatriation from a foreign country (n=14,16%), and no ICU-capacity in regional hospitals (n=3,4%). 74/85 patients (87%) had a foregoing CT. The mean Injury Severity Score of transferred patients was 25. Reasons for repeated CT were inadequate data transfer (n=29,39%), poor image quality (n=0,0%), inadequate study (n=24,33%), and follow-up of trauma injury known from previous CT (n=21,28%). The average dose-length-product of repeated CT because of incomplete and unavailable scans was 2815mGyxcm/patient.
Conclusion: Trauma patients often undergo repeated CT when being referred to a trauma-center adding additional radiation to the patients. As unavailable images were one of the main reasons for repetition, policy should be aimed for further improvement of the digital imaging transfer system.

SS124

Role of CT Radiation Dose Tracking Software for Automated Dose-Metric Analysis for Initiation of an Institutional Optimization Program and Comparison with National Diagnostic Reference Levels

A. Parakh, S. T. Schindera; Basel/CH

Purpose: To implement monitoring of various dose-metrics using a commercially available automated radiation dose tracking software (RTS) to implement a dose reduction program and compare the big-data to the national diagnostic reference levels (DRLs).
Methods and Materials: Dose-metric data from January 2013 to December 2015 was collected from an academic center using RTS (Radimetrics, Bayer). During this period, dose-data ($CTDI_{vol}$, DLP, SSDE and effective dose-ED) of 5 common CT protocols (head, thorax, abdomen-pelvis, low-dose renal-colic and low-dose pulmonary-embolism) from four scanners were tracked. This data was used for a dose reduction program that included systemic protocol changes and technologist training. The median, 25^{th} and 75^{th} percentile (institutional DRL) values of the dose-metrics, were compared to the national DRLs.
Results: The median DLP (mGycm) between 2013 and 2015 showed a decrease for most protocols: from 732 to 706 head, 132 to 82 for thorax, 565 to 504 for abdomen-pelvis and 112 to 94 for low-dose pulmonary-embolism. There was no change in DLP for low-dose renal protocol (177 mGycm). The optimization program also led to a harmonized distribution of doses.
Institutional Vs. national DRL DLP (mGycm) values for CT head was 750 Vs. 1000, for thorax was 103 Vs. 400 and for abdomen-pelvis was 651 Vs. 650. Institutional DRL for CT thorax was lower than national DRL by 74%.
Conclusion: RTS is a useful tool for visualizing large amount of data to monitor optimization processes and make executive decisions. Seamless reliable analysis of large sample sizes by RTS can provide the base for developing dose-registries and updating DRLs.

SS125

Improving Radiation Awareness and Feeling of Personal Security of Non-Radiological Medical Staff in Computed Tomography by Implementing a Traffic Light System

C. Heilmaier, A. Mayor, N. Zuber, P. Fodor, D. Weishaupt; Zurich/CH

Purpose: Non-radiological medical staff often needs to remain in the computed tomography (CT) scanning room during imaging to supervise patients in critical condition. Their position relative to the X-ray beam significantly influences the radiation dose they receive, which often causes uncertainty. The purpose of this study was to determine, if a traffic light system improves non-radiological medical staff's radiation awareness and feeling of personal security.
Methods and Materials: Phantom measurements were done in the CT room to define areas of different dose rates. Thereafter, colored stickers were mounted to the floor according to a traffic light system: green=lowest, orange=intermediate, and red=highest radiation exposure. Non-radiological medical staff with different years of working experience evaluated the system using a structured questionnaire. Kruskal-Wallis and Spearman's correlation test were applied.
Results: Overall, rating of the system by the 56 participants (30 physicians, 26 nursing staff) was very good, and almost all staff tried to stand in the green stickers during the scan. The system significantly increased their radiation awareness and feeling of personal protection, particularly in staff with ≤5 years of working experience ($p<0.05$). The majority of non-radiological medical staff stated that staying in the green stickers and patient care would be compatible. Knowledge on radiation protection was poor in all groups, especially in entrants ($p<0.05$).
Conclusion: A traffic light system in the CT scanning room indicating areas with lowest, intermediate and highest radiation exposure is much appreciated. It increases radiation awareness, and improves feeling of personal radiation protection in medical staff.

SS126

Cost-Effectiveness of Bone Strength Screening for Osteoporosis in Postmenopausal Women

C. A. Agten, S. Honig, G. Chang; New York/US

Purpose: The majority of patients with fragility fractures do not demonstrate low bone mineral density (BMD) on dual-energy x-ray absorptiometry (DXA) and are therefore insufficiently treated prior to their first fracture. Current osteoporosis research focuses on bone-strength as a parameter in addition to BMD, since patients with fragility fractures demonstrate lower bone-strength compared to non-fractured controls. The purpose of this study was to investigate whether bone-strength analysis using quantitative computed tomography (QCT) would be cost-effective as a screening tool for osteoporosis in postmenopausal women.
Methods and Materials: We developed a state-transition microsimulation model of osteoporosis to simulate age- and therapy-related changes in BMD and bone-strength, their impact on fracture risk, direct and indirect fracture costs, and quality-adjusted life-years (QALYs) in postmenopausal women over lifetime. We assessed the cost-effectiveness of different screening strategies (no screening, DXA, QCT, and combined DXA/QCT screening) using different QCT intervals and different screening initiation ages (55-75 years). Therapy was started if DXA (T-score≤-2.5) or QCT (bone-strength<3000 Newton) were positive or after first fragility fracture (hip, vertebral body, wrist, and others).
Results: The most cost-effective (<$50'000 per QALY gained) strategy was combined DXA/QCT screening starting at age 55 with QCT screening every 2 years if T-score>-2.5. Using this strategy 10% of postmenopausal women sustained hip fractures (21% with no screening). The combined DXA/QCT strategy at age 55 was cost-saving compared to no screening, DXA, or QCT screening.
Conclusion: QCT bone-strength analysis combined with DXA screening for osteoporosis in postmenopausal women could potentially prevent a substantial number of fragility fractures, while saving costs.

SS127

Green Fingerprint“ Project – An Evaluation of the “Low Power” Consumption in a Radiology Department: Part I – an Inventory.

J. Hohmann, P. Brantner, G. M. Karwacki, C. Zähringer; Basel/CH

Purpose: The power consumption of a radiology department in a University Hospital generated by the PACS equipment is a relatively small part of the total power consumption of such a department. However it is still a manifold of the power consumption of a regular family household. The aim of the first part of the project was to quantify this consumption and to find out typical consumption patterns.
Methods and Materials: We measured the power consumption of an overall of 45 devices, mainly reporting stations, over a time period of approximately six months in our radiology department. Measurements were done with Voltcraft Energy Logger 4000 (Conrad Electronic SE, Hirschau, Germany) analysers which measured the power consumption of each device approximately every minute. Therefore we got about 12 millions of measurements. Calculations were done with R statistical software (https://www.r-project.org/) using R Studio (R Studio Inc, Boston, MA, US) as the user interface.
Results: The total power consumption of 2-4 reporting stations equals that of one regular family household, which was about 5000 kWh in 2014. In addition we identified three main power consumption patterns, depending on the use of the devices under evaluation: mainly off, mainly on and always on. Especially for the letter ones the stand-by and hibernation modes were quite inefficient and due to improvement
Conclusion: The power consumption of “low power” devices is not negligible. Strategies to reduce the waste of energy in this field should be established, depending on the patterns of use and the adjustment of the devices.

SS128

Simultaneous Assessment of Cardiac Function and Infarct Size in a Mouse Model Using a 4D Strategy on a Clinical 3T MR System

L. A. Crowe[1], F. Montecucco[2], F. Burger[1], A. Roth[1], F. Carbone[1], I. Friedli[1], A.-L. Hachulla[1], V. Braunersreuther[1], F. Mach[1], J.-P. Vallee[1]; [1]Geneva/CH, [2]Genoa/IT

Purpose: Small animal cardiac imaging on clinical 3T machines is an important translational step for new contrast media and sequence validation. We developed a new 4D strategy tailored for 3T clinical systems to simultaneously assess function and infarct in mice post myocardial ischemia.
Methods and Materials: Twelve C57BL/6J mice (6 with 60min ischemia, 6 without surgery) were imaged 24hrs after reperfusion (invivo and postmortem) on a clinical 3T.
New ECG/respiratory triggered 3D flash/GRE cine: isotropic 344µm, TR/TE=7.8/2.9ms;
Classic 2D flash/GRE cine: 344x344x1000µm, (2-chamber, 4-chamber, 10 short-axes), TR/TE=11/5.4ms.
End-systolic/end-diastolic endocardial volumes and epicardial contours were measured and flow artifact scored. Serum Troponin and nitrobluetrazolium chloride histology were compared to MR infarct volumes.
Results: Scan times were 20-25min for 2D cine (35-45min for 2D cine + PSIR) and 25-35min for 3D. 3D cine required no complex planning. CNR allowed endocardial delineation in both, with 3D isotropic coverage better for apex and right ventricle (RV). Flow artifact was significantly reduced in 3D (shorter TE, p=0.008). LV, RV volumes and LV mass correlated 2D:3D and RV mass 3D:postmortem (R^2>0.70). Ejection volume correlation, left:right, for 3D (y=0.96x R^2=0.6) agrees with mouse physiology and confirms 3D cine accuracy.
In the ischemia/reperfusion group, hypokinesia/akinesia was consistent, but better delineated with 3D's increased temporal resolution.
Infarct 'late Gd enhancement' was seen in 3D (unlike 2D). Excellent correlation 3D:NBT was found for infarct location and size (R^2=0.89).
Conclusion: The new 4D strategy of isotropic 3D cardiac cine post-gadolinium in mice improved coverage and spatial/temporal resolution for more accurate function and infarct quantification in a single acquisition.

SS129

MRI-Based Approach to Measurement Disease Burden in Patients with Atrial Fibrillation

M. Pradella, S. Knecht, B. Stieltjes, M. Kühne, C. Sticherling, J. Bremerich, G. Sommer; Basel/CH

Purpose: Atrial fibrillation (AF) is a common disease affecting approx. 1% of the adult population in first world countries. We developed a new approach based on sphericity to quantitatively assess this chronical change and to correlate it with descriptive clinical parameters that aim to encompass disease burden.
Methods and Materials: 130 patients were included in our study who all received an MRI prior to pulmonary vein isolation (PVI). MRI was performed on 1.5 T Siemens (Magnetom Avanto / Espree, Siemens, Germany) using a T1-weighted spoiled gradient echo sequence (FLASH) pre and post contrast. Post processing consisted of semi-automatic, threshold-based volumetry of the left atrium (Aquarius Intuition, Terrarecon, USA). Assesment of sphericity as deviation from an ideal sphere was evaluated with a custom-written code (Mathlab, Mathworks, USA). Inter and intra reader agreement was evaluated. Overall disease burden was assessed prior to PVI according to Koci et al. and the specific risk for a cerebrovascular insult via the CHA2DS2-VASc-score.
Results: Sphericity of the fitted ellipsoid correlated significantly with burden of disease (.369, p<.001). The CHA2DS2-VASc-Score showed also a significant correlation to sphericity (.392, p<.001). ICC for intra- and inter reader agreement was strong with 0.93 and 0.84 respectively.
Conclusion: Our data suggests that sphericity of fitted ellipsoids might be used to quantitatively evaluate individual disease burden of patients suffering from AF. In the future we will analyse if it also can be used to evaluate other parameters such as recurrence of AF after PVI.

SS130

Novel Ultrasound Triggering with Spatially Resolved MR-Compatible Doppler for Cardiovascular MRI.

L. A. Crowe, G. Manasseh, T. de Perrot, H. Muller, R. Salomir, J.-P. Vallee; Geneva/CH

Purpose: Poor ECG signal encountered in obese, post-surgical patients or fetal imaging could preclude MR synchronization especially at 3T. We investigated feasibility of novel ultrasound-triggered MRI using spatially-resolved Doppler.
Methods and Materials: Retrospective ECG- (gold-standard), Doppler- and Fake-triggered (RR 20-30%>reality) MRI were compared in 5 volunteers.
Simultaneous real-time Pulse-colour Doppler used an MRI compatible, shielded transducer (128 element, 5-10MHz, 20-30 frames/second) generating trigger signal from a time-adaptive threshold.
3T MRI included 2- and 4-chamber and short-axis cines (TE/TR=1.4/39.2ms, 1.63x1.63x6mm) and aortic phase-contrast flow (TE/TR=2.5/37.1ms, 1.98x1.98x6mm).
Septum sharpness (Laplacian) in 10 cases (SA, 4C) and function (LV surface over the whole cycle, ejection volume) were quantified.
Results: MR imaging was free of US interference. Artifacts on Doppler during MR were reduced to become inconsequential by optimized signal conversion.
ECG- and Doppler-triggering produced high quality cines. Sharpness showed no significant difference ECG to Doppler in 5 cases (0.339<p<1), 3 Doppler better (0<p<0.0015) and 2 ECG better (0<p<0.005).
LV surface gave no difference between ECG and Doppler (ICC>0.85). ECG- and Doppler-triggered ejection volumes were not different, but both significantly different to Fake (p<0.04).
Ascending and descending aorta peak flow (shifted to synchronize) was not different between ECG and Doppler (p=0.475), and fake-trigger gave reduced peak.
Conclusion: We acquired artifact-free, simultaneous MR and Doppler images inside the MR scanner. Doppler-triggering Cardiac MR was successful in all volunteers. Image quality and functional parameters were not different from ECG-triggered acquisition. Quantitative images, without standard ECG signal, show strong potential for advanced cardiac imaging in difficult or still unexplored cases like fetal imaging.

SS131

Impact of Parallel Imaging, View-Sharing and Compressed Sensing Sequences on Arterial Input Function Sampling

M. Benz[1], G. Bongartz[1], S. T. Schindera[1], J. Froehlich[2], T. Heye[1]; [1]Basel/CH, [2]Zurich/CH

Purpose: To determine the effect of parallel imaging, view-sharing and compressed sensing sequences on arterial input function (AIF) sampling in comparison to non-accelerated techniques.
Methods and Materials: A custom made physiologic flow-phantom simulating the cardiopulmonary circulation and the aortic outflow was designed. The flow-phantom was scanned on a 3T MRI (Magnetom Prisma, Siemens Healthcare) together with a water-phantom and muscle-phantom. Signal over time curves after the administration of 10 ml of contrast agent (2ml/s flow-rate) (Dotarem, Guerbet) were analyzed for each phantom using fast low angle shot 2d (FLASH 2d, temporal resolution [tr] 0.6s), FLASH 3d (tr 3.9s; P2 [parallel imaging factor 2] tr 2.4s), time-resolved imaging with stochastic trajectories (TWIST, tr 2.2s), and golden-angle radial sparse parallel imaging (GRASP, tr 1.1s) sequences. Each acquisition was repeated three times. Signal over time curves were normalized and quantitatively analyzed by full width half maximum (FWHM) measurements to assess the coefficient of variation (COV) within sequences and the percentage difference between sequences.
Results: The COV of the water and muscle phantom were <0.8%. Within sequence FWHM COV was 1.0% for Flash3d, 1.0% for Flash3dP2, 9.1% for TWIST and 0.3% for GRASP. Percentage difference FWHM in comparison to Flash2d as reference standard was 2.2% for Flash3d, 0.3% for Flash-3dP2, 45.9% for TWIST, and 7.8% for GRASP.
Conclusion: 3d parallel imaging and compressed sensing did not effect AIF sampling in comparison to non accelerated 2d and 3d sequences. TWIST as a representative of view-sharing with incomplete coverage of the k-space might be less suited for precise measurements of the AIF.

SS132

Step-and-Shoot CCTA vs. High-Pitch Spiral CCTA: Comparison of Image Quality and Radiation Exposure

D. Seppelt, D. Danowski, U. Speiser, T. Brauer, C. Kolb, C. Radosa, M. Laniado, R. Strasser, I. Platzek; Dresden/DE

Purpose: The purpose of our study was to compare image quality and radiation exposure in step-and-shoot coronary computed tomography angiography (CCTA) and high-pitch spiral CCTA.
Methods and Materials: Fifty-two pairs of patients matched for weight, height, sex and heart rate were included in this retrospective study (68 m, 36 f, average age 60 y).
All patients were examined on a third generation dual-source CT. Step-and-shoot CCTA was used in 50% of patients, and high-pitch spiral CCTA in the remaining 50%. The signal-to-noise ratio (SNR) in the ascending aorta and the proximal coronary arteries were determined for each dataset. Image quality was rated using a five-point scale. We used the t-test for paired samples to compare SNR and effective dose, and the Wilcoxon test to compare image quality scores.
Results: Mean effective dose for the step-and-shoot protocol (3.3 ± 1.9 mSv) was significantly higher in comparison to the high-pitch spiral protocol (1.2 ± 0.58 mSv; $p < 0.0001$).
Mean SNR was higher with the step-and-shoot protocol compared to the high-pitch spiral protocol in the aorta ($p < 0.0001$), in the proximal right coronary artery ($p = 0.027$) and in the left main coronary artery ($p < 0.0001$).
Image quality scores were significantly better for the step-and-shoot protocol ($p = 0.046$).
Conclusion: Step-and-shoot CCTA has significantly better SNR and overall image quality compared to high-pitch spiral CCTA, but with a mean effective dose more than twice as high.

SS133

From Bench to Bedside: Clinical Evaluation of a Microbolus Contrast Agent Injection Protocol for CT Angiography Derived from a Dynamic Vascular Phantom

M. Benz[1], G. Stadelmann[1], A. Willmes[2], G. Bongartz[1], S. T. Schindera[1]; [1]Basel/CH, [2]Ulm/DE

Purpose: To investigate optimized vascular enhancement in CT angiography (CTA) protocols with long scan ranges at the lowest reasonable CA dose.
Methods and Materials: Using a custom made physiologic flow-phantom we designed a microbolus technique providing an extended plateau of peak arterial enhancement. The microbolus technique uses the capacity of state of the art CA power injectors (CT-Motion, Ulrich Medical, Germany) to rapidly switch between CA and saline boli with varying volumes. The injection protocol uses 60 ml of CA (Ultravist 370, Iopromide, Bayer, Germany) and 30 ml of saline injected at a flow rate of 4 ml/s at 100 kVp. 23 patients (16 male, 7 female; mean age 69 yrs; mean BMI 26 kg/m2, range 16-45 kg/m2) underwent thoraco-abdominal CTA using the microbulus technique. Hounsfield units were measured in the ascending aorta (ASA), thoracic descending aorta (TDA), abdominal aorta (ABA), and iliac artery (IA) and compared using the Kruskal Wallis test.
Results: In the phantom study, the micro-bolus technique increased the duration of a diagnostic aortic enhancement (>200 HU) by up to 40% in comparison to a fixed injection-rate. 21 of 23 patients showed diagnostic enhancement over the entire scan range. HU in the ASA, TDA, ABA, and IA averaged 319±71, 303±71, 294±73 and 297±81 (p=0.39).
Conclusion: The microbolus technique in CTA with long scan ranges is feasible in patients and confirmed our phantom data showing a consistently high arterial enhancement. Based on our phantom and clinical data we favor the micro-bolus injection protocol for CTA with long z-axis coverage.

SS134

Suction/Inspiration Against Resistance or Standardized Mueller Maneuver: A new Breathing Technique to Improve Contrast Density within the Pulmonary Artery: A Pilot CT Study.

A. Gutzeit, J. Froehlich, C. Reischauer; Zurich/CH

Purpose: Our aim was to prospectively investigate whether the recently introduced suction/inspiration against resistance breathing method leads to higher computed tomography (CT) contrast density in the pulmonary artery compared to standard breathing.
Methods and Materials: The present study was approved by the Medical Ethics committee and all subjects gave written informed consent. Fifteen patients, each without suspicious lung emboli, were randomly assigned to four different groups with different breathing maneuvers (suction against resistance, Valsalva, inspiration, expiration) during routine CT. Contrast enhancement in the central and peripheral sections of the pulmonary artery were measured and compared with one another.
Results: Peripheral enhancement during suction yielded increased mean densities of 138.14 Hounsfield units (HU) ($p = 0.001$), compared to Valsalva and a mean density of 67.97 HU superior to inspiration ($p = 0.075$). Finally, suction in comparison to expiration resulted in a mean increase of 30.51 HU ($p = 0.42$). Central parts of pulmonary arteries presented significantly increased enhancement values (95.74 HU) for suction versus the Valsalva technique ($p = 0.020$), while all other mean densities were in favour of suction (versus inspiration: $p = 0.201$; versus expiration: $p = 0.790$) without reaching significance.
Conclusion: Suction/Inspiration against resistance is a promising technique to improve contrast density within pulmonary vessels, especially in the peripheral parts, in comparison to other breathing maneuvers.

SS201

Multi-Slice Accelerated EPI Diffusion-Weighted Imaging versus Conventional Diffusion-Weighted Imaging in the Upper Abdomen: Influence of Acceleration Factor on Image Quality

B. K. Barth, L. Filli, D. Kenkel, A. Boss, M. Piccirelli, M. Wurnig, C. S. Reiner; Zurich/CH

Purpose: To evaluate the influence of the acceleration factor in multi-band DWI (mb-DWI) on image quality (IQ) of the upper abdomen compared to conventional DWI (c-DWI).
Methods and Materials: DWI of the upper abdomen was performed in ten healthy volunteers at 3T. Free breathing single-shot spin-echo echo-planar DWI was acquired without acceleration(c-DWI), with twofold acceleration(mb2-DWI), and threefold acceleration(mb3-DWI). Two readers evaluated aspects of image quality of liver and pancreas on b=800 s/mm² images on a 5-point ordinal scale. Estimated signal-to-noise ratio(eSNR) was calculated for both liver lobes and pancreas. Wilcoxon matched pair test and student's paired t-test were used with Bonferroni correction for statistical analysis.
Results: Acquisition time was 5:23min for c-DWI, 2:55min for mb2-DWI, and 2:14min for mb3-DWI. IQ of the liver dome was significantly deteriorated with mb-DWI (2.6 and 1.4 vs. 3.5 for c-DWI, p<0.025), while liver IQ inferior to the liver dome was similar with mb2-DWI and c-DWI (4.1vs.4.3, p=0.157), but significantly worse with mb3-DWI compared to c-DWI (3.4vs.4.3, p<0.025). Pancreas IQ was significantly higher with mb2-DWI (4.0vs.3.6, p<0.025) and equal with mb3-DWI (3.6vs.3.6, p=1.0) compared to c-DWI. There was no difference in eSNR for either sequence combination (p>0.025).
Conclusion: Mb2-DWI demonstrated similar or higher IQ compared to c-DWI in significantly reduced scan time, especially for the pancreas. Thus, slice acceleration may increase the clinical applicability of abdominal DWI. However, IQ of mb-DWI of the liver dome needs to be improved.

SS202

Impact of Vendor and Field Strength of the Magnetic Resonance Scanner on Measurements of IVIM Parameter Values in Abdominal Organs

S. Barbieri[1], O. F. Donati[2], J. Froehlich[1], H. C. Thoeny[1]; [1]Bern/CH, [2]Zurich/CH

Purpose: To quantify differences in Intravoxel Incoherent Motion (IVIM) parameter values measured in abdominal organs by magnetic resonance scanners from different vendors and at different field strengths.
Methods and Materials: Abdominal diffusion-weighted magnetic resonance images (DW-MRI) of ten healthy male volunteers (age range: 29 to 53 years-old) were acquired using five different MR scanners (1.5T Siemens Sonata, 3T Siemens Tim Trio, 1.5T Philips Achieva, 3T Philips Achieva, 3T GE Discovery MR750). Two readers independently drew regions of interest (ROI) in the left and right liver lobe, pancreas, spleen, renal cortex, and renal medulla. Average IVIM parameter values (the diffusion coefficient D_t, the perfusion fraction F_p, and the pseudo-diffusion coefficient D_p) were computed within each ROI and compared across imagers by coefficients of variation (CV) and analyses of variance (ANOVA).
Results: CVs of D_t were relatively high (> 20%) in the left liver lobe and low (< 10%) in the renal cortex and renal medulla. CVs of F_p were more uniform across anatomical regions and ranged between 14 and 24%. CVs of D_p were the highest and generally exceeded 20%. The ANOVA determined statistically significant differences in measured IVIM parameter values in the left and right liver lobe, spleen, renal cortex, and renal medulla (P<0.05).
Conclusion: The potential for clinical applications of IVIM analysis might be higher in the kidney than it is in the liver. In the context of a multi-center study making use of IVIM parameters as biomarkers, differences across MR scanners should be quantified and corrected for.

SS203

Is There Evidence for More Than Two Diffusion Components in Abdominal Organs? – Assessment in Healthy Volunteers.

M. Wurnig, M. Germann, A. Boss; Zurich/CH

Purpose: Different models of diffusion in perfused organs have been proposed with intra-voxel incoherent motion (IVIM) being the most established at present. However, recent literature suggests that besides the two diffusion components of the IVIM-model additional components may exist. In this study we assessed the number of distinguishable diffusion components using an extensive diffusion-weighted-imaging (DWI) protocol with subsequent multi-component analysis.
Methods and Materials: Diffusion data-sets of 6 healthy subjects were acquired in a 3T MR scanner using 68 different b-values during free breathing (equidistant placed in the range 0-1005s/mm²). Signal-intensity-curves as a function of the b-value were obtained in liver, spleen and kidneys via ROI-analysis. For analysis non-negative least-squares fitting of the signal-intensity-curves to a distribution of decaying exponential functions with minimum amplitude energy regularization was used.
Results: In all assessed organs the typical slow and fast diffusing components of the IVIM-model were found (liver: D=0.98±0.10x10⁻³mm²/s; D*=103±19x10⁻³mm²/s; kidney cortex: D=2.19±0.21x10⁻³mm²/s; D*=75±9x10⁻³mm²/s; kidney medulla: D=1.84±0.25x10⁻³mm²/s; D*=106±9x10⁻³mm²/s; spleen: D=0.75±0.06x10⁻³mm²/s; D*=155±177x10⁻³mm²/s). However, in the kidney a third component between D and D* was found (cortex: D´=18,4±7,5x10⁻³mm²/s; medulla: D´=25,6±9,3x10⁻³mm²/s).
Conclusion: In the present study we could not find any evidence for the existence of more than the two diffusion components in liver and spleen proposed by the IVIM-model, while in the kidneys an additional component was detected. This indicates that for a correct description of diffusion in the kidneys a more sophisticated model is needed as changes in this additional component might be misinterpreted in the IVIM model.

SS204

Reduction in Respiratory Motion Artefacts on Gadoxetate-Enhanced MRI after Training Technicians to Apply a Simple and more Patient-Adapted Breathing Command.

A. Gutzeit, J. Froehlich, O. Kolokhitas, D. Mu Koh; Zurich/CH

Purpose: To investigate whether a trained group of technicians using a modified breathing command during gadoxetate-enhanced liver MRI reduces respiratory motion artefacts compared to non-trained technicians using a traditional breathing command.
Methods and Materials: The gadoxetate-enhanced liver MR images of 30 patients acquired using the traditional breathing command and the subsequent 30 patients after training the technicians to use a modified breathing command were analyzed. A subgroup of patients (n = 8) underwent scans both by trained and untrained technicians. Images obtained using the traditional and modified breathing command were compared for the presence of breathing artefacts [respiratory artefact-based image quality scores from 1 (best) to 5 (non-diagnostic)].
Results: There was a highly significant improvement in the arterial phase image quality scores in patients using the modified breathing command compared to the traditional one (P < 0.001). The percentage of patients with severe and extensive breathing artefacts in the arterial phase decreased from 33.3 % to 6.7 % after introducing the modified breathing command (P = 0.021). In the subgroup that underwent MRI using both breathing commands, arterial phase image quality improved significantly (P = 0.008) using the modified breathing command.
Conclusion: Training technicians to use a modified breathing command significantly improved arterial phase image quality of gadoxetate-enhanced liver MRI.

SS205

MRI Texture Analysis for Differentiation of Malign and Benign Hepatocellular Tumors in the Non-Cirrhotic Liver.

D. Stocker, H. P. H. P. Marquez Masquiaran, M. Wurnig, M. W. Wagner, D. Raptis, P.-A. Clavien, M. Fischer; Zurich/CH

Purpose: To evaluate the diagnostic accuracy of 2-dimensional (2D) MR texture analysis (TA) for differentiation between hepatocellular carcinoma (HCC) and benign hepatocellular tumors of the non-cirrhotic liver.
Methods and Materials: A total of 108 non-cirrhotic patients (46 male; 45±14years) undergoing preoperative contrast-enhanced MRI due to suspicion of HCC were retrospectively included in this multi-center-study. TA including grey-level histogram, co-occurrence and run-length matrix features (in total 19 features) was performed by two independent readers using MATLAB. Native T1w and T2w as well as arterial and venous post contrast-enhanced 2D-image-slices were assessed by placing a region-of-interest (ROI) at the maximum diameter of each lesion. Differences between HCC and benign lesions were assessed using the independent sample T-tests and logistic regression analysis was performed to obtain the optimal number/combination of TA-features along with diagnostic accuracy.
Results: Interreader agreement was substantial to excellent (interclass correlation-coefficient, 0.68-0.99). The highest number of significantly differing TA-features (N=5) was found using the arterial-phase images including one grey-level histogram (skewness, p = 0.018) and four run-length matrix features (all, p<0.02). The optimal binary logistic regression model for TA features of the arterial-phase images contained 13 parameters and showed an accuracy of 84.5% (sensitivity 84.1%, specificity 84.9%) for diagnosis of HCC.
Conclusion: 2D-texture-analysis of arterial phase post contrast images allows discriminating HCC from benign hepatocellular tumors with good diagnostic accuracy and substantial to excellent inter-reader agreement.

SS206

Improving Interobserver-Agreement with a Simplified Li-Rads Algorithm

A. Becker, B. K. Barth, C. S. Reiner, O. F. Donati, C. A. Karlo, E. J. Ulbrich, M. A. Fischer; Zurich/CH

Purpose: Li-Rads is a standardized reporting system for liver lesions. Despite ongoing efforts, it has yet to demonstrate improved interreader agreement. We propose a simplified Li-Rads algorithm to improve interreader agreement while maintaining diagnostic performance for HCC.
Methods and Materials: MRI scans of 84 cirrhotic livers with 104 distinct lesions were retrospectively selected to equivocally match each of the Li-Rads grades (LR1-5) using histopathology and imaging follow up as standard of reference. Four independent radiologists categorized all lesions as benign (LR1-2) or potentially malignant (LR3-5) and determined Li-Rads based imaging features including lesion size, arterial enhancement, wash-out, capsule appearance and threshold growth for LR3-5 lesions. In regards to their imaging features, LR3-5 lesions were automatically classifed accoring to the current Li-Rads and a modified Li-Rads (mLi-Rads) version replacing the Li-Rads decision table with a sequential decision tree. Diagnostic performance and Interreader agreement were determined for Li-Rads versus mLi-Rads using receiver operating characteristics (ROC) and Kappa analysis respectively..
Results: ROC analysis revealed a similar diagnostic performance for Li-Rads (AUC = area under the curve = 0.91) and mLi-Rads (AUC = 0.90; p = 0.45). Interreader agreement was higher using mLi-Rads as compared to current Li-Rads showing an improved overall (Fleiss' Kappa; 0.52 vs. 0.47), and inter-individual agreement between all readers (Cohen's Kappa's; range 0.37-0.62 vs. 0.41-0.70).
Conclusion: Raising importance of lesion size and wash-out criteria using a stepwise Li-Rads decision tree for LR3-5 lesions allows for faster classification with higher interobserver reliability while maintaining diagnostic accuracy.

SS207

CT Perfusion for Early Response Assessment after Radiofrequency Ablation of Focal Liver Lesions

H. P. H. P. Marquez Masquiaran, G. D. Puippe, T. Pfammatter, M. P. Rishi, H. Alkadhi, M. Fischer; Zurich/CH

Purpose: To evaluate the feasibility and diagnostic performance of perfusion CT (P-CT) for early assessment of treatment response in patients undergoing radiofrequency ablation (RFA) of focal liver lesions.
Methods and Materials: 20 patients (14men; mean age 64±14) undergoing RFA due liver metastases (N=10) or HCC (N=10), were prospectively included in this study. P-CT was performed within 24 hours after RFA. Two readers determined arterial-liver-perfusion (ALP, mL/min/100mL), portal-venous perfusion (PLP, mL/min/100mL) and hepatic-perfusion-index (HPI, %) in all 20 lesions by placing a freehand volume-of-interest (VOI) in the necrotic central (CZ), the transition (TZ) and the surrounding parenchymal (PZ) zone. Patients were classified in responders (no residual-tumor) and non-responders (residual/progressive-tumor) using imaging follow-up with contrast-enhanced CT or MRI after a mean of 139±70 days. Prediction of treatment response was evaluated using receiver operating characteristics.
Results: Mean ALP/PLP/HPI of both readers was 4.89/15.44/61.25 for the CZ, 9.98/16.88/66.35 for the TZ and 20.70/29.09/61.87 for the PZ. Interreader agreement of HPI was good for the CZ (ICC=0.875) and the TZ (ICC=0.857) zone, and high for the PZ (ICC=0.920). For both readers there was significant difference in PVP/HPI of the CZ and HPI of the TZ (all, P<0.03) between responder and non-responders. HPI of the TZ showed the highest area under the curve (0.90) for prediction of residual tumor, suggesting a cut-off value of 73%.
Conclusion: Predominant arterial perfusion of the transition zone assessed directly after RFA might be an early biomarker for residual tumor/tumor recurrence in patients with focal liver lesions.

SS208

What Are the Factors Associated with an Increased Risk of Local Recurrence after Radiofrequency Ablation or Surgical Metastasectomy?

N. Vietti Violi, P. Bize, R. Duran, B. Guiu, N. Sala, C. Sempoux, N. Demartines, N. Halkic, J.-F. Knebel, A. Denys; Lausanne/CH

Purpose: To compare local recurrence rate after radiofrequency ablation (RFA) and surgical metastasectomy for colorectal cancer liver metastases and to define the best candidates for each treatment.
Methods and Materials: We analyzed, lesion by lesion, 121 metastases treated by metastasectomy (43 patients, follow up 688 days) and 110 metastases treated by RFA (in 60 patients, median follow up 552 days). We compared rate of local recurrence (LR) and hepatic recurrence (HR) between the two groups. Possible predictive factors for recurrence, were analyzed by Chi square and logistic regression in uni and multivariate analysis.
Results: We found no difference between the two groups for patients and primary tumor characteristics. Metastasis size was larger in metastasectomy group than RFA group (18mm, range 2-90mm and 15mm, range 3-55mm, respectively; p=0.03). Rate of LR and HR between were nearly statistically different in favor of RFA: LR:19% for metastasectomy group, 10% for RFA group (p=0.06, delay:245 and 289 days, p=0.56), HR: 78.5% for metastasectomy, 66% for RFA (p=0.054, delay: 226 and 235 days , p=0.81). R1 status and metastasis deepness were predictive factors for LR in the metastasectomy group (p=0.03 and p=0.02, respectively). Metastases deepness and proximity to vascular structure increased risk for R1 (p=0.04 and p<0.001, respectively). We found no predictive factor for LR in RFA group.
Conclusion: Pending proper selection, RFA tends to have a lower recurrence rate than metastasectomy. Lesions localized in depth in the liver parenchyma, close to large veins, with R1 margin are at risk of LR after metastasectomy.

SS209

The Value of Percutaneous Image Guided Fine Needle Aspiration Cytology (FNAC) in Pancreatic Lesions

A. Barras, C. Duc, A. Regnaud, J.-L. Constantin, M. E. Kamel, C. Constantin; Sion/CH

Purpose: To evaluate the clinical utility and diagnostic accuracy of percutaneous image guided fine needle aspiration cytology (FNAC) in patients with suspicious pancreatic lesions.
Methods and Materials: Twenty four patients (16 males and 8 females, age range 57 to 89 y) with suspected pancreatic lesions (20mm to 78mm, mean diameter 43mm ±17) were prospectively enrolled. Standard FNAC was performed under US (n=14) or CT (n=10) guidance by two radiologists. Four cytologic categories of the analyzed aspirates were hypothesized: malignant, benign, atypical, and nondiagnostic. All results were correlated with post-operative histological analysis or clinical and radiological follow-up >6 months. Complications rate was also documented for the entire patient cohort.
Results: Twenty three patients had malignant lesions (19 adenocarcinoma, 2 mucinous carcinoma, 1 lymphoma, and 1 adeno-squamous carcinoma), whereas, 1 had benign lesions (chronic pancreatitis). For the detection of pancreatic malignancy, cytological diagnosis was true-positive in 19 patients, true-negative in 1, and false-negative in 4. False-negative results were represented by atypical (n=2) and nondiagnostic (n=2) findings in 4 patients. No false positive results were obtained. The diagnostic accuracy was 83%, sensitivity was 83%, and specificity was 100%. Two (8%) patients had controlled hemorrhagic complications.
Conclusion: Percutaneous image guided FNAC is a safe and reliable procedure for tissue diagnosis of suspicious pancreatic lesions. Patients with nondiagnostic or atypical aspirates deserve further clinical evaluation since these features portend high risk of an underlying malignancy.

SS210

Management of Active Colonic Bleeding Detected by Angio- MDCT: Interventional Radiology versus Surgery

M. Pannatier, S. Schmidt, P. Bize, D. Hahnloser, R. A. Meuli; Lausanne/CH

Purpose: To determine radiological or clinical criteria permitting to guide emergency treatment of active colon bleeding detected by angio-MDCT
Methods and Materials: We retrospectively included 39 patients, admitted in emergency between August 2003 and July 2014 for active colonic bleeding proven by angio-MDCT. They were divided into two groups based upon the chosen emergency treatment: interventional radiology (n= 21) versus surgery (n= 18). In consensus, two observers reviewed the MDCT-images (location and density of bleeding), the delay between imaging and treatment, patients' hemodynamic parameters (shock index, lactate, and hemoglobin level), clinical data and final outcome in order to detect any differences between the two groups (Fischer, chi-square test).
Results: No significant statistical differences were observed between the two groups, neither radiologically, hemodynamically, clinically nor biologically. Only two tendencies were shown: The group treated by interventional radiology more often showed clinical symptoms, that is hematochezia or melena (p=0.0775), and a decrease of the hemoglobin level (p= 0.0893). Interventional radiology was the preferred treatment option, when the bleeding source was located in the proximal colon (p=0.0866).
Conclusion: In emergency patients with active colonic bleeding revealed by angio-MDCT, interventional radiology should be the first treatment choice, being faster, less invasive and associated with fewer complications than surgery. In case of impossible embolization or relapse of bleeding, surgery becomes the best treatment option.

SS211

Reduction of Peristalsis-Related Gastrointestinal Motion Artifacts with Dual-Energy CT: A Patient and Phantom Study.

S. Winklhofer[1], J. Lambert[2], J. Wang[2], R. Gould[2], R. Zagoria[2], B. Yeh[2]; [1]Zurich/CH, [2]San Francisco/US

Purpose: To assess the ability of Dual-Energy Computed Tomography (DECT) to reduce peristalsis-related motion artifacts.
Methods and Materials: DECT images of 100 consecutive patients (48 male, 52 female, mean age 57 years) were retrospectively evaluated in this institutional review board-approved study. Image reconstructions included virtual monochromatic 70keV and 120keV images, as well as iodine(-water) and water(-iodine) material decomposition images. We recorded the presence and severity of artifacts qualitatively (4-point scale) and quantitatively (iodine/water concentrations, Hounsfield units, grey scale values [GY]) and compared to corresponding unaffected reference tissue. Similar measures were obtained in DECT images of a peristalsis phantom. Wilcoxon signed-rank and paired t-tests were used to compare results between different image reconstructions.
Results: Peristalsis-related motion artifacts were found in 49 (49%) of the DECT examinations. Artifacts were significantly more severe in 70keV, 120keV, and water(-iodine) images than in iodine(-water) images (qualitative readout P<0.001, each). Quantitative measurements were significantly different between the artifact and the reference tissue in 70keV, 120keV, and water(-iodine) images (P<0.001 for both HU and GY for each image reconstruction), but not significantly different in iodine(-water) images (iodine concentrations P= 0.088 and GY P=0.111). Similar results were seen in the peristalsis DECT phantom study.
Conclusion: Peristalsis-related motion artifacts seen in 70keV, 120keV, and water(-iodine) images are significantly reduced in iodine(-water) images at DECT.

SS212

Comparison of Shear Wave Velocity Measurements assessed with Two Different Ultrasound Systems in an Ex-vivo Tendon Strain Phantom

A. B. Rosskopf, E. Bachmann, J. Snedeker, C. W. Pfirrmann, F. M. Buck; Zurich/CH

Purpose: To assess the reproducibility and accuracy of shear wave (SW) velocity measurements with two different ultrasound (US) systems in a load bearing tendon model against direct biomechanical measurements.
Methods and Materials: A bovine tendon was fixed in a custom-made stretching device. Applied force was increased step-wise from 0 up to 18 Newton (N) in steps of 2N ranging from an unloaded tendon to simulated physiological maximal contraction. The elastic modulus at each strain state was determined (E;N/mm2) by the stress-strain-output of the stretcher device and by SW velocities. SW velocities were measured two-times during each tendon strain state using a Siemens S3000, and two-times using a Supersonic Aixplorer US-machine. Descriptive statistics, Pearson correlation coefficient, coefficient of determination, paired t-test and intraclass correlation coefficients were calculated to compare measurements.
Results: A strong significant positive correlation for all transducers was found between SW velocity and E-modulus (r=989-0.994,p<0.001), yet all SW velocity based calculations dramatically underestimated the reference tissue elastic modulus. Mean difference of SW velocities with the S3000 was 0.46 m/s±0.3(p=0.002), and with the Aixplorer 0.32 m/s±0.3(p=0.034). Mean difference of SW velocity between the two US-systems was 0.37 m/s±0.3 (p=0.012).
Conclusion: SW velocities in healthy tendon tissue are highly dependent on mechanical forces in the tissue, but for controlled mechanical loads appeared to yield reproducible, sensitive, and comparable measurements using different US-systems. Because small differences in tissue loads can heavily affect measurement outcome, care must be taken in using SW velocity as a clinical indication of an underlying biomechanical deficiency.

SS213

Value of Acromiohumeral Distance and Critical Shoulder Angle Measurements for the Prediction of Rotator Cuff Tendinopathies

M. Q. Hamie, V. Grunder, T. Pfammatter, G. Andreisek, R. Guggenberger; Zurich/CH

Purpose: The purpose of this study was to investigate whether there is an association between the critical shoulder angle (CSA), the acromiohumeral distance (AHD) and rotator cuff tendinopathies (RCTs) in the shoulder joint.
Methods and Materials: In this ethical board approved, retrospective study in 194 patients referred to our institution for unspecific shoulder pain CSA and AHD were measured on conventional antero-posterior radiographs. MR examination reports acquired at 1.5 Tesla were screened for presence of partial or total rotator cuff tears.
Statistical analysis with independent t-testing, Pearson-rank correlation and stepwise multiregression analysis was performed.
Results: In 90 patients (mean age 36+/-14.1, female 17) no RCTs were found on MR imaging and thus served as control group. Patient group consisted of 104 patients (mean age 50+/-15.9, female 27) with at least one partial or total tear of a rotator cuff tendon. The control group had a mean AHD of 10.8mm+/-2.2mm and a mean CSA of 33.1°+/-3.5° with no significant correlation of both with age or gender (p=0.28 and p=0.74). The patient group had a mean AHD of 10.1mm +/- 2.5mm and a mean CSA of 34.0° +/- 5.7°. Significant differences were found between control and patient group for AHD and CSA (p<0.01). Multi regression analysis showed RCT of the infraspinatus tendon to best correlate with AHD and CSA (R= -0.258 and R=0.251, p<0.05).
Conclusion: The AHD and CSA do not depend on age or gender. CSA and AHD significantly correlate with RCTs, especially with infraspinatus tendinopathy.

SS214

The Legend of the Luschka's Tubercle and Its Association with Snapping Scapulae: Osseous Morphology of Snapping Scapulae on 2D and 3D CT Images

T. Dietrich[1], C. A. Agten[2], P. Fürnstahl[1], L. Vlachopoulos[1], C. W. Pfirrmann[1]; [1]Zurich/CH, [2]New York/US

Purpose: To determine the osseous morphology of snapping-scapulae on CT images.
Methods and Materials: Two and three-dimensional CT images of scapulae of 34 patients with snapping-scapulae were compared to 34 age-and-gender matched control-group patients. Two observers analyzed the following parameters: Presence of the Luschka's tubercle, shape of superior angle of the scapula, abnormalities of ribs and periscapular soft tissues, thickness and length of superior angle of the scapula, craniocaudal length of scapula, minimal distance between scapula and ribs, depth of subscapular fossa, and superomedial angle.
Results: In snapping-scapula patients observer 1 did not find any Luschka's tubercle while observer 2 detected one Luschka's tubercle compared to two Luschka's tubercle in the control-group for both observers (p-values>0.48). One scapular osteochondroma was detected in a 29-year-old snapping-scapula patient. No abnormalities of the ribs and periscapular soft tissues were found in snapping-scapula patients. The superior angle of the scapula was significantly thicker in the snapping-scapula group compared to the control-group (4.8±1.3 mm versus 4.1±1.1mm, p-values<0.02). The subscapular fossa was significantly deeper in snapping-scapula patients compared to control-group patients (21.9±5.0mm versus 18.8±4.5mm, p-values<0.035). Comparison of the remaining parameters did not differ significantly between the groups.
Conclusion: The Luschka's tubercle was rarely observed and not associated with a snapping scapula. In contrast a scapular osteochondroma may be found in patients with a snapping scapula. The superior angle of the scapula was significantly thicker and the subscapular fossa was significantly deeper in patients with a snapping scapula compared to control-group patients.

SS215

Shoulder Muscle Volume and Fat Content in Healthy Adult Volunteers as Quantified with DIXON MRI: Influence of Age, Gender and Handedness

P. Kälin[1], R. Crawford[2], M. Marcon[1], A. Manoliu[1], S. Bouaicha[1], M. Fischer[1], D. Nanz[1], E. J. Ulbrich[1]; [1]Zurich/CH, [2]Winterthur/CH

Purpose: Define normative reference standards of fat-fraction and volume for healthy rotator cuff and deltoid muscles. This study should benefit clinicians in determining modifiable risk factors for successful outcomes in the treatment of shoulder pathology.
Methods and Materials: Seventy-six healthy, asymptomatic volunteers (39F, 37M) with normal BMI (18.5-25 kg/m^2) were included in the study. Eight to ten participants per gender represented each decade age-group (20-29, 30-39, 40-49, and 50-60). Shoulder MRI was performed at 3.0T using 3-point DIXON sequences. Volume and fat-signal fraction (FSF) of supraspinatus (SSP), infraspinatus (ISP), subscapularis (SSC), teres minor (Tm) and deltoid (Delt) muscles were determined with semi-automated segmentation with linear interpolation. Student's t-test and ANOVA evaluated differences according to age, gender and handedness per muscle. Correlations of FSF with anthropometric and bioelectrical impedance measurements as well as sports activity, and hand dominance were evaluated using Pearson's and Spearman`s correlation coefficient.
Results: FSFs were comparable between genders and muscle groups (total mean FSF in women/men: 7.0±1.6%; 3.3-12.3, 6.8±1.4; 3.0-12.7) with exception of significant lower FSF of ISP (5.7±1.2%/5.8±0.8%, p<0.001). Trends towards higher shoulder muscle volume and lower FSF in the dominant arm were shown and significant particularly in Tm and Delt (p<0.01). FSF showed trends for an age-effect although not significant. Body fat parameters related to FSF for all shoulder muscles (R>0.34) while sporting activity did not.
Conclusion: Normative shoulder muscle FSF and volume in healthy 20-60 year-old adults provide reference for clinicians. Our findings warrant extension into younger and older groups to establish further trends.

SS216

Real T1 Relaxation Time Measurement and Diurnal Variation Analysis of Intervertebral Discs in a Healthy Population of 50 Volunteers

J. Galley, G. Maestretti, H.-M. Hoogewoud; Fribourg/CH

Purpose: To measure the real T1 relaxation time of lumbar intervertebral discs in a young and healthy population, using different inversion recovery times, and assess diurnal variation.
Methods and Materials: Lumbar intervertebral discs of 50 healthy volunteers from 18 to 25 years old were evaluated twice a day, morning and afternoon. Dedicated MRI sequences with different inversion recovery times (from 100 to 2500ms) were used to calculate the real T1. Three regions of interest were defined, the middle representing the nucleus pulposus (NP) and outer parts the annulus fibrosus (AF) anterior and posterior. Diurnal variation was analyzed.
Results: T1 values in the NP were 1142 ± 12 ms in the morning and 1085 ± 13 ms in the afternoon, showing a highly significant decrease of 57 ms ($p < 0.001$). Each level was found to be significantly different from the others except comparing L2-L3/L5-S1 and L3-L4/L5-S1 for the morning and L2-L3/L5-S1 for the afternoon. T1 of the anterior part of the AF was 577 ± 9 ms in the morning and 554 ± 8 ms in the afternoon. For the posterior part, the values were 633 ± 8 ms in the morning and 581 ± 7 ms in the afternoon. It shows a highly significant decrease of 23 ms for the anterior part and 51 ms for the posterior part ($p < 0.001$).
Conclusion: T1 mapping is highly sensitive for disc hydration and shows diurnal variation. It seems to have great potential for longitudinal study, e.g. in post-operative follow up and sport medicine.

SS217

High-Resolution 3T MR Imaging of Bone Microarchitecture and MRI Quantification of Bone Marrow Fat in Osteoporosis

C. A. Agten[1], A. Welbeck[1], D. Xia[1], C. Sudesh[2], C. Chen[3], P. Parasoglou[1], P. Saha[3], S. Honig[1], G. Chang[1]; [1]New York/US, [2]Philadelphia/US, [3]Iowa City/US

Purpose: Elevated bone marrow fat content increases the risk for osteoporotic fracture, but it is unknown if such changes are associated with detrimental changes in bone microarchitecture and bone mass. Our goal was to determine the association between femoral neck bone marrow fat with femoral neck bone microarchitecture and femoral neck bone mineral density (BMD).
Methods and Materials: Hips of forty-two consecutive patients referred from the osteoporosis clinic at our institution (mean-age 60.2±7.5 years) underwent dual-energy X-ray absorptiometry (DXA), high-spatial resolution three-dimensional 3T-MRI with volumetric topological analysis (VTA-MRI), and fat quantification with IDEAL-MRI. Femoral neck BMD T-scores (DXA) and trabecular bone microarchitecture parameters (VTA-MRI) were calculated. Proton density fat fraction (IDEAL-MRI) of the femoral neck bone marrow (FFmarrow) was measured by two independent readers. Inter-reader agreement was calculated. FFmarrow was correlated with BMD, bone microarchitecture parameters, age, and body-mass-index (BMI).
Results: FFmarrow (mean from both readers 70.2±6.5%) measurements showed excellent inter-reader agreement (ICC=0.955; $p<0.0005$). No statistically significant correlation between FFmarrow and BMD was found ($r=-0.257$, $p=0.155$). Age- and BMI-adjusted FFmarrow inversely correlated with trabecular plate-to-rod ratio ($r=-0.335$; $p=0.049$) and trabecular plate-width ($r=-0.345$; $p=0.042$), but not with bone volume fraction ($r=0.155$; $p=0.374$). FFmarrow correlated with age ($r=0.383$; $p=0.021$), but not with BMI ($r=0.132$; $p=0.445$).
Conclusion: Bone marrow fat content inversely correlated with trabecular plate-to-rod ratio and plate-width, but not BMD, suggesting that the increased fracture risk in the setting of elevated bone marrow fat content may in part be mediated via microarchitectural deterioration, rather than via reduced BMD.

SS218

In Vivo Evaluation of Bound and Pore Water Components in Cortical Bone Using Ultrashort-TE MRI in Mice: Initial Experience.

M. Marcon, C. Eberhardt, D. D. Keller, M. Weiger, M. Wurnig, D. Eberli, A. Boss; Zurich/CH

Purpose: Separation and quantification of collagen bound water (CBW) and pore water (PW) components of cortical bone are important due to their different contribution to the bone mechanical properties. We tested the feasibility of ultra-short echo-time (UTE) measurements in a murine model for quantification of transverse relaxation of CBW and PW in vivo.
Methods and Materials: UTE sequences were applied at 4.7T in 6 mice with 10 different echo-times (50-5000 µs). T2* of CBW, PW and CBW fraction (BWF) were computed using a mono-exponential (ME) and a standard bi-exponential (SBE) model. Additionally, for the first time, a multistep bi-exponential (MBE) approach was applied. Region-of-interests were drawn at multiple levels of femur and vertebral body cortical bone for each mouse. The sum of the squared residuals (Res) and homogeneity of variance were tested to compare the different methods.
Results: In femur mean ME T2*±standard deviation(SD) was 657 ±234µs. With the SBE approach CBW T2*, PW T2* and BWF were 463±152µs, 15777±10863µs and 57.6±9.9%, respectively. Applying the MBE approach CBW T2*, PW T2* and BWF were 387±108µs, 7533±2764µs and 42.5±6.2%. Similar values were obtained from vertebral bodies. Mean Res was lower for SBE than both ME and MBE ($p<0.007$). BWF and PW variance was lower with MBE than SBE ($p<0.048$).
Conclusion: Separation and quantification of cortical bone water components with a UTE sequence is feasible in vivo in murine models. The SBE approach showed lower residuals of curve fitting, however, the new MBE approach demonstrated higher stability.

SS219

Metal Artifact Reduction of Hip Prostheses: Comparison of an Iterative Algorithm with Virtual Monoenergetic Extrapolations from Dual-Energy CT

K. Higashigaito[1], F. M. Angst[1], V. M. Runge2, H. Alkadhi[1], O. F. Donati[1]; [1]Zurich/CH, 2Bern/CH

Purpose: To directly compare virtual monoenergetic extrapolations (VME) from dual-energy CT with iterative metal artifact reduction (iMAR) in human pelvis with hip prostheses.
Methods and Materials: A human pelvis phantom with uni-/bilateral metal inserts of different material (steel/titanium) was scanned with third-generation dual-source CT using single (120kVp) and dual-energy (100/150kVp) at similar radiation dose ($CTDI_{vol}$:7.15mGy). Three image series for each phantom configuration were reconstructed: uncorrected, iMAR from single-energy, and VME from dual-energy. Two independent, blinded radiologists assessed quantitative (noise and attenuation) and qualitative image quality. Intraclass correlation coefficients (ICC) and Cohen's kappa was calculated to evaluate inter-reader agreements. Repeated measures ANOVA was used to compare reconstruction algorithms regarding quantitative, Friedman-test regarding qualitative image quality. Post-hoc testing was performed for pairwise comparisons using a corrected (Bonferroni) p-value<0.017.
Results: Agreements between readers were high for noise (all,ICC≥0.975) and attenuation (all,ICC≥0.986); agreements for qualitative assessment were good to perfect (all,k≥0.678). Compared to uncorrected images, iMAR resulted in significantly lower noise in all regions and phantom configurations (all,$p<0.017$), whereas VME showed noise reduction ($p<0.017$) in the phantom with titanium only. In all phantom configurations, deviations of attenuation were smallest in images reconstructed with iMAR. Compared to uncorrected images, iMAR had significantly higher image quality in all phantom configurations (all,$p<0.017$). VME showed higher quality in phantoms with titanium compared to uncorrected images, however, without reaching statistical significance ($p>0.017$).
Conclusion: In all phantom configurations, iMAR showed better metal artifact reduction capabilities than VME, whereas VME showed good results only in phantom configurations with titanium prostheses.

SS220

Hip MRI: Prevalence of Defects of the Articular Cartilage and Labrum in Asymptomatic Volunteers and Patients with Femoroacetabular Impingement (FAI)

F. Tresch, T. Dietrich, C. W. Pfirrmann, R. Sutter; Zurich/CH

Purpose: To prospectively compare defects of the articular cartilage and labrum in asymptomatic volunteers and patients with femoroacetabular impingement (FAI) matched for age and gender.
Methods and Materials: This cross-sectional study was institutional review board approved, all participants provided signed informed consent. 63 asymptomatic volunteers and 63 patients with symptomatic FAI between 20 and 50 years were included and underwent MR imaging. Two radiologists independently assessed defects of the acetabular and femoral cartilage and the labrum at six positions. Mann-Whitney-U-test and Spearman's rho were used for statistics.
Results: A defect of the articular cartilage and/or labrum was present in 57% of asymptomatic volunteers, compared to 80% of symptomatic patients. 14% of volunteers had acetabular cartilage defects, and 6% had femoral cartilage defects (compared to 47% and 30% in patients, respectively). Labrum defects were seen in 44% of volunteers versus 61% of patients. Joint damage was more commonly present in male volunteers than in female volunteers, with the largest difference seen for the acetabular cartilage ($P \leq 0.02$). In all groups, the majority of cartilage and labrum defects were encountered in the anterior, anterosuperior, and superior position of the hip joint.
Conclusion: Quite a large number of asymptomatic volunteers had labral tears, defects of the acetabular cartilage, and to a lesser degree, defects of the femoral cartilage. Our data demonstrates that not all cartilage and labral defects of the hip joint are symptomatic.

SS221

Do Iliopsoas and Gluteus Maximus Change with Aging? A MRI Investigation in Healthy Adult Volunteers.

R. Crawford[1], S. Franckenberg[2], P. Kälin[2], M. A. Fischer[2], D. Nanz[2], E. J. Ulbrich[2]; [1]Winterthur/CH, [2]Zurich/CH

Purpose: Evaluate changes to iliopsoas (IP) and gluteus maximus (GM) volume and fat content in healthy adult volunteers using mDIXON whole-body MRI.
Methods and Materials: IRB approved. Fat-signal fractions (FSF) and normalised volumes (Vi) of IP and GM were determined from two-point mDIXON sequences of 80 adults (Women/men n=40; age 20-62yrs), using semi-automated segmentation of 3T whole-body MRI. T-tests analyzed sex, side and leg-dominance differences. ANOVA (Bonferroni) compared FSF and Vi between sub-groups. Pearson's and Spearman analysis described correlations ($p<0.05$).
Results: FSF-IP increased with age for both sexes (Women/men: $p<0.01/p<0.001$) and for FSF-GM in men ($p<0.01$). No sex-dependence was shown for FSF-IP (10.1±1.2/10.2±1.5). FSF-GM was higher in women (13.0±2.7/11.1±3.0;$p<0.001$). IP- and GM-FSF correlated strongly on the dominant ($R=0.60$, $p<0.001$) and non-dominant sides ($R=0.52$, $p<0.01$) in men only. Women had lower muscle volumes ($p<0.001$) and Vi-IP showed age-dependent decline in men ($p<0.01$). Muscle volume showed strong correlation to each other on both sides in both sexes ($R>0.45$, $p<0.01$). BMI strongly correlated with FSF-IP for men ($R=0.48$, $p<0.001$). Normalised TAT (MR-based total adipose tissue) moderately to strongly correlated with FSF-IP (R=0.37/0.66;$p<0.001$) and FSF-GM (R=0.48/0.64;$p<0.001$) for both women/men; normalised TLMT (MR-based total lean muscle tissue) inversely correlated with FSF-IP (R=-0.42/-0.47;$p<0.001$) and FSF-GM (R=-0.49/-0.59;$p<0.001$).
Conclusion: Age-dependent muscle decline in iliopsoas and gluteus maximus is stronger in men. Other adipose content relates to primary hip flexor and extensor muscle quality. The functional significance warrants investigation.

SS222

Magnetization Transfer Ratio (MTR) and Diffusion-Tensor Imaging (DTI) for In-Vivo Muscle Regeneration after Cell Therapy.

D. Keller, C. Eberhardt, M. Rottmar, D. Haralampieva, T. Sulser, D. Eberli, A. Boss; Zurich/CH

Purpose: Urinary incontinence compromises a patient's quality of life and inflicts tremendous health care costs. Recent advances using cell therapy such as muscle precursor cells (MPC) show promising results towards correcting the underlying etiology, but evaluating the success of such treatments in vivo is difficult. We show that Magnetic Resonance Imaging (MRI) using novel sequences for alignment and complex macro molecules enables monitoring of adult stem cell myogenic differentiation in a mouse model.
Methods and Materials: We have isolated, characterized and expanded human MPCs followed by injection into a tibialis anterior and quadriceps femoris muscle crush mouse model. We followed the in situ differentiation via MRI (4.7 T scanner) for 21 days focusing on Magnetization Transfer Ratio (MTR) and Diffusion-Tensor Imaging (DTI) properties of the de novo tissue and confirmed the results by histology, immunohistochemistry, western blot and real time PCR.
Results: MT measurements showed an initial MTR decrease before increasing steadily and approximating the MTR values of reference skeletal muscle tissue. DTI revealed that de novo generated muscle fibers are orientated in the same direction as the surrounding fibers which were not affected by the initial muscle crush injury. Cell differentiation and myofibers formation could be confirmed by increased expression of skeletal muscle-associated markers.
Conclusion: MT-MRI allows to directly assess muscle fiber formation as a measure of myogenic differentiation. DTI highlights the direction of the newly formed fibers. These results will be transferable to the clinical setting as a non-invasive biomarker for the assessment of muscle tissue regeneration in patients.

SS223

Effect of Topogram Projection Angle on Organ Dose in Chest CT with Tube Current Modulation.

N. N. Saltybaeva, H. Alkadhi; Zurich/CH

Purpose: It was recently suggested to use the postero-anterior (PA) projection of the topogram instead of antero-posterior (AP) one to reduce radiation dose to the breast in chest CT. However, the choice of projection angle affects tube current modulation (TCM) and thus the dose from the subsequent CT examination. Our study investigates the cumulative effect of the topogram projection angle on patient dose.
Methods and Materials: The measurements were performed on third-generation CT scanner using an anthropomorphic Rando-Alderson phantom with and without breast attachments. A standard chest CT protocol with TCM at tube voltages of 120kV was used after two different topograms (AP/PA) were applied. Dose distributions were obtained by Monte Carlo simulations based on phantom voxelized data. For topogram simulations tube position was fixed at 0° and 180° for AP and PA projections, respectively. For CT examinations spiral trajectory with TCM was simulated. TCM-profiles were generated based on the topogram data and the assumption of phantom elliptical geometry. Total doses for lungs, heart and breast were calculated as a sum of topogram- and CT- dose values.
Results: Dose values from the PA topogram alone were lower than from the AP one, however, using the PA topogram yielded higher TCM values in subsequent CT examination, resulting in significant increase in total organ doses ($p<0.001$). Using AP instead of a PA topogram allows for dose reductions of about 16%, 11% and 9% for breast, lungs and heart, respectively.
Conclusion: Using AP projection of topogram in chest CT with TCM is associated with substantially lower total radiation dose.

SS224

Chest CT with Radiation Dose Equivalent to Chest Radiography: Prospective Evaluation of Pulmonary Nodules and Infection

K. Martini, B. K. Barth, S. Baumüller, T. D. L. Nguyen, H. Alkadhi, T. Frauenfelder; Zurich/CH

Purpose: To compare prospectively standard dose chest CT with an redused dose protocol for follow–up of pulmonary nodules and lung-pathologies evaluating image quality and diagnostic accuracy.
Methods and Materials: One-hundred patients (64 male, 36 female; median age 56years) who were referred to our department for follow-up of pulmonary nodules or lung consolidations underwent chest CT with both standard-dose protocol and reduced-dose protocol at 100kVp,16mAs and 100kVp,46mAs, respectively. Images were reconstructed with iterative reconstruction algorithms (ADMIRE). One reader measured image noise. Two blinded readers evaluated lung-nodules and –pathologies and determined overall image quality (4-point Likert-scale). Interclass correlation coefficient (ICC) between the two protocols was calculated. The study was approved by ethical committee.
Results: CTDIvol of the standard protocol (mean 2.41mGy, SD +/-0.87mGy) was significantly higher compared to the reduced-dose protocol (mean0.06mGy, SD +/-0.03mGy). Overall image quality was lower for all images scanned with ULD-protocol using ADMIRE, but all images were diagnostic. Inter-observer agreement for image quality was substantial for both ADMIRE strength levels. Image noise has been significantly reduced using ADMIRE5 compared to ADMIRE3 (52.42% for ultra-low-dose, $p=0.001$). ICC for lung pathology detection was high for both IR (atelectasis: ICC = 0.812 vs. 0.889; consolidations: ICC = 0.857 vs. 0.891, interstitial lung changes: ICC = 0.780 vs. 0.807).
Conclusion: With tin-filtration in combination with IR reduced-dose protocols do not significantly influence the detection of lung consolidations, but have a lower sensitivity for detection of small nodules.

SS225

Non-Invasive Pulmonary Nodule Characterization Using Bio-Conductance; Preliminary Results

J. Gariani, S. Martin, A.-L. Hachulla, W. Karenovics, P. Gasche, C. D. Becker, X. Montet; Geneva/CH

Purpose: To analyze the use of an EPN scanner (Freshmedx, Utah, USA) in the non-invasive characterization of pulmonary lung nodules using bio-conductance.
Methods and Materials: Prospective study approved by the local ethics committee with consent from each patient. The scan was performed by a trained physician, bio-conductance curves were obtained at 62 different points for each patient on the chest, arms and hands. Analysis of the bio-conductance curves provided a score for each patient with a cut-off of 0.292 to distinguish between benign and malignant lesions. This was then correlated with pathology results obtained after surgery or percutaneous biopsy.
Results: A total of 8 patients were included at the time of submission. Average lesion size was of 37mm, pathology revealed 7 malignant lesions (adenocarcinoma, squamous cell carcinoma, carcinoid tumor) and 1 benign lesion (necrotic nodule with granuloma). The EPN scanner had a sensitivity of 57% and a specificity of 100%.
Conclusion: EPN scanner is a tool that merits further investigation with a larger patient population in the non-invasive characterization of lung nodules.

SS226

Impact of Iterative Reconstructions on Emphysema Quantification by Computed Tomography Scanner

S. Martin, J. Gariani, A.-L. Hachulla, D. Botsikas, D. Adler, W. Karenovics, C. D. Becker, X. Montet; Geneva/CH

Purpose: To prospectively evaluate the impact of iterative reconstructions (IR) as compared to filtered back projection (FBP) reconstructions on objective and subjective emphysema assessment.
Methods and Materials: The local ethics committees approved this study. Multiple-level IR of 110 unenhanced thoracic CT scans (M:F ratio 11:4, mean age 62 [range, 18-92]) acquired on two different units (GE Discovery 750HD; Siemens Somatom Definition Flash) were compared to FBP reconstructions on the basis of emphysema index, lung volume and voxel densities. Objective emphysema (based on a lung density<950HU) assessment was performed with software provided by each manufacturer. Subjective emphysema analysis was performed as double-blinded visual assessment, based on a 5-point likert scale (0=no emphysema, 5=emphysema present). The quantitative values were compared using repeated ANOVA analysis with a p value <0.05 considered statistically significant. The subjective values were compared using a Kendall's W.
Results: The use of IR modified the emphysema index. Quantification goes from 3.57+/-0.53%(FBP) to 2.38+/-0.48%(IR) ($p<0.0001$) on the GE unit and from 3.13+/-0.59(FBP) to 2.00+/-0.58%(IR) ($p<0.0001$) on the Siemens unit. The use of IR does not change lung volume ($p>0.05$). Significant differences in minimal lung density were found (FBP vs IR, $p\leq0.003$). Subjective evaluation reveals a good intra- and inter-observer agreement on emphysema detection ($W\geq0.77$).
Conclusion: Even at the lowest levels of IR, emphysema quantification was modified, due to differences in minimum voxel density. IR does not alter visual assessment of emphysema. Hence, the use of IR technique for emphysema quantification should be strongly discouraged.

SS227

Magnetization Transfer as a Biomarker for Acute Graft Rejection

D. Kenkel, M. Weiger, W. Jungraithmayr, Y. Yamada, M. Wurnig, A. Boss; Zurich/CH

Purpose: To investigate the value of magnetization transfer measurements for assessment of acute rejection (AR) in a murine lung transplantation model.
Methods and Materials: 30 mice including 15 mice C57BL/10 serving as donors and 15 mice C57BL/6 as recipients were examined in this study. Datasets were acquired on a 4.7-T magnetic-resonance small animal scanner using a 3D zero-echo-time sequence (ZTEisotropic) with a Gaussianshaped MT pre-pulse, and MT imaging was performed with 1000° or 3000° flip angle and systematic variation of off-resonance frequencies between 1000 and 15000 Hz. After image acquisition lungs were taken for histologic examination including staining with hematoxylin/eosin, Masson's trichrome stain (collagen) and α-smooth muscle (fibroproliferative tissue).
Results: Lung transplantation was successfully performed in all 15 mice. All animals showed AR characterized by the presence of interstitial mononuclear cell infiltrates. There were significant differences of magnetization transfer ratio (MTR) in lungs with and without AR (p=0.007). With a flip angle of 1000°, largest differences between the MTR of healthy lungs and lungs with AR were observed for an off-resonance frequency of 10000 Hz (difference MTR 1.80%) and 15000 Hz (1.91%) and with a flip angle of 3000° at off-resonance frequencies of 6000 Hz (1.37%) and 8000 Hz (1.70%).
Conclusion: MT measurements may provide a suitable tool for the quantitative assessment of AR.

SS228

Necrotizing Pneumonia in Children: Radiological Aspects

J. Carrard[1], E. Tenisch[2], L. Alamo[2], G. Hafen[2], F. Gudinchet[2]; [1]Vevey/CH, [2]Lausanne/CH

Purpose: Necrotizing pneumonia (NP) is characterized by the development of necrosis within an infected lung. It has been increasingly reported in children. The aim of our study was to describe the typical radiological aspect of NP and to investigate the respective role of CT and US in the diagnosis and management of the disease.
Methods and Materials: We retrospectively reviewed 39 patients (male: 21; female: 18; mean age: 4.2 years old) with NP treated in our institution between 01/01/2000 and 30/06/2015. The radiological features assessed included: location and aspect of the consolidations (parenchymal enhancement), presence of pleural effusion, atelectasis and pneumothorax. Clinical features such as: type of bacteria, presence of fever, need of O2 and duration of hospitalization were also considered.
Results: Every patient had a mean of 15 x-rays, 1.3 US and 2 CT. On CT, consolidations were heterogeneous in 97.5% of the patients. This correlated well with US findings when available (N=20). On CT, 85% of the patients had a pleural effusion of which, a fifth were loculated. 82.5% complicated by cavitation and 17.5 % by bronchopleural fistula. Adenopathies were present in only 25% of the cases.
Conclusion: Both US and CT were complementary in the diagnosis and in the treatment of NP. On one hand, CT helped in the diagnosis of early necrosis and to evaluate its extension. CT was mandatory to detect bronchopleural fistulae. On the other hand, US was useful in the follow up of lung necrosis and to assess the evolution of pleural effusion.

SS229

Functional Pulmonary Perfusion with Dual-Energy CT in Children with Pulmonary Hypertension, Preliminary Results

A.-L. Hachulla, F. Lador, S. Noble, J. Gariani, M. Laurent, X. Montet, Y. Aggoun, M. Beghetti, J.-P. Vallee; Geneva/CH

Purpose: To assess pulmonary perfusion with dual-energy CT in order to better understand morphological pulmonary or vascular abnormalities and their functional consequences in the pediatric population.
Methods and Materials: Four children with pulmonary hypertension confirmed by right heart catheterism underwent a dual-energy chest CT scan for parenchymal and vascular assessment. 2 patients (2 and 8 months old) had bronchopulmonary dysplasia, 1 patient (1 month-old) a patent ductus arteriosus with treated right diaphragmatic hernia, and 1 patient (13 years-old) with tricuspid endocarditis. Each CT-scan corresponded to an irradiation dose of 0.38, 0.49, 0.28 and 1.3 mSv respectively. Parenchymal and arteries abnormalities were noted. Perfusion maps were reconstructed for functional lung analysis. Pulmonary perfusion was also rated qualitatively as severe hypoperfusion, moderate hypoperfusion or normal perfusion using a color-scale map. Iodine parenchymal lung concentrations (C_{lung},mg/mL) were measured and normalized by the left atrial concentration. Then, a morphological and functional correlation was realized.
Results: 2 patients had pulmonary fibrosis with honeycombing, cysts and bronchiectasis responsible for severe hypoperfusion (C_{lung}=2.0); surrounded by normal morphological areas with normal (C_{lung}=5.3) or moderate hypoperfusion (C_{lung}=2.9).
1 patient had right pulmonary artery hypoplasia responsible for extensive and severe right lung hypoperfusion (C_{lung}=1.2) but normal left lung perfusion (C_{lung}=3.8).
The last patient had chronic pulmonary embolism due to tricuspid endocarditis with severe systematized hypoperfusion defects (C_{lung}=0.8).
Conclusion: Chest DE-CT can allow complete assessment of vascular anatomy, parenchymal morphology and functional pulmonary imaging in different pediatric pathologies, particularly when the lung seems morphologically normal.

SS230

A micro CT Study in Patients with breast Microcalcifications Using a Mathematical Algorithm to Assess 3D Structure

D. Kenkel, Z. Varga, H. Heuer, K. Dedes, L. Filli, A. Boss; Zurich/CH

Purpose: The aim of this study was to evaluate the relevance of the 3-dimensional structure of microcalcifications (MC) as a predictor of malignancy using highly resolved micro-computed-tomography (microCT) datasets of biopsy samples.
Methods and Materials: The study included 28 women with suspicious microcalcifications in the mammogram (BIRADS classification 3-5) undergoing vacuum-assisted biopsy. Directly after the intervention, the specimen were scanned in a microCT with an isometric spatial resolution of 9 µm. Datasets were analyzed regarding the number, volume and diameter of MC, morphology (suspicious non-monomorphic MC: fl fine linear, fp fine pleomorph, ch: coarse heterogeneous), and the structure model index (SMI). Histological evaluation was performed according to the B-classification: benign (group A: B1, B2), unclear malignant potential (group B: B3, B4) and malignant lesions (group C: B5).
Results: In all groups, suspicious non-monomorphic MC were found: Group A exhibited fp MC in 38.5% of samples, no fl/ch; group B: fl 14.3%, fp 28.6%, ch 14.3%; group C always at least one type of fl (57.1%) or fp (57.1%) in each sample. The different histologic groups showed a similar mean SMI (benign: 2.97±0.31, malignant: 3.02±0.10, unclear: 2.90±0.28). Between the three groups, no significant differences were found regarding number, volume, diameter and SMI value of MC.
Conclusion: The 3D structure of MC analysed with highest spatial resolution is not significantly associated with the B-classification of breast lesions. Thus, magnification views of microcalcifications may be omitted in the analysis of MC detected in mammograms.

SS231

Fat Suppression Techniques for Breast MRI: Dixon versus Spectral Fat Saturation for 3D T1-Weighted Sequence at 3 T.

N. Firmenich, A. Kalovidouri, B. Delattre, M. Picarra, C. D. Becker, X. Montet, D. Botsikas; Geneva/CH

Purpose: To compare two fat suppression techniques used for 3D T1-weighted sequence in breast MRI, namely Dixon versus spectral fat saturation in classical THRIVE.
Methods and Materials: All breast MRI examinations performed in a Philips 3T unit between March 2013 and October 2015 including either a Dixon or a THRIVE sequence were retrospectively recalled from the PACS of our institution. The examinations were subjectively evaluated by two independent experienced readers in a scale of 5 for overall quality of fat suppression, homogeneity of fat suppression, definition of anatomic structures and pathologic lesions, diagnostic confidence for axillary and internal mammary regions and presence of artifacts, 1 corresponding to excellent and 5 to non-diagnostic quality. Contrast-noise-ratio(CNR) measurements for muscle and pathologic lesions were also performed.
Results: Overall 161 women (mean age 51.6 +/-12.0 years) underwent 189 MR examinations, 113 with the VIBE and 76 with the Dixon sequence. Interobserver variability was good (kappa=0.757). In all subjectively evaluated parameters the Dixon sequence was superior to the THRIVE ($p<0.05$). Mean values of CNR for muscle and pathologic lesions were 9.98(+/-4.2), 17.9 (+/-7.53) for the THRIVE and 18.3 (+/-10.4), 29.3 (+/-14.1) for the Dixon sequence respectively ($p<0.001$).
Conclusion: 3D T1 Dixon sequence is superior to THRIVE for dedicated breast MRI at 3T, in terms of efficiency of fat suppression and image quality with the added advantage of optimal exploration of the axillary areas.

SS232

Abbreviated Breast MRI for Cancer Screening: Are MIP Projections of DCE Sufficient for Cancer Detection?

N. Vietti Violi, E. Tenisch, L. Alamo, R. A. Meuli, J.-Y. Meuwly; Lausanne/CH

Purpose: Accurate detection of breast cancer is limited in women with dense breast. Sonography may help in these cases, but at the price of considerable increase in false positive. MRI is the most sensitive technique for cancer detection, with high specificity. Today, due to long examination time, it cannot be used for screening in normal risk population. The aim of this study was to determine if interpretation of one sequence amongst those obtained for a complete examination may be sufficient to identify cancer.
Methods and Materials: Two readers consensually reviewed the MIP images of DCE sequences of 60 breast MRI examinations performed in women over 50 for preoperative assessment in our breast center. The presence, visibility, shape, size and location of suspicious enhancement were reported. In case of multiple suspicious enhancements, index lesion was determined. Data were compared to the results of the complete MRI examination.
Results: Cancer was identified on the MIP projection in 97% of cases. Failures of identification were observed in some cases of DCIS or low grade ILC. False positive cases were related to intraglandular lymph nodes, hyperplasia without atypia or papillary lesions.
Conclusion: Assessment of MIP images from DCE series was sufficient to identify almost all breast cancers. Abbreviated breast MRI should be considered for shorten breast MRI examination's duration.

SS233

Site and Rate of Arterial Anomalies in Acute Ischemic Stroke: A CT-Angiography Study of 50'807 Cervico-Cerebral Arterial Segments

D. Rotzinger, P. Mosimann, R. A. Meuli, P. Maeder, P. Michel; Lausanne/CH

Purpose: CT angiography (CTA) can rapidly and accurately depict arterial anomalies in patients with acute ischemic stroke (AIS). Our purpose was to determine the pattern of significant stenoses and occlusions at admission based on CTA in a representative AIS population.
Methods and Materials: Data from consecutive AIS patients admitted to a single centre (CHUV) between 2003 and 2012 were prospectively collected in the Acute STroke Registry and Analysis of Lausanne (ASTRAL) database. All patients with a good quality CTA within 24 hours from symptom onset were selected. All intracranial and cervical arterial stenoses ≥50% or occlusions were registered and classified according to 31 pre-specified segments per patient.
Results: Among 2'209 patients (42.6% females, median age 71 years), 1'177 (53.3%) had significant arterial CTA anomalies. Among the 50'807 examined arterial segments, 2'259 were abnormal: 1'851 (82%) were within the ischemic territory, whereas 408 (18%) were considered asymptomatic. The arteries most frequently affected by symptomatic anomalies were the proximal MCA (20.1% of all segments), followed by the cervical ICA (16.7%) and the distal MCA (12.1%). In AIS patients imaged by CTA within 6 hours of onset, 40.7% had occlusions potentially amenable to endovascular therapy.
Conclusion: This study shows that CTA obtained within 6h of symptom onset can depict large, proximal segmental arterial anomalies amenable to endovascular therapy in more than 40% of AIS patients. The annual case load of CTAs performed in AIS patients may therefore serve to estimate how many acute endovascular treatments can be expected per stroke center or region.

SS234

Dose Reduction in Dynamic Perfusion CT of the Brain: Effects of the Scan Frequency on Calculated Infarct Core and Penumbra Volume

G. M. Karwacki, C. Stippich; Basel/CH

Purpose: CT Perfusion technique (CTP) is a highly sensitive and specific imaging method for detection of ischemic brain changes. Based on calculated parameters the size of penumbra (tissue at risk, TAR) and irreversibly damaged infarct core (non-viable tissue, NVT) can be judged. We wanted to evaluate whether an increased time interval between sequential CTP scans affects the volume of calculated TAR and NVT and thus if it could affect further therapeutic procedures and if potential radiation dose reduction is possible.
Methods and Materials: We have included 20 patients (7 male, 13 female, age 77,9±9,6) who had an occlusion of M1 and/or M2 segment of MCA. The sizes of NVT and TAR have been evaluated using CT Neuro Perfusion application in Syngo.Via (Siemens, Germany). CTP scans were first analyzed in a standard fashion according to our in house stroke protocol. Resulting NVT and TAR volumes measured in ml were recorded in a database. Second analysis was conducted after retrospectively increasing the time interval between sequential CTP scans up 3 seconds (by excluding some of time points of original studies) in the same group of patients. Measurements of NVT and TAR volumes were repeated, recorded and compared to values obtained using our standard methods.
Results: There was no statistically significant difference between IR and TAR volumes between two compared CTP protocols (p>0,05).
Conclusion: Reduction of CTP scan frequency without objective loss of accuracy of NVF and TAR calculation and a reduction of patient exposure to radiation are feasible.

SS235

Texture Analysis Features Reveal Selective Vulnerability of Thalamic Nuclei in Mice after Hypoxic-Ischemic Injury

M. W. Wagner[1], M. Wurnig[1], A. K. Narayan[2], T. A. Huisman[2], F. J. Northington[2], A. Boss[1], A. Poretti[2]; [1]Zurich/CH, [2]Baltimore/US

Purpose: Neonatal hypoxic-ischemic injury (HII) damages the thalamus, with the ventrolateral nuclei being a selectively vulnerable target. We aimed to identify thalamic nuclei damage in HII mice to assess the role of hypothermic management using texture analysis (TA) features of diffusion tensor imaging (DTI) data.
Methods and Materials: HII was induced at postnatal day 10 by a right carotid artery ligation followed by 45 minutes of hypoxia. Mice were randomized to a healthy control group (N=20) and a hypothermia (31°C) (N=32) or normothermia (36°C) (N=25) group following HII. DTI data were acquired at postnatal (p) day 11, 18, and 30. Fractional anisotropy (FA) and mean diffusivity (MD) maps were generated. Single slice regions of interest were drawn manually to cover the entire thalamus at its greatest diameter on FA and MD maps. TA features were calculated using a MATLAB based algorithm.
Results: Quantitative evaluation of TA features of the right thalamus on both FA and MD maps revealed statistically significant results ($p < 0.005$) for 1st, 2nd, and 3rd order texture features comparing p11, p18, and p30 control mice and mice with hypothermia and normothermia therapy. Statistically significant differences were predominant in 3rd order texture features.
Conclusion: TA identifies thalamic injury in mice after HII. Our results most likely reflect the selective vulnerability of the ventrolateral nuclei. Immunohistochemistry is needed to confirm these findings. In addition, studies correlating TA features with neurodevelopmental outcome of children with HII are needed to assess the potential role of TA features as outcome biomarker of neonatal HII.

SS236

MR Brain Volumetry May Help to Diagnose PSP in Elderly Patients

V. Dunet[1], J. Deverdun[2], C. Charroud[2], E. Le Bars[2], F. Molino[2], C. Geny[2], N. Menjot de Champfleur[2]; [1]Lausanne/CH, [2]Montpellier/FR

Purpose: Progressive supranuclear palsy (PSP) is a difficult differential diagnosis in elderly subjects. We aimed at identifying specific morphometric markers in the brain of elderly patients with progressive PSP compared to age-matched patients with Parkinson's disease (PD) or vascular parkinsonism (VP) and healthy controls.
Methods and Materials: Fourty-four patients (79±5yo; M/F: 31/13) with parkinsonism (9 PSP, 27 PD and 8 VP) and 29 controls (78±3yo; M/F: 21/8) prospectively underwent brain MRI on a 3-T scanner including T1 MPRAGE sequence. Volumetric morphometry was obtained using Morphobox software. Receiver operating characteristics curve analysis with computation of area under the curve (AUC) was used to compare diagnostic values.
Results: Among all brain structures, mesencephalon appeared significantly smaller and third ventricle significantly larger in PSP than in PD, VP patients and controls. Normalized mesencephalic volume of less than 0.58% accurately distinguished between PSP and PD patients (AUC: 0.90[0.79-1.0]), VP patients (AUC: 0.86[0.7-1.0]) and controls (AUC: 0.85[0.71-0.99]). Normalized third ventricular volume of at least 0.23% accurately distinguished between PSP and PD patients (AUC: 0.81[0.63-0.98]), VP patients (AUC: 0.72[0.49-0.94]) and controls (AUC: 0.84[0.69-1.0]). Mesencephalic and third ventricular volumes had similar performance (p>0.28).
Conclusion: Mesencephalic and third ventricular MR volumetry could be used to identify elderly patients with PSP.

SS237

A Novel Non-Parametric Algorithm for Intravoxel Incoherent Motion Analysis in the Brain: Test-Retest Reliability, Correlation to Arterial Spin Labeling and Preliminary Results in Glioblastoma Patients

S. Stieb, A. Boss, M. Wurnig, P. S. Özbay, D. Nanz, T. Weiss, O. Riesterer, C. Rossi; Zurich/CH

Purpose: Quantitative monitoring of tissue cellularity and perfusion in heterogeneously vascularized lesions can be potentially achieved using intra-voxel incoherent motion (IVIM) model, which predicts a dependence of the diffusion-weighted MR-signal from diffusion (D) and perfusion (D*, f_p) correlates. However, standard IVIM-algorithms suffer from poor stability. In this study a novel non-parametrical IVIM-algorithm was tested for reliability in healthy volunteers. IVIM was performed in patients with malignant intracranial lesions and correlated with Arterial Spin Labeling (ASL).
Methods and Materials: IVIM-parameters (non-parametric and standard algorithm) and Cerebral Blood Flow (CBF) values were computed within gray and white matter (GM, WM), and cerebrospinal fluid (CSF) in eleven healthy volunteers and nine patients. Healthy volunteers' data were acquired twice during the same imaging session. For patients, mean values were computed over lesions (L), edema (E), and necrotic areas (N). Intra-class correlation coefficients (ICCs) and Pearson's coefficients were computed.
Results: The non-parametric algorithm provided in healthy volunteers the following mean values: D_{GM}=0.76±0.06*10^{-3}mm^2/s, D_{WM}=0.54±0.04*10^{-3}mm^2/s, D_{CSF}=1.04±0.22*10^{-3}mm^2/s, D^*_{GM}=8.3±3.2*10^{-3}mm^2/s, D^*_{WM}=4.7±1.2*10^{-3}mm^2/s, D^*_{CSF}=11.4±5.9*10^{-3}mm^2/s, $f_{P,GM}$=0.14±0.03, $f_{P,WM}$=0.13±0.02, $f_{P,CSF}$=0.47±0.13. Corresponding CBF values were: CBF_{GM}=71±13ml/100g/min, CBF_{WM}=45±6ml/100g/min, CBF_{CSF}=53±10ml/100g/min.The novel IVIM-algorithm resulted in higher stability (non-parametric-algorithm: $ICC_{min,max,mean}$=0.53,0.65,0.59; standard-algorithm: $ICC_{min,max,mean}$=0.40,0.65,0.52). In patients, mean values were: D_N=0.97±0.24·10^{-3}mm^2/s, D_E=1.06±0.19*10^{-3}mm^2/s, D_L=0.88±0.14*10^{-3}mm^2/s, D^*_N=9.9±5.3*10^{-3}mm^2/s, D^*_E=19.1±29.3*10^{-3}mm^2/s, D^*_L=11.6±9.5*10^{-3}mm^2/s, $f_{P,N}$=0.14±0.05, $f_{P,E}$=0.12±0.05, $f_{P,L}$=0.20±0.13, CBF_N=50±12ml/100g/min, CBF_E=41±12ml/100g/min, CBF_L=53±19ml/100g/min. Perfusion estimates of the non-parametric algorithm better correlated with ASL (.53≤r_{CBF,D^*}≤.76, -.98≤r_{CBF,f_P}≤-.80).
Conclusion: The non-parametric algorithm performed better in terms of reliability and correlation with ASL. Reliable IVIM-biomarkers may support the clinical management of intracranial lesions.

SS238

Neuroimaging of the Pituitary Gland - GRASP Sequence at 1.5 T and 3.0 T

A. Bink, J. Lieb, C. Stippich; Basel/CH

Purpose: Report on advantages with the Golden-angle RAdial Sparse Parallel MRI sequence (GRASP) in patients with pathologies of the pituitary gland. The GRASP sequence combines the techniques of compressed sensing and parallel imaging for rapid continuous acquisition with the advantages of flexible spatiotemporal resolution using the golden-angle radial sampling scheme.
Methods and Materials: The GRASP sequence was implemented on 5 MR scanners (Prisma, Skyra, Verio, Avanto, Espree, Siemens Medical Solutions, Erlangen, Germany). The GRASP sequence parameters were: TR/TE 4.42/2.13 msec, image matrix 256 x 256 mm, voxel size 1.0 x 1.0 x 1.0 mm, temporal resolution 4 s, TA 4:07 min. Images were read by two neuroradiologists with respect to delineation of pathologies and artifacts. Data were compared to standard T1w post CE and standard dynamic T1w post CE measurements.
Results: 40 patients were retrospectively included. In 7 patients no pituitary pathology was detected. 33 patients had the following reports: preoperative macroadenoma (10x), postoperative makroadenoma (8x), microadenoma (9x), cyst (3x); craniopharyngeoma (1x), infarction (2x). In the GRASP sequence arrival of contrast media and distribution over time was well visible in all patients with additional high regional resolution. Both readers evaluated all pathologies in detail. Image quality was assessed comparable to standard sequences. Pulsation artifacts were not observed.
Conclusion: With the GRASP sequence all pituitary pathologies were well visible by simultaneously providing high temporal and high spatial resolution. We assume that a significant reduction of examination time will be achieved for these patients in the future by using the GRASP technique.

SS239

Do Quantitative Diffusion Weighted MRI Parameters Reflect Human Papilloma Virus Status in Oropharyngeal and Oral Cavity Head and Neck Squamous Cell Carcinoma?

T. de Perrot, M. Domingos, V. Lenoir, S. S. Stefanelli, P. Dulguerov, M. Pusztaszeri, M. Becker; Geneva/CH

Purpose: Infection with the human papilloma virus (HPV) is a well-established cause for the development of head and neck squamous cell carcinoma (HNSCC). The purpose of this retrospective study was to compare quantitative diffusion-weighted imaging (DWI) parameters in HPV positive (HPV+) and HPV negative (HPV-) HNSCC based on radiologic-pathologic correlation.
Methods and Materials: 89 lesions in 87 consecutive patients (mean age = 65 years) with primary oropharyngeal (n= 41) and oral cavity (n= 48) HNSCC underwent MRI with routine anatomic and DWI sequences. Apparent diffusion coefficient (ADC) maps were calculated. Measurements were obtained by contouring the largest tumor areas on two consecutive slices. A voxel by voxel histogramm analysis was performed for ADC values. Images and quantitative data were analyzed by two experienced readers who were blinded to the standard of reference, which included histology and HPV status in all tumors.
Results: There were 17 HPV+ and 72 HPV- HNSCCs. 53% of HPV+ tumors and 83% of HPV- tumors were keratinizing HNSCC, whereas 47% of HPV+ and 17% of HPV- cancers were of the non-keratinising subtype (p<0.02). The mean tumor diameter was 30mm in HPV+ and 20mm in HPV- HNSCC (p<0.05). Mean and median ADCs were significantly lower in HPV+ (1010x10-6mm2/s and 964x10-6mm2/s) than in HPV- tumors (1143x10-6mm2/s and 1116x10-6mm2/s, p <0.05), whereas kurtosis and skewness were significantly higher in HPV+ (1.598 and 0.975) than in HPV- (0.677 and 0.535) cancers, respectively (p<0.001).
Conclusion: Significant differences in quantitative DWI parameters of HPV+ and HPV- HNSCCs exist reflecting their distinct histopathological microstructure.

SS240

Multiparametric MR Neurographic Orthopantomogram of the Mandibular Bone and Nerve

M. Ho, A. Manoliu, D. Nanz, M. Piccirelli, E. Dappa, L. Filli, A. Boss, G. Andreisek, F. P. Kuhn; Zurich/CH

Purpose: Panoramical radiographs or cone-beam CT are the standard-of-care in dental imaging to assess teeth, mandible, and mandibular canal pathologies, but do not allow assessment of the inferior alveolar nerve itself nor of its branches. We propose a new technique for 'MR neurographic orthopantomograms' exploiting ultrashort echo-time (TE) imaging of bone and teeth complemented with high-resolution morphological and functional MR neurography.
Methods and Materials: IRB approved study in 10 healthy volunteers. Whole mandibles were imaged at 3.0T (MAGNETOM Skyra, Siemens-Healthcare) using a 64-channel head coil with isotropic spatial resolution for subsequent multi-planar reformatting. Bone images were acquired using a 3D PETRA sequence (TE, 0.07ms). Morphological nerve imaging was performed using a dedicated 3D PSIF and 3D SPACE STIR sequence. Functional MR neurography was accomplished using a new accelerated diffusion-tensor-imaging (DTI) prototype sequence (2D SMS-accelerated RESOLVE). Qualitative and quantitative image analysis was performed and descriptive statistics were provided.
Results: Image acquisition and subsequent post-processing into 'MR neurographic orthopantomogram' by overlay of morphological and functional images were feasible in all 10 volunteers without artifacts. All mandibular bones and mandibular nerves were assessable and considered normal. Fiber tractography with quantitative evaluation of physiological diffusion properties of mandibular nerves yielded the following mean±SD values: FA, 0.43±0.07; mean diffusivity (mm^2/s), 0.0014±0.0002; axial diffusivity, 0.0020±0.0002, and radial diffusivity, 0.0011±0.0001.
Conclusion: The proposed technique of 'MR neurographic orthopantomogram' exploiting ultrashort TE imaging complemented with high-resolution morphological and functional MR neurography was feasible and allowed comprehensive assessment of osseous texture and neural microarchitecture in a single examination.

NSS101

Regadenoson for Stress Testing in Myocardial Perfusion Scintigraphy in Comparison to Dipyridamole

M. Koßert, F. Forrer, K. Szentesi, M. Buser; St. Gallen/CH

Purpose: Adenosine and Dipyridamole are well established agents for pharmacological stress testing in myocardial perfusion scintigraphy (MPS). However, the procedure is time-consuming and associated with significant side effects. Recently Regadenoson is available in Switzerland, allowing for a shorter protocol that is potetentially associated with less side effects.
Methods and Materials: We retrospectively analysed 42 patients that underwent pharmacological stress testing during MPS at our centre. Group A consisted of 21 patients tested with Regadenoson (m/f, mean age 68.3 ± 11.0 years). Group B consisted of 21 patients tested with Dipyridamole (m/f, mean age 70.1 ± 8.2 years). The time of procedure, side effects of stress testing (headache, nausea/vomiting, dyspnae), heart rate difference rest/stress, and the number of patients with pathologic scintigraphic images (scar and/or ischemia) were analysed.
Results: In all 42 patients the stress test was classified adequate. The mean duration of stress testing was 5.4 ± 1.0 minutes in group A versus 18.2 ± 4.6 minutes in group B. The overall incidence of side effects was higher in group B (52%), compared to group A (47%). In group A dyspnae was the most common side effect (43% vs. 5% in Group B), whereas in group B headache was predominat (38% vs. 0% in group A). The number of pathological findings in the scans was equal in the two groups.
Conclusion: Regadenoson allows fast stress testing in MPS featuring less side effects compared to Dipyridamole. The time safed during the procedure will most likely outweigh the higher costs for regadenosn.

NSS102

Functional Imaging in Extra-Adrenal Paragangliomas with 18F DOPA PET/CT and 123I MIBG SPECT/CT Imaging

A. S. Kroiss[1], C. Uprimny[1], B. Shulkin[2], L. Gruber[1], C. Url[1], G. Sprinzl[3], G. Fraedrich[1], G. Gastl[1], I. Virgolini[1]; [1]Innsbruck/AT, [2]Memphis/US, [3]St. Poelten/AT

Purpose: We compared functional imaging modalities in the diagnosis and staging of extra-adrenal paragangliomas (PGLs), using ^{18}F-DOPA PET/CT (diagnostic CT) and ^{123}I-MIBG imaging including SPECT/CT ("low dose" CT).
Methods and Materials: Three male and seven female patients (age range 31 to 73 years) with anatomical and/or histologically proven disease were included in this study. Three patients were either suffering from metastatic head and neck paragangliomas (HNPGLs) or multifocal PGLs and seven patients from nonmetastastic disease. Comparative evaluation included morphological imaging with CT, functional imaging with ^{18}F-DOPA PET and ^{123}I-MIBG imaging including SPECT/CT. Imaging results were analyzed on a per lesion basis.
Results: On a per lesion basis, ^{18}F-DOPA showed a sensitivity of 66.7% (McNemar p<0.01), when compared with anatomical imaging. Sensitivity of ^{123}I-MIBG was 3.7% (McNemar p<0.0001), and that of SPECT/CT 7.4% (McNemar p<0.0001), respectively. Overall, ^{18}F-DOPA PET identified 18 lesions, anatomical imaging identified 27 lesions, and ^{123}I-MIBG imaging identified only 1 lesion and SPECT/CT 2 lesions, respectively.
Conclusion: ^{18}F-DOPA PET/CT is more sensitive than ^{123}I-MIBG imaging including SPECT/CT, providing valuable clinical information for staging of paragangliomas.

NSS103

Utility of 68Ga-NODAGA-RGD in Osteoarticular Disease: Preliminary Results and Generation of Hypothesis

F. Tabotta, M. Nicod Lalonde, F. Buchegger, J. Delage, M. Straub, J. Prior, P. N. Schaefer; Lausanne/CH

Purpose: RGD is an analogue of $\alpha_v\beta_3$ integrins, which is used to target neoangiogenesis. αVβ3 integrins are also known to be overexpressed on osteoclasts, activated T cells and neutrophils. Gallium-68-NOGADA-RGD (RGD) PET/CT has been described to delineate neoangiogenesis in different tumors. This preliminary study does investigate the role of this radiopharmaceutical in osteoarticular disease.
Methods and Materials: We analyzed the PET/CT images of 9 patients with known cancer (3 head and neck, 2 stomach, 1 esophagus, 1 pancreas, 1 leiomyosarcoma) included in our prospective ^{68}Ga-NODAGA-RGD (100–200MBq) versus ^{18}F-FDG (3.5MBq/kg) study. All studies were analyzed for benign and malignant bone lesions, articular alterations or periarticular accumulation of FDG and RGD. Lesions were classified as benign or malignant based on all available information and compared with the FDG-PET findings.
Results: In total, 7/9 (78%) patients had articular or periarticular accumulation of RGD. All articular or periarticular changes found with RGD were visible with FDG (n=41). In particular, findings in large joints (shoulder/hips, n=13 of 26 joints) were predominantly seen with RGD (2.4±0.7 vs. 2.0±0.5, p=0.03). One patient showed predominant regression of the RGD accumulation in a metastatic bone lesion with morphologic changes after chemotherapy. On patient with known Paget's disease showed specific uptake in the Pagetic lesion.
Conclusion: RGD-PET targeting the $\alpha_v\beta_3$ integrins identifies inflammatory and osteolytic bone lesions. This hypothesis-generating analysis might leads to new indications for RGD-PET.

NSS104

Diuretic (F+30) All-in-One Whole Body 18F-Choline PET/CT in Prostate Cancer

V. Soubeyran, O. Özsoy, C. Duc, Y. Zarkik, J.-P. Coppey, M. E. Kamel; Sion/CH

Purpose: To evaluate the practical use of forced diuresis preceded by adequate hydration in eliminating the residual urinary activity of ^{18}F-Choline in patients with prostate cancer.
Methods and Materials: Twenty patients with prostate cancer underwent dual-phase ^{18}F-Choline PET/CT that consisted of an early dynamic pelvic acquisition and late whole body scan. Oral and parenteral hydrations were started directly after the end of dynamic acquisition. Thirty minutes after tracer injection, each patient received 20 mg of i.v. furosemide then whole body PET/CT started within 30min. To manage any potential urinary output during data acquisition, an external urine collection device was applied for each patient before whole-body PET acquisition. Analysis of urinary tract activity and that of background were done besides the analysis of pathological tracer uptake.
Results: Forced diuresis (F+30) preceded by adequate hydration was efficient in eliminating any residual ^{18}F-Choline activity in all patients. A high image quality in the pelvic region was achieved especially in the prostatic bed. All patients tolerated the procedures and no data acquisition interruption was recorded. Fourteen (70%) patients had active tumor manifestations in the form of locally recurrent foci (n=6) that stood out clearly after discarding the residual urinary activity, regional lymph node metastases (n=22), and distant metastases (n=9). The mean SUVmax of these lesions were: 5.4 ±1.9, 8.8 ±4.2, and 10.2 ±5, respectively.
Conclusion: Forced diuresis (F+30) preceded by adequate hydration has the potential to successfully resolve the inherent ^{18}F-Choline contrast handicap in the lower urinary tract.

NSS201

Radiosynthesis and Biological Evaluation of a Novel Pyrazole-Based CB2 Radioligand designated [11C]RO6753361

A. Haider[1], A. Müller Herde[1], U. Grether[2], L. Gobbi[2], J. Fingerle[2], R. Schibli[3], S. Ametamey[1], L. Mu[1]; [1]Zurich/CH, [2]Basel/CH, [3]Villigen/CH

Purpose: Under physiological conditions, the abundancy of cannabinoid receptors type 2 (CB2) in the central nervous system (CNS) is considered very low to negligible. However, CB2 can be upregulated on activated microglia in patients suffering from different neurodegenerative diseases such as amyotrophic lateral sclerosis, multiple sclerosis, Parkinson's disease and Alzheimer's disease. Our aim is to develop a suitable brain tracer for non-invasive imaging of CB2 expression in patients with CNS diseases. Here we report the radiosynthesis and biological evaluation of a novel CB2 radioligand designated [^{11}C]RO6753361.
Methods and Materials: Radiosynthesis of [^{11}C]RO6753361 was successfully achieved using dry toluene as solvent. Autoradiography was performed with rodent brain and spleen tissue. Wistar rats and CD1 mice were used for the *in vivo* evaluation.
Results: Radiochemical yields ranged from 6.5 – 19.5 % (n=28, dc) with an excellent specific activity of > 500 GBq/µmol and a synthesis time of 40 minutes. Autoradiography revealed high binding in rodent spleen tissue. The binding was blocked by excess CB2 specific ligand GW405833, indicating specific binding of the radioligand towards CB2. Unlike the spleen, radioactivity accumulation in rodent brain tissue was not blocked by GW405833, thus confirming the very low to negligible CB2 expression level in healthy brain tissue. Upon injections of [^{11}C]RO6753361 into rats and mice, acquired PET scans showed tracer accumulation in the spleen. However, this uptake could neither be blocked nor displaced *in vivo*.
Conclusion: [^{11}C]RO6753361 is a selective CB2 tracer when tested *in vitro*. However, *in vivo* specificity could not be demonstrated probably due to stability issues.

NSS202

64Cu-Labeled Folate Radioconjugate for PET Imaging of Folate Receptor-Positive Tumors

R. Farkas, K. Siwowska, N. van der Meulen, R. Schibli, C. Mueller; Villigen-PSI/CH

Purpose: Folate radioconjugates are promising for imaging of folate receptor (FR)-positive tumors. The aim of this study was to develop an albumin-binding folate conjugate (RF42) with a NODAGA-chelator for labeling with ^{64}Cu (Eβ$^+$=278 keV, $T_{1/2}$ = 12.7 h). The ^{64}Cu-RF42 was investigated in vitro and in vivo.
Methods and Materials: ^{64}Cu was produced at the research cyclotron at PSI. RF42 was synthesized in eight steps in an overall yield of 5 %. The radioconjugate was prepared by incubation of RF42 with $^{64}CuCl_2$ in a mixture of HCl/Na-acetate (pH ~5.5) at 45°C for 15 min. FR-positive KB tumor cells were used for in vitro experiments. Biodistribution and PET imaging studies were performed with KB tumor-bearing nude mice.
Results: The radiochemical purity of ^{64}Cu-RF42 was >99% at a specific activity of 10 MBq/nmol. Cell internalization studies showed high and FR-specific uptake of ^{64}Cu-RF42. In vivo, high uptake of ^{64}Cu-RF42 was found in KB tumor xenografts (16.20 ± 3.58% IA/g, 24 h p.i.). Accumulation of ^{64}Cu-RF42 was also found in the kidneys resulting in a tumor-to-kidney ratio of 0.55 ± 0.11 at 24 h p.i. PET/CT imaging studies allowed excellent visualization of tumor xenografts up to 60 h after injection of ^{64}Cu-RF42.
Conclusion: ^{64}Cu-RF42 showed FR-specific tumor cell accumulation in vitro and in vivo. The half-life of ^{64}Cu is well suited to the enhanced circulation time of the novel albumin-binding conjugate RF42. Based on the excellent PET images obtained with ^{64}Cu-RF42, it may have the potential for future application in the clinics.

NSS203

68Ga-Labeled Neurotensin and Bombesin Analogs for Targeting Human Ductal Pancreatic Cancers and Glioblastoma

D. Viertl[1], J. Delage[1], F. Buchegger[1], R. Mansi[2], H. Maecke[3], D. Tourwe[4], N. Riggi[1], T. Stora[5], L. Bühler[5], J. Prior[1]; [1]Lausanne/CH, [2]Basel/CH, [3]Freiburg/DE, [4]Brussels/BE, [5]Geneva/CH

Purpose: Neurotensin and bombesin receptors are overexpressed in several cancers, such as pancreatic adenocarcinoma and glioblastoma. Biodistributions and microPET imaging of neurotensin and bombesin analogues radiolabeled with 68Ga were studied in mice bearing human pancreatic xenografts or an orthotropic glioblastoma.
Methods and Materials: MiaPaCa2 and Capan-2 human pancreatic cancer cells and MGH4 glioblastoma expressing neurotensin and bombesin receptors were grafted in SCID mice, either subcutaneously (MiaPaCa2+Capan-2) or orthotopically (MGH4). The neurotensin analogue DOTA-NT20.3-Ile and the bombesin-analogue (NODAGA-MJ9) were radiolabeled with generator-eluted ^{68}Ga. Mice were injected with 0.1-0.2µg of ^{68}Ga DOTA-NT20.3-Ile (n=12) or NODAGA-MJ9 (n=4) corresponding to 0.3–7MBq 90 minutes before biodistributions or microPET acquisitions.
Results: Labelling of DOTA-NT and NODAGA-MJ9 analogues with ^{68}Ga yielded radiotracers of high radiochemical purity (>95%). In MiaPaCa2 and Capan-2 cancer cells, 68Ga-DOTA-NT and ^{68}Ga-NODAGA-MJ9 specifically localized in tumours with an uptake of 3.3±1.6 and 4.2±1.2 %ID/g for ^{68}Ga-DOTA-NT20.3-Ile and ^{68}Ga-NODAGA-MJ9, respectively. Beside tumour uptake, ^{68}Ga-DOTA-NT20.3-Ile accumulated in the kidney and ^{68}Ga-NODAGA-MJ9 in the pancreas. Overall radiotracers accumulation was at least 3 times higher than in normal tissues. MicroPET imaging supported the biodistribution results with high tumour uptake and very-low unspecific binding 90 minutes *p.i.* The first microPET acquisitions in orthotopic MGH4 glioblastoma model showed a ^{68}Ga-NODAGA-MJ9 accumulation of 0.6±0.07 %ID/g at 90 minutes *p.i.*, leading to a tumour-to-normal-brain ratio of 3.
Conclusion: ^{68}Ga-DOTA-NT-Ile and 68Ga-NODAGA-MJ9 were specific for the two human pancreatic tumours studied with a good tumour-to-normal-tissue-ratio. Interestingly, a accumulation of ^{68}Ga-NODAGA-MJ9 in the orthotopic glioblastoma was observed. Those results warrants further study for peptide receptor targeted radiotherapy.

NSS204

The Use of 149Tb and 152Tb in Preclinical Investigations: Mass Separation and Subsequent Application for Imaging and Therapy

N. van der Meulen[1], C. Vermeulen[1], U. Koester[2], K. Johnston[3], S. Haller[1], A. Tuerler[4], R. Schibli[1], C. Mueller[1]; [1]Villigen/CH, [2]Grenoble/FR, [3]Geneva/CH, [4]Bern/CH

Purpose: Terbium is a unique element as it provides radionuclides suited for diagnostics and therapy in nuclear medicine. As part of the PSI-ISOLDE collaboration, we concentrated on the collection and purification of ^{149}Tb (α-emitter, $T_{1/2}$ = 4.1 h – for therapy) and ^{152}Tb (β$^+$-emitter, $T_{1/2}$ = 17.5 h – for PET).
Methods and Materials: Mass-separated beams of ^{149}Tb and ^{152}Tb, respectively, were implanted into Zn-coated Au foils. The irradiated foils were shipped to PSI for processing.
The Tb radionuclides were dissolved in HNO_3/NH_4NO_3, loaded onto a macroporous cation exchange resin and the Tb radionuclides eluted using dilute α-hydroxyisobutyric acid (α-HIBA). The product eluent was used directly for the radiolabeling process.
Healthy mice, without tumors, were injected with increasing activities to investigate kidney damage with ^{149}Tb-folate. DOTANOC and DOTA-RGD were also labeled with ^{152}Tb and injected into AR42J and U87MG tumor-bearing mice, which were imaged using a benchtop small-animal PET/CT scanner.
Results: The ^{149}Tb (~100 MBq) and ^{152}Tb (~500 MBq) were effectively separated from impurities, yielding a radionuclidically pure product. The product in question was successfully labeled to DOTANOC at a specific activity of 10 MBq/nmol. The ^{149}Tb-folate dose escalation study was conducted with six mice, while three untreated controls were injected with α-HIBA only.
Tumor visualization was readily achieved with ^{152}Tb-DOTANOC.
Conclusion: ^{149}Tb and ^{152}Tb were harvested successfully and its subsequent chemical separation from impurities performed reproducibly. The product was successfully labelled to a peptide and folate and injected into mice for imaging and long-term studies to determine kidney damage (^{149}Tb).

NSS205

Therapeutic Potential of 47Sc in Comparison to 177Lu and 90Y: Preclinical Investigations

K. Siwowska[1], K. Domnanich[1], U. Koester[2], B. Ponsard[3], R. Schibli[1], N. van der Meulen[1], C. Mueller[1]; [1]Villigen-PSI/CH, [2]Grenoble/FR, [3]Mol/BE

Purpose: Recently, the concept of theragnostic application (PET/β⁻-therapy) with the matched pair of Sc-nuclides (^{44}Sc/^{47}Sc) was proposed. The aim of this study, therefore, was to evaluate ^{47}Sc ($T_{1/2}$ = 3.35 d, Eβ⁻ = 162 keV, Eγ = 159 keV) for therapeutic purposes and compare it to the clinically-established radionuclides ^{177}Lu and ^{90}Y.
Methods and Materials: ^{47}Sc was produced by irradiation of a ^{46}Ca target at a reactor and separated by chromatographic methods, while ^{177}Lu and ^{90}Y were obtained from commercial suppliers. Radiolabeled DOTA-folate conjugates were used for in vitro experiments with folate receptor (FR)-positive IGROV-1 tumor cells and for in vivo therapy with tumor-bearing mice.
Results: Cell internalization studies showed FR-specific uptake of all folate radioconjugates. ^{47}Sc-folate was effective in killing tumor cells in vitro, as was the case for ^{177}Lu-folate and ^{90}Y-folate. The in vivo effect of ^{47}Sc-folate was significant and corresponded well with the deposited calculated tumor dose in comparison to ^{177}Lu-folate and ^{90}Y-folate. At activities that reduced tumor growth significantly, undesired side effects of ^{47}Sc-folate were not observed.
Conclusion: In vitro and in vivo studies confirmed a dose-dependent and FR-specific therapeutic efficacy of ^{47}Sc-folate. The shorter half-life of ^{47}Sc may be advantageous over ^{177}Lu in combination with small molecules, while its low β⁻-energy is clearly preferred to the β⁻-particles emitted by 90Y, which comprise a higher risk of undesired side effects to the kidneys and the bone marrow.

NSS206

Targeted Radionuclide Therapy with 161Tb: Investigation of Anti-Tumor Effects and Undesired Side Effects

C. Mueller[1], S. Haller[1], C. Vermeulen[1], U. Koester[2], G. Pellegrini[3], R. Schibli[1], N. van der Meulen[1]; [1]Villigen-PSI/CH, [2]Grenoble/FR, [3]Zurich/CH

Purpose: The radiolanthanide ^{161}Tb ($T_{1/2}$ = 6.89 d) emits β⁻-particles (Eβ⁻ = 154 keV) similar to ^{177}Lu, but also a significant number of Auger electrons (~12e⁻/decay). Herein, we investigated ^{161}Tb in combination with folate and somatostatin analogs in vitro and in vivo and compared the results to those obtained with the ^{177}Lu-labeled pendants.
Methods and Materials: A DOTA-folate conjugate was labeled with ^{161}Tb and ^{177}Lu and investigated in mice. The tumor sizes were measured and undesired side effects were monitored by determination of body weights and blood plasma parameters (BUN, creatinine), as well as histological investigation. DOTATOC and its analog, which comprises a nuclear localizing signal (DOTATOC-NLS), were labeled with ^{161}Tb (30 MBq/nmol) and investigated using AR42J rat tumor cells. Viability and survival assays were performed in vitro.
Results: Application of ^{161}Tb-folate (10 MBq) resulted in reduced tumor growth and. as a consequence. in an increased survival time (54 d) of mice compared to the effects of ^{177}Lu-folate (10 MBq, 35 d). ^{161}Tb-folate did not cause more renal damage than ^{177}Lu-folate, however. In vitro the fraction of ^{161}Tb-DOTATOC-NLS, which was targeted to the nucleus (~3%), was significantly higher than the fraction of ^{161}Tb-DOTATOC (<0.5%). AR42J cell killing after application of ^{161}Tb-DOTATOC-NLS was more effective (IC_{50} ~1.5 MBq/mL) than after treatment with 161Tb-DOTATOC (IC_{50} ~8 MBq/mL).
Conclusion: The emission of Auger electrons and β⁻-particles makes ^{161}Tb attractive for therapeutic purposes. The concept of targeting the cellular nucleus to profit from Auger electron emission of ^{161}Tb-labeled compounds warrants further investigations.

NSS301

New imaging agents – Bench to bedside: How to obtain the regulatory approval for non registered radiopharmaceuticals within Swiss small-scale radiopharmacies (ex. 68Ga-PSMA-617)

D. Judith, J. Prior, J. Caputo, N. Schaefer, M. Straub; Lausanne/CH

Purpose: Special authorizations provide one possibility to employ established, non-registered radiopharmaceutical products in Switzerland under condition that the product is registered at a foreign regulatory instance recognized by Swissmedic. To comply with the regulatory criteria if no foreign registration exists remains challenging. We aim to present a guide for the bench to bedside process through the regulatory affairs for novel theragnostics imaging agents in the example of 68Ga-PSMA-617 to image prostate cancer by PET/CT.
Methods and Materials: The labeling of 68Ga-PSMA-617 is done using a commercial GMP precursor (ABX-Nr.9934), synthesized by an automated synthesis module (Eckert & Ziegler-EC154). Test syntheses are produced and quality controls are performed complying with the general quality control criteria for radiopharmaceutical preparations of the European Pharmacopoeia.
Results: For the submission at the regulatory instance (Swissmedic), the producing radiopharmacy needs to possess an authorization for the fabrication. The production process has to be validated by a responsible person being a radiopharmacist (minimum requirement EANM certificate). A detailed report containing information on general indication, justification, safety, dosimetry, production process, quality control, results of test preparations and first existing images has to be prepared, a validation by the responsible person before submission is necessary.
Conclusion: Submitting a protocol for new radiopharmaceutical tracers remains a challenging, but feasible process. The Swiss authorities are actually revising and clarifying their legal requirements to obtain approval to introduce new imaging agents in nuclear medicine. With this general guideline we aim to facilitate this complicated process to make non registered, GMP peptides available for other small scale radiopharmacies.

NSS302

Assessment of Detectability and Quantification at Early Dynamic and Late Acquisitions with Ga-68-NODAGA-RGDyK PET/CT

A. A. van der Gucht, P. Mitsakis, A. Pomoni, M. Jreige, G. Allenbach, M. Nicod-Lalonde, N. Schaefer, J. Prior; Lausanne/CH

Purpose: Several preclinical and clinical studies have demonstrated that radiolabelled Arg-Gly-Asp (RGD) peptides and positron emission tomography (PET) allow non invasive monitoring of αvβ3 integrin expression, a molecular target involved in angiogenesis. We aimed at assessing respective value of early dynamic and late acquisitions with Ga-68-NODAGA-RGDyK PET/CT in terms of lesion detectability and quantification.
Methods and Materials: We consecutively included 11 patients (mean age=59.8±7y, n=3 women) followed at our center for gastric cancer (n=2), esophageal cancer (n=4), upper respiratory tract cancer (n=3), glioblastoma (n=1) and Diffuse Large B-Cell Lymphoma (n=1). Patients underwent a 10-min dynamic acquisition centred on the primary tumour after injecting 3.1±0.9MBq/kg of Ga-68-NODAGA-RGDyK. Whole-body PET/CT images were acquired at 1 h after injection (Discovery D690 TOF, GE Healthcare). SUVmax and target-to-background ratio (TBR, defined as the SUVmax of the lesion divided by the SUVmax of a region of interest drawn in nearby healthy tissue) were compared for both early (10-min) and late (60-min) acquisitions.
Results: Among the 11 primary tumours, NODAGA-RGD uptake was seen in 9/11 (82%) at early phase and in all cancers at late phase. The 2 primary cancers not seen at early phase were a gastric and a oesophageal cancer. Comparing early to late acquisitions, TBR increased significantly (1.4±0.6 vs. 2.5±1.2 vs., p=0.02), whereas SUVmax did not (3.4±1.0 vs. 4.1±1.6, p=0.28).
Conclusion: The late phase acquisition led to increased detectability and quantification compared to the early dynamic acquisition with Ga68-NODAGA-RGDyK PET/CT.

NSS303

In Vivo Stabilization of Radiolabelled Gastrin Analogues May Improve Peptide Receptor Radionuclide Therapy of Cholecystokinin 2 Receptor (CCK2) Positive Tumours

R. Mansi[1], A. Sauter[1], I. E. Valverde[1], U. Hassiepen[1], M. Behe[2], D. Wild[1], M. Fani[1]; [1]Basel/CH, [2]Villigen/CH

Purpose: Radiolabelled gastrin analogues are useful for the therapy and imaging of different tumours expressing CCK2, including medullary thyroid cancer. However, their quick degradation by proteases in vivo decreases their potential therapeutic efficacy. We aimed at improving their stability by co-administration of protease inhibitors.
Methods and Materials: *In vitro* stability against selected regulatory proteases was assessed for the minigastrin-based radiotracers ^{177}Lu-MG11 (^{177}Lu-DOTA-D-Glu-Ala-Tyr-Gly-Trp-Met-Asp-Phe-NH$_2$) and ^{177}Lu-PP-F11N (^{177}Lu-DOTA-(D-Glu)$_6$-Ala-Tyr-Gly-Trp-Nle-Asp-Phe-NH$_2$), a stabilized analogue that is currently in a clinical phase I/II study. Two protease inhibitors, phosphoramidon (PA) and thiorphan (TH), were then selected for co-administration. Their effect on the radiotracers' stability was evaluated in healthy mice. Biodistribution studies of ^{177}Lu-MG11 and ^{177}Lu-PP-F11N alone or in combination with the inhibitors were performed in A431-CCK2 xenografts 4h post injection (p.i.).
Results: ^{177}Lu-MG11 showed very low stability *in vivo* (<4% intact peptide in blood, 5 min p.i.) and was drastically stabilized in the presence of PA or TH (>70% and >90%, respectively). ^{177}Lu-PP-F11N was more stable *in vivo* (39% intact peptide, 5 min p.i.). The effect of PA or TH in combination with ^{177}Lu-PP-F11N was less profound (60% and 66%, respectively). Thanks to the improved stability, the tumour uptake of ^{177}Lu-MG11 increased by a factor of 6.6 (PA) or 4 (TH). Tumour uptake of ^{177}Lu-PP-F11N was increased by 1.5- and 1.3-fold, respectively.
Conclusion: The use of enzyme inhibitors impacts on the in vivo stability and tumour uptake of gastrin-based radiotracers. Drastic improvement can be achieved on the highly unstable radiotracers and moderate improvement on the "stabilized" ones.

NSS304

Somatostatin Receptor PET/CT with Radiolabelled Antagonist is Twice as Effective as the Agonist for Detecting Liver Metastases: Results of a Phase 1/2 Study Comparing 68Ga-OPS202 with 68Ga-DOTATOC PET/CT in Gastro-Entero-Pancreatic NET Patients

G. Nicolas[1], F. Kaul[1], N. Schreiter[2], J. Uiters[2], R. Mena[2], A. Bauman[1], H. Bouterfa[2], J. Rivier[3], J. C. Reubi[4], H. Maecke[5], R. Cathomas[6], E. Christ[4], M. Fani[1], D. Wild[1]; [1]Basel/CH, [2]Berlin/DE, [3]La Jolla/US, [4]Bern/CH, [5]Freiburg/DE, [6]Chur/CH

Purpose: ^{68}Ga-DOTATOC PET/CT is a reference method for imaging somatostatin receptor (sstr) expressing neuroendocrine tumors (NET). Presence and extent of liver metastases impact on patient management and prognosis. Our aim was to investigate safety and diagnostic accuracy of ^{68}Ga-OPS202, a radiolabelled sstr antagonist for PET/CT imaging of gastroenteropancreatic (GEP) NET (ClinicalTrials.gov NCT02162446).
Methods and Materials: Twelve metastatic G1/G2 GEP-NET patients were enrolled in a prospective phase 1/2 imaging study to investigate two single doses of ^{68}Ga-OPS202 (A: 15µg & B: 50µg) in comparison with ^{68}Ga-DOTATOC PET/CT. Scans were reviewed by 2 independent blinded readers. Follow-up imaging and biopsy were used as standard of reference.
Results: No adverse reaction to ^{68}Ga-OPS202 required treatment.Both ^{68}Ga-OPS202 doses showed lower uptake than ^{68}Ga-DOTATOC in the normal liver, the pancreas and the gastro-intestinal (GI) tract ($p<0.05$) and similar uptake in malignant lesions, thus significantly improving the image contrast: e.g. liver-lesions-to-normal-liver uptake ratios (mean±σ) were 5.7±6.9 (A)/6.0±7.4 (B) for ^{68}Ga-OPS202 vs 3.0±4.1 for ^{68}Ga-DOTATOC ($p<0.05$). A total of 102 lesions were detected with ^{68}Ga-DOTATOC vs 187 (A) and 221 (B) with the antagonist. Accuracy data will be presented.
Conclusion: ^{68}Ga-OPS202 is well tolerated, improves imaging contrast and tumor detection in the liver over ^{68}Ga-DOTATOC PET/CT. The lower GI and pancreatic uptake may increase the PET sensitivity and accuracy for detecting sites of primary tumour.

NSS305

Comparison of 68Ga-DOTA-TOC PET/CT and 18F-DOPA PET/CT in Metastatic Extra-Adrenal Paraganglioma Diesease

A. S. Kroiss[1], C. Uprimny[1], A. Frech[1], B. L. Shulkin[2], L. Gruber[1], C. Thomé[1], G. M. Sprinzl[3], G. Gastl[1], G. Fraedrich[1], I. Virgolini[1]; [1]Innsbruck/AT, [2]Memphis/US, [3]St Poelten/AT

Purpose: ^{18}F-DOPA PET offers high sensitivity in the imaging of nonmetastatic extra adrenal paragangliomas (PGLs) but lower sensitivity in metastatic disease. These tumors can be detected by ^{68}Ga-DOTA-TOC PET. We compared ^{68}Ga-DOTA-TOC and ^{18}F-DOPA PET/CT imaging for staging of malignant extra adrenal PGLs.
Methods and Materials: 2 men and 4 women (age range 22 to 60 years) with anatomical and/or histologically proven malignant extra adrenal PGLs were included. 2 female patients suffered from metastatic head and neck PGL disease, while the remaining 4 patients were diagnosed as extra adrenal multifocal PGL disease. The imaging results were analyzed on a per-patient and a per-lesion basis. The maximum standardized uptake value (SUV_{max}) of each functional imaging modality in concordant tumor lesions was measured.
Results: Compared with anatomical imaging,^{68}Ga-DOTA-TOC PET and ^{18}F-DOPA PET each had a per-patient detection rate of 100% in metastatic extra adrenal PGLs. However, the per-lesion detection rate of ^{68}Ga-DOTA-TOC was 100% (McNemar, P<1.0), and that of ^{18}F-DOPA PET was 59.3% (McNemar, P<0.001) in metastatic extra adrenal PGLs. Overall, ^{68}Ga-DOTA-TOC PET identified 28 lesions; anatomical imaging identified 27 lesions, and ^{18}F-DOPA PET identified 16 lesions. The SUV_{max} (mean +/- SD) of all concordant lesions was 31.4 +/- 22.3 for ^{68}Ga-DOTA-TOC PET and 9.2 +/ 9.0 for ^{18}F-DOPA PET (Mann Whitney U test, P<0.001).
Conclusion: ^{68}Ga-DOTA-TOC PET may be superior to ^{18}F-DOPA PET and even to diagnostic CT in providing valuable information for pretherapeutic staging of metastatic paraganglioma disease.

NSS306

Predictive Value of the 18FDG Baseline PET-Derived Quantitative Parameters in Diffuse Large B-Cell Lymphoma (DLBCL) Patients (ABREOC 08-002 Study)

L. Ceriani[1], T. Ruberto[1], L. Mazzucchelli[2], A. Moccia[1], F. Pavanello[1], E. Zucca[1], L. Giovanella[1]; [1]Bellinzona/CH, [2]Locarno/CH

Purpose: To assess the prognostic value of the main 18FDG PET-derived quantitative parameters, in a retrospective cohort of DLBCL patients uniformly treated with doxorubicin and rituximab-based regimen (R-CHOP).
Methods and Materials: Maximum Standard Uptake Value (SUVmax), metabolic tumor volume (MTV) and total lesion glycolysis (TLG) were measured baseline, following a standard protocol, in 82 DLBCL patients. Cut-off values of MTV, TLG and SUVmax were calculated using the Receiver Operating Characteristic (ROC) curve. Univariate and multivariate models were used to analyze their effect on the progression-free (PFS) and overall survival (OS).
Results: After a median follow-up of 4.2 years (interquartile range 2-6.1) the global 5-years PFS and OS rate were 71% and 73%, respectively. Among quantitative PET parameters only MTV and TLG predict OS but not PFS demonstrating high Negative Predictive (>0.85) but low Positive Predictive Value (<.41). The 5-year OS for patients with low TLG was 88% vs. 58% for those with high TLG (Log-rank test p<.008) and 86% vs. 62% for MTV values (p= .03). By multivariate analysis including also the main clinical parameters, TLG (p<.005) and MTV (p<.001) were shown, in separate models, to predict longer OS with the IPI score (p<.01).
Conclusion: Baseline wholebody metabolic tumor burden as measured on 18FDG PET images is a prognostic measure independent of the clinical factors and may be used to further risk stratify patients with DLBCL. Among the PET-derived functional parameters TLG and MTV demonstrated a similar prognostic power.

PO01

OHVIRA Syndrome – Clinical and Radiological Correlation Across the Ages

K. Lai, E. S. M. Hamouda, M. V. Fortier; Singapore/SG

Learning Objectives: After viewing this exhibit, readers would be able to:
- Understand the embryological underpinnings of OHVIRA syndrome
- Learn about its various clinical presentations
- Recognise OHVIRA syndrome and its variants in imaging studies
- Be aware of treatment options available

Background: Obstructed hemivagina and ipsilateral renal anomaly (OHVIRA) syndrome, or Herner-Werner-Wunderlich syndrome, is a rare urogenital anomaly.
It is thought to have an embryological basis in the Wolffian and Mullerian ducts. Abnormal development of a Wolffian duct causes anomalies in the ipsilateral kidney and structures arising from the ipsilateral Mullerian duct (namely the fallopian tubes, uterus, cervix and upper two thirds of the vagina).
Detection of OHVIRA syndrome is important as it is associated with pelvic inflammatory disease, infertility, obstetric complications, and acute urinary retention.
Resection of the vaginal septum decompresses the obstructed hemivagina.
Imaging Findings or Procedure Details: Uterine didelphys, ipsilateral hematometrocolpos and ipsilateral renal agenesis are the prototypical imaging findings.
Other possible findings include complications of infection such as pyosalpinx and tubo-ovarian complex, and other renal anomalies such as crossed-fused ectopia and cystic dysplasia.
OHVIRA syndrome can also be associated with other congenital abnormalities, such as VACTERL and ectopic insertion of the ureter. MRI is probably the best modality for demonstrating both OHVIRA syndrome as well any associated findings.
Conclusion: OHVIRA syndrome is a rare congenital urogenital anomaly with significant clinical consequences. Patients with ipsilateral renal agenesis or ipsilateral Mullerian duct abnormalities should be further investigated for the other companion anomaly.

PO02

Gadoxetic Acid (Primovist) – Enhanced MR Imaging for Characterization of Focal Liver Lesions Developed on Healthy Liver.

L. Paulatto[1], G. Brancatelli[2], M. Dioguardi-Burgio[2], M. Lagadec[3], R. Breguet[1], C. Hansen[1], S. Terraz[1], C. D. Becker[1], V. Vilgrain[4], M. Ronot[3]; [1]Geneva/CH, [2]Palermo/IT, [3]Paris/FR, [4]Clichy/FR

Learning Objectives: To understand the contribution of gadoxetic acid (GA) for differential diagnosis of benign hepatic lesions.
Background: GA is a hepatospecific contrast agent. After intravenous injection it is uptaken by hepatocytes. Aside from the classical dynamic phases, the exploration of the liver requires the acquisition of hepatocellular phase images (HP) on which functional hepatocytes show marked signal hyperintensity, while non-hepatocellular lesions and lesions containing impaired hepatocytes show hypointensity.
In the absence of chronic liver disease or malignancy, most focal liver lesions are benign. The most frequent are hemangiomas, focal nodular hyperplasia (FNH), and hepatocellular adenomas (HCA). The use of GA may help characterizing these lesions, but some pitfalls and limitations are to be known.
Imaging Findings or Procedure Details: Hemangiomas are characterized by a nodular enhancement with progressive centripetal filling. Due to the rapid uptake of GA by the surrounding liver parenchyma, this classical presentation is modified, most haemangiomas show a pseudo-wash out during the transitional phase and appear hypointense on the HP.
Most FNH show iso/hyperintensity on the HP, while the majority of HCA are hypointense. GA-enhanced-MRI has been shown highly accurate for the differentiation between FNH/HCA. Nevertheless, up to 50% of inflammatory/telangiectatic HCA show iso/hyperintensity and mimic the appearance of FNH. As a consequence, HCA subtyping as been shown to be less accurate with GA, when compared to extracellular contrast agents.
Conclusion: Radiologists should be aware of the modified appearance of haemangiomas on GA-enhanced-MRI to avoid misdiagnosis, especially with liver malignancies. GA may be helpful for the differentiation between FNH/HCA, but HCA subtyping may be difficult.

PO03

Pelvic Congestion Syndrom

B. Freiwald, R. Omidi, R. A. Kubik-Huch, C. L. Zollikofer; Baden/CH

Learning Objectives: To raise awarness and improve the understanding for this underdiagnosed but treatable condition and to learn how to evaluate and treat pelvic congestion syndrom (PCS).
Background: Chronic pelvic pain (CPP) is a common condition in women of reproductive age and ist defined as pain that has been present für 6 Month or more. The list of differential diagnosis for CPP includes urological and gastrointestinal pathologies, e.g. irritable bowel syndrom, psychosocial factors or gynacologic problems such as menstruation pains, hydrosalpinx, endometriosis, adenomyosis and adhesions. CPP with associated ovarian vein insufficiency is termed pelvic congestion syndrome (PCS), but it is important to acknowledge that only 10% of CPP present as PCS.
Imaging Findings or Procedure Details: Patients history and clinical examination as well as ultrasound (US) and computed tomography (CT) plays an important role to exclude differential diagnosis. Magnetic resonance imaging MRI of the abdomen including time-resolved MR angiography of the ovarian veins has become a mainstay for diagnosis. It allows to identify pathologies of the ovarian veins (the left side more commonly affected) and to depict the main vein that need to be treated and visualizes the pelvic anatomy.
Conclusion: For most patients, PCS is a treatable disease. This educational poster aims to highten awareness for this entity. The optimal MR imaging approach, diagnostic criteria to establish the correct diagnosis as well as treatment options will be discussed.

PO04

Errors in Abdominal Doppler Sonography

L. Trachsel, N. Kotalawala, M. Roux, R. A. Meuli, J.-Y. Meuwly; Lausanne/CH

Learning Objectives: The aim of this educational exhibit is to review the main causes of misdiagnosis in abdominal Doppler sonography and to propose solutions to avoid them.
Background: Sonography is a highly operator dependant imaging technique. Due to their important technical difficulties and complex images and Doppler spcectral curves interpretations, abdominal Doppler examinations are particularly subject to errors.
Imaging Findings or Procedure Details: Medical errors may be shared out in observer errors, interpretation errors, failure to suggest an appropriate subsequent procedure and failure to communicate.
From our daily activity, we have retrieved typical cases related to one or other cause of potential error. Examples cover the different indications to abdominal Doppler, from hepatic veins to renal arteries.
Conclusion: Observation errors are the main source of mistake in abdominal Doppler sonography. Next to Doppler analysis of the vessels, organ's morphology and topography have to be closely observed.
Strategies may be applied to reduce errors in abdominal Doppler sonography. They include continuous improvement in knowledge et regular review of misdiagnosis.

PO05

Pre-Operative Imaging Evaluation of Pancreatic Tumors: What the Surgeons Want to Know before Resection

M. Pregarz[1], R. de Robertis[1], M. D'onofrio[1], P. Pederzoli[2], P. Tinazzi Martini[2]; [1]Verona/IT, [2]Peschiera del Garda (Verona)/IT

Learning Objectives: The purpose of this exhibit is: 1. To combine thorough understanding of the technical aspects of pancreatic surgery with pre-operative imaging findings;2. To provide practical examples regarding imaging features that should be always evaluated before pancreatic resection (relationships with peri-pancreatic vessels, assessment of anatomical variants, prediction of pancreatic texture to prevent post-operative fistula, and assessment of feasibility of enucleation).
Background: Computed Tomography (CT) and Magnetic Resonance Imaging (MRI) criteria of resectability of pancreatic neoplasms are discussed.
Imaging Findings or Procedure Details: CT and MR studies of pancreatic lesions are presented.
Conclusion: Evaluation of vascular involvement (type of vessel, linear and circumferential involvement) to assess resectability and plan vascular resection;2. Description of anatomical variants (vascular, biliary, parenchymal and ductal) relevant for surgery;3. Prediction of pancreatic texture to stratify the risk of post-operative fistula;4. Assessment of enucleation feasibility.

PO06

PI-RADS Version 2.0: Practical Guide for Adequate Analysis and Reporting of Prostate MRI Examinations

M. Roux, M. Hauser, M. Valerio, R. A. Meuli, J.-Y. Meuwly; Lausanne/CH

Learning Objectives: The aim of this educational exhibit is to present the PI-RAD v. 2.0 and to explain, with practical examples, how to use it.
After viewing this educational exhibit, the reader should be able to correctly categorize prostate lesions identified on prostate MRI and adequately communicate with other professionals involved in prostate cancer treatment.
Background: PI-RADS lexicon has been developed in order to improve consensual communication between professionals dealing with prostate cancer. Used since 2012, version 1.0 has shown some limitations, particularly for detailed assessment of individual MRI sequences. Version 2.0 has been recently introduced, simplifying the process.
Imaging Findings or Procedure Details: The PI-RADS v. 2.0 needs the observation of T2w, DWI, ADC and DCE series of prostate MRI. We describe image acquisition, image analysis and the scoring process, using practical examples from our daily practice.
Conclusion: FDG-PET/CT allows for monitoring of PVGI and treatment response. It appears to be superior to blood biomarkers by suggesting alternative infectious sites impacting on therapeutic regimens.

PO07

PI-RADS Version 2.0: How Accurate Are You for a Proper Communication?

M. Hauser, M. Roux, M. Valerio, R. A. Meuli, J.-Y. Meuwly; Lausanne/CH

Learning Objectives: The aim of this educational exhibit is to provide the reader the opportunity to practice prostate MRI evaluation with PI-RADS v. 2.0 categorization.
After viewing this educational exhibit, the reader should be able to correctly categorize prostate lesions identified on prostate MRI and adequately communicate with other professionals involved in prostate cancer treatment.
Background: PI-RADS v. 2.0 is the new version of reporting categories for prostate MRI. It promotes standardization in image acquisition and interpretation, and aims at reducing variability. Nevertheless, prostate MRI interpretation and reporting entails a learning curve.
Imaging Findings or Procedure Details: The reader will be confronted with 30 cases of prostate MRI. For each case, T2w, DWI, ADC and DCE images of the same plan will be available. From these images, the reader should determine if a lesion is present, its location and PI-RADS v. 2.0 categorization. Immediate feedback will be supplied through an internet link.
Conclusion: The PI-RADS v. 2.0 systems is easy to use. The reporting physician needs training in order to become familiar with it.

PO08

Role of Diffusion MRI in Evaluating Liver Fibrosis

C. Ozturker[1], E. Karagoz[2], K. Kara[3], G. Sonmez[3], H. Mutlu[3]; [1]Canakkale/TR, [2]Van/TR, [3]Istanbul/TR

Purpose: Liver fibrosis is frequently seen in patients with chronic liver disease and responds positively to antifibrotic therapy, when detected in early stages. In routine daily practice, liver fibrosis is usually diagnosed by means of parenchymal biopsy but alternative non-invasive diagnostic methods are required. The aim of this study was to determine the apparent diffusion coefficient (ADC) values of liver fibrosis in diffusion MRI and investigate their role in detecting fibrosis.
Methods and Materials: In the study a total of 43 patients [31 chronic hepatitis B, 7 non-alcoholic steatohepatitis patients] were examined with 1.5 T, respiratory triggered DW-SS-EP MRI technique. (b value of 1000 s/mm^2). Patient's diagnosis were determined by means of histopathological evaluation. ADC values were measured in the lateral and medial segment of the left lobe, anterior and posterior segment of the right lobe. ISHAK score was used for pathologic grading of fibrosis.
Results: There was a significant difference between the ADC values of nonfibrotic and moderate-to-severe fibrotic liver of the patients. Also there was a significant difference between patients with mild fibrosis and patients with medium and advanced fibrosis. However, there were no significant differences between non fibrotic patients and patients with mild fibrosis. Also there were no statistically significant differences in terms of ADC values between patients with moderate and severe fibrosis.
Conclusion: The ADC values of moderate and severe fibrotic liver were found significantly lower compared to nonfibrotic and mild fibrotic liver of patients. Still, ADC values cannot take the place of percutaneous liver parenchymal biopsy.

PO09

Pelvic Artifacts in Material Decomposition Images from Dual Energy CT: A Phantom and Patient Study.

S. Winklhofer[1], J. Lambert[2], Y. Sun[2], J. Wang[2], B. Yeh[2]; [1]Zurich/CH, [2]San Francisco/US

Purpose: Aim of the study was to describe the frequency, appearance and severity of pelvic beam hardening artifacts
on material decomposition images from rapid-kV switching Dual-Energy Computed Tomography (rsDECT).
Methods and Materials: Monochromatic (70keV, 52keV, 120keV) and material decomposition images (iodine(-water), water(-iodine)) reconstructed from pelvic rsDECT scans of 41 patients (22 male, mean age 57±6 years, range 22-86 years) were retrospectively evaluated. We qualitatively analyzed the presence, type (hyperdense vs. hypodense) and severity of artifacts and the diagnostic capability of anatomic details (5-point scales). Quantitative measurements included CT numbers, iodine and water concentrations, grayscale values (GY), and standard deviations (SD) of the artifact-affected regions, compared with corresponding unaffected reference tissue. A pelvic phantom was constructed and scanned to validate the presence of artifacts. Wilcoxon signed-rank and paired t-tests were used to compare results between the different image reconstructions.
Results: Beam hardening artifacts were seen in all 41 patients in all datasets. The median artifact severity score was higher in water(-iodine) and iodine(-water) images (3, each) compared to 70keV (1), 52keV (2), and 120keV (1) (P<0.001, each). The diagnostic capability for pelvic organ depiction was lower (P<0.001) in water(-iodine) and iodine(-water) images compared to monochromatic images. Higher SD values of CT number, concentrations, and GY value were revealed for areas affected by artifacts compared to reference tissues in all data sets (each P<0.001). Similar results were seen in the phantom study.
Conclusion: Beam hardening artifacts are prevalent in pelvic material decomposition rsDECT images, show inverted high and low signal and should not be misinterpreted as disease in the pelvis.

PO10

Accessory Spleen versus Lymph Node: Added Value of Iodine Quantification with Dual-Energy Computed Tomography

S. Winklhofer[1], W.-C. Lin[2], J. Lambert[2], B. Yeh[2]; [1]Zurich/CH, [2]San Francisco/US

Purpose: To evaluate whether iodine quantification with Dual-Energy Computed Tomography (DECT) improves the differentiation of accessory spleens (AS) from lymph nodes (LN) compared to CT number measurements.
Methods and Materials: Abdominal DECT images of 75 patients with either AS (n=35) or LN (n=48) were retrospectively evaluated. CT numbers (Hounsfield Units [HU]) and iodine concentrations of AS, LN and the main spleen were measured. Receiver operating characteristics (ROC) were performed to calculate an optimal threshold for distinguishing AS from LN. Sensitivity, specificity, and accuracy were calculated for distinguishing AS from LN by iodine concentration measurements.
Results: Mean CT numbers and iodine concentrations were higher for AS (148±29 HU and 48.2±11x100 µg/cc) than LN (83±19 HU and 31.5±6.2x100 µg/cc, respectively, P<0.001 each). Mean CT numbers were lower for AS compared to the main spleen (161±29 HU, P<0.01), whereas mean iodine concentrations (47.7±10x100 µg/cc) were not significantly different (P=0.095). An iodine concentration greater than 38 x 100 µg/cc suggested AS with a sensitivity, specificity and accuracy of 91%, 85%, and 88%, respectively (Area under ROC curve 0.941).
Conclusion: Iodine measurements at DECT improve the differentiation of AS from LN. Iodine concentrations similar to that of the main spleen help confirm the diagnosis of AS.

PO11

Diagnostic Performance of Late-Phase Contrast Enhanced MRI of the Liver for the Distinction of Hemangiomas versus Metastases Using Gadoteridol or Gadoxetate Disodium.

O. Mühlebach[1], C. A. Binkert[1], J. Froehlich[2], O. Kolokythas[1]; [1]Winterthur/CH, [2]Zurich/CH

Purpose: To assess differentiation between hemangiomas and metastases comparing late-phase contrast enhanced-MRI (CE-MRI) images with either extracellular or hepatobiliary contrast agents.
Methods and Materials: 53 hemangiomas and 55 histopathologically verified metastases in 73 patients were included. Qualitative lesion assessment was done using typical imaging criteria on T2-, diffusion-weighted and dynamic CE-MRI. Quantitative enhancement analysis was evaluated on the delayed phase images by positioning standardized regions-of-interest inside the lesions, in adjacent hepatic parenchyma and in venous intrahepatic vessels of one slice. Two-tailed unpaired Student t-test was used to analyse differences of signal ratios, χ^2-test to assess the diagnostic performance of late-phase enhancement.
Results: With the extracellular agent gadoteridol (28 hemangiomas, 26 metastases) the signal intensities of hemangiomas, which were all hypointense, did not differ significantly from late-phase vascular enhancement (-92.2 +/- 157.3 SI, p=0.49), while metastases, which were mixed hypo- and hyperintense, showed a significant difference in their signal intensities towards vessels (-308.5 +/- 234.9 SI, p<0.05). Qualitatively the diagnosis could be confirmed in all 54 lesions (100%).
With the hepatobiliary agent gadoxetate disodium (25 hemangiomas, 29 metastases) the enhancement of hemangiomas, which were all hypointense, did not differ from intrahepatic vessels (-0.7 +/- 95.8 SI, p=0.99), neither did metastases, which were all hypointense compared to liver parenchyma (-56.0 +/- 76.1 SI, p=0.13). Qualitative diagnosis was possible in 7 lesions (12.9%).
Conclusion: Based on late-phase enhancement properties gadoteridol is superior to gadoxetate disodium in distinguishing hepatic hemangiomas from metastases. Quantitative analysis does not add further value to the characterization of the two entities in MRI.

PO12

The Role of Magnetic Resonance Cholangeopancreatography in the Investigation of Choledocholithiasis

D. Pathmajothy[1], S. Batra[1], M. Owen[2]; [1]London/UK, [2]Pembrokeshire/UK

Purpose: This study aimed to investigate whether MRCP could be used more selectively in patients being investigated for choledocholithiasis based on liver function tests (LFTs) and ultrasonography (USS) findings.
Methods and Materials: Consecutive MRCPs performed between 1/11/2014-31/10/2015 for suspected choledocholithiasis were studied. Association between clinico-pathological variables with choledocholithiasis on MRCP were determined using multivariate logistic regression.
Results: Of 131 patients included, choledocholithiasis was diagnosed in 40(30.5%). Mean bilirubin levels were significantly higher in patients with choledocholithiasis (49+/-6mmol/L) compared to those without (31+/-4mmol/L), p=0.027. The mean ALP tended to be higher in those with choledocholithiasis (229+/-16 IU) compared to those without (178+/-16 IU), p=0.065. The mean CBD diameter on USS was similar in those with choledocholithiasis (9.9mm+/-0.6mm) compared to those without (8.8+/-0.4mm), p=0.16. Using received operating characteristic analysis we found that bilirubin >20mmol/L was 78% sensitive and 59% specific, ALP >170 IU was 69% sensitive and 67% specific and CBD diameter on USS >8mm was 76% sensitive and 44% specific at detecting choledocholithiasis on MRCP.
The final multivariate model revealed bilirubin> 20mmol/L (OR: 8.1; 95% CI 2.9-22.9) and CBD diameter>8mm (OR: 2.9; 95% CI: 1.2-8.5) as significant predictors of CBD stone after adjusting for age and gender. The criteria requiring total bilirubin >20mmol and CBD diameter >8mm had sensitivity of 57% , positive predictive value of 57% , specificity of 83% and negative predictive value of 83%.
Conclusion: LFTs and USS criteria lack sensitivity and specificity to robustly select patients with suspected choledocholithiasis for MRCP.

PO13

Prostatic Fiducial Marker Placement and Recto-Prostatic Separation by Hydrogel Injection under Echographic Guidance: The Transperineal Pathway

T. de Perrot, M. Scheffler, T. Zilli, J.-P. Vallee; Geneva/CH

Purpose: Rectal toxicity following radiation therapy of prostate cancer can be reduced by increasing the distance between the prostate and the rectum. The aim of this study is to assess the technic of a transperineal pathway in order to place intraprostatic fiducial markers and perform recto-prostatic separation by gel instillation.
Methods and Materials: The radiology database was searched for patients adressed by the radiotherapy department for fiducial marker placement and recto-prostatic hydrodissection between January 2012 and November 2015. The reports were studied for immediate complications after the intervention, the best achieved distance between the rectum and the prostate in the median line, and the volume of injected gel spacer.
Results: All interventions were performed under local anesthesia in outpatients. 56 patients were retrieved (mean age = 72 years, range 56-81). Restylane (n=34) and space-OAR (n=20) were used as hydrogel spacers. In two cases (n=2), no gel was injected because of uneffective NaCl hydrodissection in locally advanced tumors (n=1) or because of technical reasons (n=1). The mean volume of injected gel was 6.7 ml (+/- 2.8 ml). The mean rectum-prostate separation distance was 8.8 mm (+/- 2.2 mm). In 39 patients, the fiducial markers were placed using a template grid, and in 17 patients without one. No early complications and no infection were reported.
Conclusion: Recto-prostatic separation by gel spacer injection and intraprostatic fiducial marker placement by the ultrasound-guided transperineal approach are safe procedures. Fiducial marker placement can be performed without the need of the classical template grid used in the transperineal ultrasound-guided procedure. (preliminary results).

PO14

Computed Tomographic Perfusion Imaging for Monitoring of Transarterial Chemoembolization Treatment of Hepatocellular Carcinoma

H. P. H. P. Marquez Masquiaran, H. Alkadhi, M. Fischer; Zurich/CH

Purpose: to prospectively monitor changes in tumor perfusion of hepatocellular carcinoma (HCC) in response to transarterial chemoembolization (TACE) using perfusion CT (P-CT).
Methods and Materials: 19 patients (mean age 69±6) undergoing P-CT before and directly after TACE treatment due to multifocal HCC were prospectively included in this dual center study. Two readers determined arterial-liver-perfusion (ALP, in mL/min/100mL), portal-liver-perfusion (PLP in mL/min/100mL) and hepatic-perfusion-index (HPI, in%) by placing circular regions of interest (ROI) covering the maximum diameter of each lesion (N=19) before and after TACE. Imaging follow-up with contrast-enhanced CT or MRI was used to distinguish responders (complete response/partial response) from non-responders (stable disease/progressive disease) following EASL criteria. Diagnostic performance of percentual changes in perfusion parameters before and after treatment (Δ) for early assessment of response was determined using receiver operating characteristics.
Results: Mean ALP, PLP and HPI were 36.5, 16.6 and 75.9 before and 11.9, 23.3 and 46.8 after TACE, resulting in a Δ ALP, PLP and HPI of -53%, 17% and -25%. Interreader agreement was fair to high for all perfusion parameters (ICC, 0.758–0.978). Before TACE, no significant correlations were found between perfusion parameters and treatment response (all $p>0.05$). After TACE, PLP significantly correlate with treatment response ($p<0.003$) showing a high accuracy identifying TACE non-responders (AUC 0.943, 95% confidence interval 0.808-1.000, $p<0.01$).
Conclusion: P-CT is useful for monitoring the effects of TACE in HCC patients. Decreased PLP after TACE has potential as a biomarker for tumor progression.

PO15

Assessment of Cytoreduction after Radiofrequency Ablation of Unresectable Pancreatic Adenocarcinoma: Correlation between Variation of CA 19.9 and Dimension of Necrosis at CT.

M. Pregarz[1], P. Tinazzi Martini[2], R. de Robertis[1], R. Girelli[2], A. Giardino[2], F. Scopelliti[2], M. D'onofrio[1]; [1]Verona/IT, [2]Peschiera del Garda (Verona)/IT

Purpose: To evaluate the correlation between variation of Ca 19.9 levels and dimensions of necrotic area at CT after radiofrequency ablation of unresectable pancreatic adenocarcinoma.
Methods and Materials: Patients with diagnosis of pancreatic ductal adenocarcinoma, expressing tumoral marker Ca 19.9, unresectable and not metastatic treated with RFA ablation procedure were included. CT study was performed one week after RFA. The dosage of Ca 19.9 levels was performed one month after RFA. Dimensions of necrosis at CT, expressed in percentage compared to the original lesion, were evaluated and compared by using T-test.
Results: 51 patients were included. After the procedure, Ca 19.9 levels reduced in 26/51 (51%), remained stable in 12/51 (24%) and increased in 13/51 (25%).Differences in the average percentage of necrotic area between the group with Ca 19.9 levels stable or reduced less than 30% and the group with Ca 19.9 reduced more than 30% was statistically significant ($p<0.05$). The average percentage of necrotic area in the group of Ca19.9 levels reduction of more than 30% was 43%.
Conclusion: Radiofrequency ablation of unresectable pancreatic adenocarcinoma induces cytoreduction as proved by the reduction of Ca 19.9 levels in 51% of the cases. The larger is the ablated area, the more is the decrease of Ca 19.9 levels in the subgroup of patients with post treatment tumoral marker reduction. To reach more than 30% reduction of Ca 19.9 levels an ablation area of 40% has to be obtained.

PO16

Brain Imaging Findings in Carbon Monoxide Poisoning

S. Kok, S. Kumar; Singapore/SG

Learning Objectives: Carbon monoxide poisoning is associated with a spectrum of imaging findings in the acute and delayed stages which are usually well characterized on CT and MRI imaging. In this poster, we review the imaging patterns of brain injury in several patients following carbon monoxide poisoning.
Background: Carbon monoxide poisoning usually presents as a deliberate suicide attempt or accidental poisoning due to poor ventilation in motor vehicles and in rooms with heating systems. Worldwide, it is a common and lethal cause of poisoning and can be associated with severe neurologic sequelae. Central to its underlying pathophysiology in the acute stage is the strong affinity for carbon monoxide (CO) with heme protein, 250 times that of oxygen (O2), resulting in the formation of carboxyhaemoglobin which consequently results in tissue hypoxia. Other studies have postulated that there is also brain lipid peroxidation and leukocyte-induced inflammatory damage, possibly accounting for the delayed imaging findings.
Imaging Findings or Procedure Details: We review the brain imaging findings of 4 patients and illustrate the various patterns of brain injury: diffuse hypoxic-ischemic encephalopathy, necrosis of the globus pallidus, basal ganglia abnormalities, diffuse brain atrophy and cerebral white matter demyelination.
Conclusion: Radiologists should be familiar with the brain imaging findings of carbon monoxide poisoning and the possible evolution of imaging features in the acute and delayed stages.

PO17

Neuroimaging of Acute and Chronic Unilateral and Bilateral Thalamic Lesions

C. Tuttle, J. Boto, A. M. Korchi, V. Zhekova, K.-O. Lovblad, M. I. Vargas; Geneva/CH

Learning Objectives: Our aim is to provide a comprehensive approach to the thalamus focusing on its anatomy, the main pathologies affecting this structure and their radiological semiology on CT and MRI. We will also illustrate the importance of multimodal MR imaging (morphologic sequences, diffusion tensor imaging, perfusion, spectroscopy) for the diagnosis and treatment of these conditions.
Background: The thalami are gray matter cerebral bilateral structures which participate in several functions such as relaying of sensory and motor signals, regulation of consciousness, sleep, and alertness. Pathologies affecting the thalamus can therefore cause a variety of symptoms, be unilateral or bilateral, and isolated or associated with involvement of neighboring structures.
Imaging Findings or Procedure Details: We will present the imaging findings of common pathologies affecting the thalamus illustrated by cases found in our daily practice. Thalamic lesions fall into different categories such as congenital (peroxisomal disorder, Fahr disease), vascular (arteriovenous malformation, ischemia, hemorrhage), metabolic (Wernicke's encephalopathy, Wilson disease), neoplastic (gliomas, metastasis), and infectious (Creutzfeld-Jacob disease, Behçet disease). We will also include cases with artefacts mimicking disease to illustrate potential pitfalls of brain MRI. Finally, we will address high-resolution imaging and new sequences, essential for surgical planning, such as for positioning electrodes in Parkinson disease.
Conclusion: Imaging, particularly multimodal MRI, plays a crucial role in the detection and characterization of thalamic lesions, as well as in the detailed analysis of this structure and its anatomical boundaries. Correct interpretation of imaging findings in the light of the clinical context is nevertheless essential for an accurate diagnosis and guiding therapeutic strategy.

PO18

A Case of Superficial Siderosis and Overview of the Literature.

R. Marasco, G. Iussich, J. Heinkel; Locarno/CH

Learning Objectives: SS represents a rare and under-recognized condition that must be considered in all patients with cerebellar syndrome of unknown cause.The aim of this poster is to present a rare case of SS and to review the related literature.
Background: Superficial siderosis (SS) is caused by chronic subarachnoid bleeding and is characterized by free iron and hemosiderin deposition along the pial and subpial structures of central nervous system. SS leads to progressive and irreversible CNS damage. The most common causes of chronic subarachnoidal bleeding are tumors, head and spinal cord trauma, arteriovenous malformations and aneurysms. SS is characterized by a clinical triad: sensorineural hearing loss, cerebellar ataxia and piramydal signs. Brain MR imaging is the investigation of choice for the diagnosis of SS.Typical findings include hypointensities seen on T2-weighted MR imaging around the brain, cerebellum, brain stem, spinal cord, VIII cranial nerve and atrophy of cerebellum and medulla.
Imaging Findings or Procedure Details: Brain MRI GRE sequence demonstrating linear hypointensity of signal within the superior cereberllar folie (tipical finding of SS).
Review of the similar cases in the literature.
Conclusion: SS is a rare disease and often misdiagnosed, therfore it is important to know the clinic of the disease and the related MRI findings because the early diagnosis of SS allowes therapeutic interventions that may prevent further progression of the disease.

PO19

Key Imaging Findings Regarding some Tumor of the Nasal Cavity

S. Durante, V. Dunet, R. A. Meuli, P. Hagmann; Lausanne/CH

Learning Objectives: Describe the key imaging findings regarding some tumor of the nasal cavity Elaborate differential diagnosis of lesions of the nasal cavity Correctly perform initial staging of malignant tumors
Background: Malignant tumors of the nasal cavity are rare (3% of upper airway cancer). Professional exposure or smoking is usually involved. Early symptoms and imaging signs are similar to rhinosinusitis and therefore neglected. Staging includes CT to determine size and local bony extent, MRI to evaluate soft tissue involvement and ^{18}F-FDG PET-CT to explore lymph nodes and metastasis.
Imaging Findings or Procedure Details: We present here relevant imaging findings in some of primary tumor like adenocarcinoma, rhabdomyosarcoma, squamous cell carcinoma, osteosarcoma and metastatic melanoma.
Conclusion: Characteristics of nasal mass are often unspecific and should be correlated with clinical history. The use of correct imaging modality and semiology can help differentiating primary tumor from metastasis and benign lesions.

PO20

Cerebral Infections and Immunodepression Outside of HIV

J. Forget, P. Maeder, P. Hagmann, R. A. Meuli; Lausanne/CH

Learning Objectives: To know the main aetiologies, the semiology and the pathogenicity of brain infections in immunosuppressed patients outside of HIV.
To know the adequate sequences to use with MRI and the limits of CT.
To know some challenging differential diagnosis than can mimic brain infections in immunosuppressed patients.
Background: Brain infections in immunosuppressed patients are mostly opportunist infections occuring also in HIV. Their prevalency increased dramatically in the last three decades with the treatment of oncologic diseases and transplantation development. In our series at CHUV, they occured after chemotherapy, corticotherapy, in diabetes, or organ transplant.
Imaging Findings or Procedure Details: The most frequent cerebral infections found in altered immunity are brain abscesses due to toxoplasmosis, aspergillosis, candidosis, cryptococcosis, nocardiosis, pyogenic germs, candidodis and tuberculosis. They may be identified with MRI by post-gadolinium annular enhancement, restricted diffusion, peripheral edema with T2 & FLAIR hypersignal, and central necrosis. Aspergillosis abscesses may present signs of bleeding found on SWI/T2* sequences or through spontaneous T1 hypersignal. Empyemas are less frequent but also occur in immunosuppressed patients. PML and PML-IRIS due to JC virus can be a challenging diagnosis. Such as in immunocompetent patients, some rare cases of encephalitis (VZV, HSV) have been observed.
Conclusion: Situations such as chemotherapy, organ transplant, metabolic diseases such as diabetes, may lead to brain infections, mainly brain abscesses. MRI is a sensitive exam and must include T2, FLAIR, Diffusion and post Gadolinium sequences. For better specificity, perfusion, spectroscopy and gradient echo sequences may be included. CT stays limited especially at the early stage of the disease.

PO21

3D Quantification of Basal Ganglia Susceptibility in Elderly Subjects: A Validation Study

V. Dunet[1], J. Deverdun[2], C. Charroud[2], E. Le Bars[2], F. Molino[2], C. Geny[2], N. Menjot de Champfleur[2]; [1]Lausanne/CH, [2]Montpellier/FR

Purpose: Quantitative susceptibility mapping (QSM) allows non-invasive quantification of iron deposition in the brain. We aimed at validating three-dimensional estimation of basal ganglia susceptibility and interobserver reproducibility in a elderly population.
Methods and Materials: Twenty-eight healthy elderly (aged>70 years) subjects (mean age 78±3y; range 71-87y, male: 20) prospectively underwent 3-T brain MRI including quantitative susceptibility maps obtained from 3D multi-echo spoiled gradient echo sequence. Volume-of-interest (VOIs) were manually delineated to obtain left and right basal ganglia (caudate nucleus, globus pallidus, putamen, substantia nigra, red and dentate nucleus) susceptibility values and compared to age/sex expected susceptibility values by Student t-test. For the ten first subjects (120 VOIs), VOIs were delineated twice to assess interobserver reproducibility by Lin test.
Results: In total, 336 VOIs values were obtained. Left and right basal ganglia had similar values (0.088±0.025 vs. 0.087±0.026 ppm, p=0.62). Observed basal ganglia susceptibility values were not statistically significantly different from age/sex expected susceptibility values except for globus pallidus (0.108±0.028 vs. 0.127±0.001 ppm, p=0.0012) and dentate nucleus (0.065±0.005 vs. 0.099±0.001ppm, p<0.0001), which displayed lower values than expected. Interobserver reproducibility was very good without systematic bias (Pearson's rho=0.974, rho-c=0.973, Cb=0.999).
Conclusion: Three-dimensional QSM is a reliable method to assess basal ganglia susceptibility values in elderly subjects.

PO22

Estimation of the Effect of Stenosis on Carotid and Intracranial Blood Flow Using Quantitative Magnetic Resonance Angiography

A. Sobieh[1], A. Hackbart[2], T.-K. Hauser[1], U. Klose[1]; [1]Tuebingen/DE, [2]Stuttgart/DE

Purpose: Determine influence of stenosis on blood flow and pattern of affection to enhance better diagnosing and grading stenosis using quantitative magnetic resonance angiography.
Methods and Materials: We constructed a flow phantom mimicking normal carotid and middle cerebral arteries made of 8 and 4 mm tubes connected in Y shaped form. 500 ml pulsatile flow at 60 beat/min was applied. One limb was patent while in other limb, different stenosis degrees were induced. We scanned orthogonal to flow direction with Phase contrast sequence. We scanned also 27 healthy subjects and 14 patients with stenosis subsequently.
Results: As the stenosis degree increased, flow showed a non linear behavior, flow remained stable up to 75% in 8 mm tubes while it was up 65% in 4 mm tubes then it declined with higher stenosis degrees. In-vivo, we calculated % flow between right and left arteries with range -11 to 11% in healthy subjects while in patients, it was more than 16% and varied according to stenosis degree. Patients suffered declined flow compared to that in healthy subjects.
Conclusion: QMRA is a potential non invasive tool for stenosis detection and grading allowing for adequate patient management and could be applied in stented arteries.

PO23

Quantitative Evaluation of Lateral Pterygoid Muscles in Patients with Temporomandibular Joint Disorders by Intravoxel Incoherent Motion MRI.

S. Ngamsom, S. Nakamura, J. Sakamoto, S. Kotaki, T. Kurabayashi; Tokyo/JP

Purpose: To quantitatively evaluate the changes of lateral pterygoid muscles (LPM) in patients with temporomandibular joint disorders (TMDs) using intravoxel incoherent motion (IVIM) parameters.
Methods and Materials: Twenty-six patients were included in this prospective study. After conventional MRI on closed- and open-mouth position, diffusion-weighted imaging using 8 b-values (0, 50, 100, 150, 200, 300, 400, 500s/mm^2) was performed (single-shot echo planar sequence, TR/TE/TI = 6800/72/250 ms). According to the conventional MRI findings, the disk position of 52 temporomadibular joints (TMJs) was classified into two: normal and anterior disk displacement (ADD). Then, on the diffusion-weighted images, regions of interest were drawn at the level of superior lateral pterygoid muscle (SLP) and inferior lateral pterygoid muscle (ILP) for the measurement of signal decay. To evaluate IVIM parameters indicating diffusion and perfusion, bi-exponential fittings based on the Levenberg-Marquardt algorithm were performed. Those parameters were compared with the conventional MRI findings. Statistical analysis was carried out using Student's t-test. All p values of < 0.05 were considered as statistically significant.
Results: Among 52 TMJs, 27 showed normal disk position, whereas 25 showed ADD. For ILP, both normal TMJs and TMJs with ADD showed similar f parameters (0.31±0.07 and 0.35±0.08, respectively). However, for SLP, f parameter in TMJs with ADD was significantly higher than that in normal TMJs (0.41±0.09 vs 0.33±0.08, p=0.002).
Conclusion: ADD of TMJ causes microvascular changes of LPM, which may be greater in SLP than in ILP. IVIM is considered useful for evaluating such changes quantitatively.

PO24

Contrast Enhancement in Multiple Sclerosis is Dependent on the MR Sequence Used - in Vitro and in Vivo Results

F. J. Ahlhelm[1], D. U. Müller-Pfister[1], S. Ulmer[2], J. M. Fröhlich[2], R. A. Kubik-Huch[1], M. Klarhoefer[3], M. Steinhauser[2], P. D. P. Sandor[1]; [1]Baden/CH, [2]Zurich/CH, [3]Basel/CH

Purpose: Multiple sclerosis (MS) is the most common inflammatory disease of the central nervous system. Magnetic resonance (MR) imaging with the use of gadolinium-based contrast agents (CM) has become the imaging modality of choice in the initial diagnosis of MS but also for therapy monitoring.
The purpose of this study was to compare the sensitivity for the depiction of a pathologic CM-uptake using 2D TSE and 3D GRE MR imaging in patients with MS at 1.5 T.
Methods and Materials: In-vitro MRI tests analysed different dilution series (n=15) of CM to control both for data consistency and differed only for the used Gadolinium contrast agents.
In 24 patients with a clinical diagnose of a relapsing-remitting MS MRI examinations including both GRE as well as TSE sequences for T1W imaging after CM application using a standard 20-channel head coil and standard single dose CM-administration were available.
Results: In-vitro tests demonstrated that depending on the CM concentrations the SNR varied among the sequences used.
In 11 MR examinations of MS patients pathologic CM-uptake was found. Altogether 14 lesions could be identified using the TSE technique. Only five of these lesions were also found using the GRE sequences.
Conclusion: For evaluation of contrast enhancement in MS patients both of these techniques should be considered.

PO25

More Precise Placement of External Ventricular Drainages by Combining CT-Planning and Angel-Guidance

F. A. Burn, M. Baumann, C. E. Eisenring, J. Beck, A. Raabe, M. Oertel; Bern/CH

Purpose: External ventricular drainages (EVD) placement is an important and common procedure to monitor and treat elevated intracranial pressure and pathological cerebrospinal fluid circulation. Nowadays up to 40% of conventionally inserted EVD are shown to be displaced on post-interventional imaging. Therefore, the authors developed a new implantation method based on MPR-CT dataset and angle-guided EVD insertion.
Methods and Materials: Pre-interventional CT images were used for planning. A trajectory from Kocher's point to the center of the ipsilateral ventricular frontal horn was determined according to the horizontal and vertical diameter. Intracranial length and the angle of the trajectory towards the midline were measured. A commercially available protractor App of a sterile packed smartphone was implemented to adjust and monitor the insertion angle.
Results: In total, 20 EVD were inserted successfully in an ex-vivo model within the ipsilateral ventricle by first attempt. We measured a mean tip-deviation from the ventricular center of 0.4 cm. The maximal deviation was 0.86 cm. With a mean duration of 7 min more, the procedure took only slightly longer than by conventional free-hand methods.
Conclusion: In summary combining CT- and angle-guidance based planning for EVD insertion results in higher precision, time-efficiency and less malpositions when compared to conventional freehand techniques. Future in vivo studies might help to further implement our method into clinical routine.

PO26

Imaging of Intracranial Tumors – First Experiences with GRASP Sequence at 1.5 T and 3.0 T

A. Bink, C. Stippich; Basel/CH

Purpose: Report on advantages with the Golden-angle Radial Sparse Parallel MRI sequence (GRASP) in patients with intracranial tumors. The GRASP sequence combines the techniques of compressed sensing and parallel imaging for rapid continuous acquisition with the advantages of flexible spatiotemporal resolution using the golden-angle radial sampling scheme.
Methods and Materials: The GRASP sequence was implemented on 5 MR scanners (Prisma, Skyra, Verio, Avanto and Espree, Siemens Medical Solutions, Erlangen, Germany). The parameters were: TR/TE 4.42/2.13 msec, image matrix 256 x 256 mm, voxel size 2.0 x 1.1 x 1.1 mm, temporal resolution 3.5 s, TA 4:07 min. Images were read by two neuroradiologists with respect to delineation of pathologies and artifacts. Data were compared to standard 3D MPRAGE post CE.
Results: 22 patients were retrospectively included. The reports were as follows: glioma (10x), lymphoma (1x), metastasis (3x), meningeoma (5x), vestibular schwannoma (3x). All pathologies were correctly detected by the readers. Image quality was judged at least comparable to standard 3D T1w images, especially the possibilities to see distribution of contrast media over time and measurement of enhancement pattern in all pathologies with additional high regional resolution was appreciated. Due to retrospective reconstructions from the continuously acquired data the arterial phase was never missed. No Pulsation artifacts occured.
Conclusion: With the GRASP sequence all intracranial tumors were well visible by simultaneously providing high temporal and high spatial resolution. In the future we want to add detailed perfusion postprocessing, in order to get anatomic and perfusion data with only one sequence which will reduce scanning time for patients.

PO27

Effect of Splenomegaly on Resistive İndex Values of Extrinsically Compressed Left Kidney

K. Yalçin-Şafak, A. Akça; İstanbul/TR

Purpose: The aim of our study was to prospectively evaluate the effect of splenomegaly on renal resistive index (RI) values and sphericity indices (long axis/short axis) of extrinsically compressed left kidney by using renal gray scale and Doppler ultrasonography (USG).
Methods and Materials: Fifty seven patients with splenomegaly with measurement of greater than 130 mm diameter in abdominal USG were studied. Patients right kidneys were accepted as control group. The bipolar lengths and transverse diameters of both kidneys in each patients were measured. Three Doppler waveform tracings were obtained from each kidney by sampling the interlobar arteries in the superior, middle, and inferior portions of the kidney. The difference of mean RI values and sphericity indices between two kidneys were compared.
Results: The average spleen diameter of the patients was 165.21 ± 29.45 mm. The mean RI of the compressed left kidney and contralateral right kidney were 0.61 ± 0.04 and 0.59 ± 0.04 respectively. The mean RI value of the left kidney is statistically higher than right kidney($p:0.001$; $p > 0.01$). The mean sphericity indices value of the left kidney is statistically higher than right kidney($p:0.001$; $p < 0.01$).
Conclusion: We conclude that the compression on left kidney due to splenomegaly can increase the RI value of the left kidney. During the renal Doppler examination, it should be remembered that the left kidney RI value could be significantly higher than the right kidney in patients with splenomegaly due to compression of splenomegaly.

PO28

Triple Rule-Out CT in the Emergency Department Patient – Should We Just Do It?

F. Morsbach, K. Higashigaito, D. Benz, R. M. M. Hinzpeter, H. Alkadhi; Zurich/CH

Purpose: To evaluate the frequency of further testing for coronary artery disease (CAD) in patients after receiving a chest CT for simultaneous aortic and pulmonary artery evaluation.
Methods and Materials: This retrospective study was conducted over a 3-year period including all patients that visited the emergency department of a 150'000 annual-visit European maximum care academic medical center. In the final patient population all patients were included that received CT testing for chest pain asking simultaneously for two or more of the following diagnoses: aortic dissection (AD), pulmonary embolism (PE) or CAD. Patients with CT testing for AD and PE were further evaluated whether they received further testing for coronary artery disease during their visit to the emergency department or up to 1 month after their initial visit.
Results: The final patient population included 229 patients. The majority were tested simultaneously for AD and PE (n=160, 60%), followed by AD, PE and CAD (n= 42, 18%). Patients receiving simultaneous testing for AD and PE received additional testing for CAD afterwards (n=54, 34%), most commonly coronary catheter angiography (n=31, 19%).
Conclusion: Most patients presenting at the emergency department with unclear chest pain commonly receive further testing for CAD after a chest CT for simultaneous evaluation of AD and PE. Evaluating patients for CAD routinely in cases of simultaneous testing for PE and AD is feasible and could reduce additional testing.

PO29

Intentional Assisted Recanalization of Challenging Chronic Total Occlusions Using a High Frequency Vibrational Device

S. D. Hajdu, C. Sotiriadis, A.-M. Jouannic, F. Glauser, S. D. Qanadli; Lausanne/CH

Purpose: Recanalization of challenging peripheral artery chronic total occlusions (CTOs) using an effective first line device could decreasing procedure time, radiation dose and injected contrast media. The use of a high frequency vibrational device, the Crosser, has been to used as a second line device in the recanalization of CTO when refractory to a standard guidewire. The aim of this retrospective study is to assess the safety and the efficacy of the Crosser as a first line treatment in CTO.
Methods and Materials: Fifty patients with proven CTO were treated with the Crosser as a first line device. Challenging CTO cases were defined as pre- or in-stent and/or heavily calcified occlusions. Patient demographics and risk factors were collected along with lesion characteristics. Crosser generator time, total fluoroscopy time, technical success and revascularization localisation were collected. Patients were followed-up for 12 months following recanalisation to assess complication and rule out restenosis.
Results: Patients included in our study exhibited the hallmark signs of peripheral artery disease with the majority moderate to severe claudicants. Among lesions, 20% and 10% were in- or pre-stent occlusions respectively. The mean recanalized length and time was 96 mm and 5 minutes respectively. The technical recanalisation success rate was 90% of which 80% were endoluminal. There were no adverse events related to the Crosser device. Clinical success was 91% and 85% at 3 and 12-months.
Conclusion: The Crosser is a safe and effective first line device in challenging CTOs decreasing time to angioplasty and stenting.

PO30

Cardiac Findings on Routine Non-Gated Computed Tomography in Comparison with Cardiac MRI

M. Cristallo Lacalamita[1], M. A. Scardapane[2], P. Q. R. Santini[1], G. Angelelli[2], R. Wyttenbach[1]; [1]Bellinzona/CH, [2]Bari/IT

Purpose: Cardiac evaluation is frequently neglected on chest and abdomen CT studies.
We aimed to evaluate cardiac anatomic features and pathologic findings on non-gated CT using cardiac MRI (CMR) as reference.
Methods and Materials: Out of 601 patients with CMR studies (2007-2014) 132 with concomitant non-gated CT were selected.
Two readers retrospectively analysed in consensus: chamber size potential anatomical pitfalls (crista terminalis, moderator band, left atrial appendage and papillary muscles) pathological findings (LHIS, non-compaction cardiomyopathy (CMP), ischemic CMP, endocavitary thrombus, masses and pericardial disease).
Results: Cardiac chamber measurements (mm) did not differ significantly ($p > 0.05$) for left atrium (CT: 38.8 ± 7.4 DS, CMR: 39.4 ± 7.7), right ventricle (CT: 38 ± 6.6, CMR: 39 ± 6.2) and right atrium (CT: 44.3 ± 6.8, CMR: 44.6 ± 6.1).
Frequency of visualization of potential anatomical pitfalls was relatively high in non-gated CT (81.8% papillary muscles, 76.5% moderator band, 61.4% crista terminalis, 53% left appendage).
Cardiac pathologies were recognized with good sensibility and high specificity compared to CMR: LHIS (1/132, 100% sensibility, 100% specificity) Non-compaction CMP (2/132, 66%, 100%) Ischemic CMP (LV wall thinning: 13/132, 65%, 100%; lipomatous metaplasia: 3/132, 100%, 99%; aneurysm: 1/132, 50%, 99%) Endocavitary thrombus (1/132, 100%, 100%) Masses (3/132, 100%, 100%) Pericardial disease (cyst: 2/132, 100%, 100%; thickening: 5/132, 83%,100%; effusion 13/132, 59%, 100%).
Conclusion: Even non-gated CT studies allow assessment of cardiac anatomy, dimensions and common cardiac pathologies emphasizing the importance of active search for cardiac findings.

PO31

Triple Rule out CT in Patients with Acute Chest Pain: Watch out the Myocardium

K. Higashigaito, F. Morsbach, D. Benz, R. M. M. Hinzpeter, S. Baumüller, H. Alkadhi; Zurich/CH

Purpose: To evaluate the frequency and significance of hypodense myocardium in emergency patients with acute chest pain referred to tripe rule out (TRO) computed tomography (CT).
Methods and Materials: TRO-CT examinations of 300 patients (mean age 59±17, 71% male) with acute chest pain referred between June 2012 and November 2015 were reviewed. Myocardium was assessed for presence of focal hypodense regions. Attenuation of hypodense myocardium in comparison with normal appearing myocardium were assessed. Furthermore, differences in attenuation between normal appearing and hypodense myocardium of patients with acute MI were compared to those with known old MI. Patient histories were reviewed for cardiovascular risk factors, known previous old myocardial infarction (MI), and final diagnosis causing acute chest pain.
Results: Hypodense myocardium was identified in 30/300 patients (10%). Mean difference of attenuation between normal appearing and hypodense myocardium was 66±38 HU. In 17/30 patients (57%) with hypodense myocardium, final diagnosis was acute MI; in 13/30 patients (43%) previous old MI was found in the patients' history. Mean differences of attenuation between healthy and hypodense myocardium were significantly smaller in patients with acute MI (55±20 HU) as compared to those with old MI (87±49 HU), ($p=0.033$).
Conclusion: Hypodense myocardium is encountered in TRO-CT in a relevant number of patients and allows for the diagnosis of acute MI. Differences in attenuation between normal appearing and hypodense myocardium allows distinguishing acute from old MI.

PO32

Triage CT (Triple rule out): The Plenty and the Pearls

G. Bodendörfer[1], J. Burnand[1], H. Bänziger[1], T. Wantz[2], Y. Agrebi[1]; [1]Riaz/CH, [2]Magnedens/CH

Purpose: Our study concerrns plausibility, feasibility, and results of triage CT in a peripheral hospital setting while maintaining acceptably low radiation dose and reliable results.
Methods and Materials: We examined 311 non-selected patients (178 male, 133 female) with suspicious or equivocal clinical findings, predominantly in an emergency setting by ecg-gated whole-chest computed tomography from november 2011 to december 2015. Age was below 50 years in 41 patients, 50-70 in 130, 70-80 in 86 and 54 beyond (range 15-96 years).
Patients were examined at a 256-slice Scanner (Philips I-CT) in a step & shoot protocol at 100 (80) or 120 kV, at 70-78% or 40% cardiac cycle prospective gating.
Results: X-Ray dose could be kept reasonably low < 3mSv or less in the < 100kV whole thoracic exams.
There was a minor increas of i.v.contrast <20ml and time - 10 min preparation- and <30min reading-time.
About 1/3 of exams showed no pathology, yielded pulmonary disease (embolism & else) or vascular disease, (mostly coronary, few aortic). Some peculiar findings of the "3 classics" and some more rare ore otherwise non-detectable pathologies are described (arteriitis, valvular disease, bronchocoronary arterial fistula).
Conclusion: ECG-gated Triage CT is feasable in a peripheral setting (community hospital) with good stability and acceptable radiation dose.
The technique grants early recognition of pulmonary, aortic or cardiovascular disease with emergency transfers for surgery or coronary intervention while necessary.
It allows for the recognition of previously undetected pathologies.
I offers new challenges and opportunities for the radiology team.

PO33

The Most Common Idiopathic Interstitial Pneumonias: What the Radiologist Should Know.

P. Douek, L. Crivelli, S. Grosfilley, S. D. Hajdu, R. Lazor, I. Letovanec, C. Beigelman; Lausanne/CH

Learning Objectives: To review the typical computed tomography (CT) findings of the most common idiopathic interstitial pneumonias (IPPs) along with their histological correlation highlighting their potential pitfalls.
Background: The final diagnosis of idiopathic pulmonary fibrosis (IPF) and idiopathic nonspecific interstitial pneumonia (NSIP), the most common forms of major IIPs, are based on typical CT and/or histological patterns. Secondary causes must be excluded such as drug toxicity, inhalation exposure, connective tissue disease and hypersensitivity pneumonitis as well as esophageal dilatation and pleural plaques by clinicians and radiologists respectively.
Imaging Findings or Procedure Details: Subpleural honeycombing and reticulations of basal predominance with or without traction bronchiectasis in the absence of features listed as inconsistent with usual interstitial pneumonia (UIP) allow a definite diagnosis of UIP.
Subpleural and basal predominance of reticulations without features listed as inconsistent with UIP pattern suggest a possible UIP pattern.
Any of the following six features are inconsistent with UIP pattern: upper or mid-lung predominance, peribronchovascular predominance, extensive ground glass abnormality, profuse micronodules, discrete cysts, diffuse mosaic attenuation/air-trapping, and consolidation in bronchopulmonary segment(s)/lobe(s).
The most frequent CT findings of NSIP are ground-glass opacities with reticulations in a basal and subpleural distribution, or a lower lobe peribronchovascular predominance with subpleural sparing, and varying degrees of distorted bronchiectasis and bronchiectasis. Potential pitfalls will be emphasized.
Conclusion: An accurate diagnosis of UIP is of utmost importance because it may avoid surgical biopsy and help guide a specific therapeutic approach. Potential pitfalls must be known.

PO34

Acute Complications after Lung Transplantation: Radiologic-Pathologic Correlation

C. I. Habre, A.-L. Hachulla, J. Gariani, S. Martin, L. Lucker, F. Lador, J.-C. Pache, C. D. Becker, P. Gasche, X. Montet; Geneva/CH

Learning Objectives: To recognize acute complications following lung transplantation on chest CT scan confirmed by pathology obtained by transbronchial biopsy or broncho-alveolar lavage.
Background: Increasing lung transplantations for end-stage pulmonary diseases prompt regular assessment of patients by CT scan for graft dysfunction. Acute pathologies may induce non-specific clinical signs regardless of their origin. Radiologists should be aware of specific signs and their delay of occurrence to improve medical management and bronchoscopic procedures..
Imaging Findings or Procedure Details: Acute complications following lung transplantation correlated to pathology could be classified as:
Infections – Gram-negative bacilli, such as Pseudomonas aeruginosa, may manifest as disseminated patchy consolidations and centrilobular nodules. Angioinvasive aspergillosis typically demonstrates solid nodules and ground glass halo sign. Cytomegalovirus pneumonia may be suggested by consolidation or ground glass opacities and reticular interstitial pattern.
Alloimmune responses – Acute rejection episodes are recurrent and should be emphasized with new or persistent pleural effusions, lung volume loss and septal thickening. Chronic rejection occurs in half of patients as constrictive bronchiolitis with typical air-trapping on expiratory chest CT scan.
Post-surgical issues – Acute graft dysfunction is transient and appears as pulmonary oedema of noncardiogenic origin. Vascular complications may involve pulmonary artery stenosis with right ventricule or pulmonary dilatation and decreased perfusion of the ipsilateral lung. Bronchial anastomosis dehiscence manifests as focal parietal defect, adjacent air collection and persistent pneumothorax.
Conclusion: Chest CT scan is an important tool in the follow-up of lung transplantation allowing the identification of complications and aiding in the guidance of transbronchial biopsies and broncho-alveolar lavage for pathologic diagnosis.

PO35

Systemic Air Embolism During Transthoracal Biopsies: Risk Factors and Preventive Measures

R. Rehwald, J. Petersen, M. C. Freund, E. Schönherr, M. Haslauer, A. E. Grams, A. Loizides, B. Glodny; Innsbruck/AT

Purpose: Systemic air embolism (SAE) is a rare, but feared complication of transthoracic biopsy (TTB) with potentially fatal consequences. The aim of the study was to assess the effect of positioning measures to prevent SAE.
Methods and Materials: A comparison was made between a group of 610 patients who underwent transthoracic biopsies before and a group of 1258 patients who were biopsied after the implementation of measures to prevent SAE during TTB.
Results: TTB in an ipsilateral dependent position reduced the rate of SAE from 3.8% to 0.16% (odds ratio 24.61; - 91.3%; $p < 0.0001$), and the rate of pneumothorax from 15.4% to 6.1% (OR 2.833; -19.15%; $p < 0.0001$). Logistic regression analyses identified needle penetration depth, prone position, height above the level of the left atrium, needle path through ventilated lung, and intubation anaesthesia as independent risk factors for SAE ($p < 0.05$). Propensity score matched analyses identified the number of biopsies as an additional risk factor ($p = 0.003$).
Conclusion: To prevent SAE, patients should be placed in an ipsilateral dependent position so that the lesion is located below the level of the left atrium. Needle path through ventilated lung and intubation anaesthesia should be avoided whenever possible.

PO36

Influence of Model Based Iterative Reconstruction Algorithm on Image Quality of Multiplanar Reformations in Reduced Dose Chest CT

H. Barras[1], V. Dunet[1], A.-L. Hachulla[2], C. Beigelman[1]; [1]Lausanne/CH, [2]Geneva/CH

Purpose: To evaluate the influence on image quality (IQ) of Model-Based-Iterative-Reconstruction (MBIR) on native, minimal Intensity Projection (mIP), Maximal Intensity Projection (MIP) axial and coronal reformats of reduced dose computed tomography (RD-CT) chest acquisition.
Methods and Materials: Raw data of 50 patients, who underwent a standard dose CT (SD-CT) and a follow-up RD-CT with a CT Dose Index (CTDI) of 2-3 mGy, were reconstructed by MBIR and FBP. Native slices, 4-mm-thick MIP and 3-mm-thick mIP axial and coronal reformats were generated. The relative IQ, subjective IQ, image noise and number of artefacts were determined in order to compare different reconstructions of RD-CT with reference SD-CT.
Results: The lowest noise was observed with MBIR. RD-CT reconstructed by MBIR exhibited the best relative and subjective IQ on coronal view regardless of the post-processing tool. MBIR generated the lowest rate of artefacts on coronal mIP/MIP reformats and the highest one on axial reformats, mainly represented by distortions and stairsteps artefacts.
Conclusion: MBIR algorithm reduces the image noise but generates more artefacts than FBP reconstruction on axial views of RD-CT with mIP and MIP post-processing techniques. Conversely, it significantly improves the IQ on coronal views, without increasing artefacts, regardless of the reformation type.

PO37

Dual Energy CT Pulmonary Angiography with 15 ml Contrast Media – a Propensity Score-Matched Study

A. Meier, K. Higashigaito, K. Martini, M. Wurnig, B. Seifert, D. Keller Lang, T. Frauenfelder, H. Alkadhi; Zurich/CH

Purpose: To evaluate the performance of low contrast media (CM) dose computed tomography pulmonary angiography (CTPA) using dual-energy with advanced monoenergetic reconstructions in patients with suspicion of pulmonary embolism (PE).
Methods and Materials: The study had local ethics committee approval; all patients gave written informed consent. Sixty-five patients undergoing low CM dose (15ml,400mg/ml,6g iodine) CTPA with advanced monoenergetic reconstructions were matched via propensity-scoring based on logistic regression analysis with 75 patients undergoing standard CM dose (80ml,300mg/ml,24g iodine) CTPA. Both subjective (noise, artifacts) and objective (contrast-to-noise ratio (CNR)) image quality was assessed by two blinded, independent readers. All patients underwent clinical three month follow-up for evaluation of adverse events.
Results: CTPA was diagnostic in 76/83 patients (92%) in the standard CM and in 65/82 patients (79%) in the low CM dose group. Interrater agreement for subjective image quality ranged from fair to excellent (ICC:0.456-0.84) for both groups. There was no significance between the low and the standard CM dose subgroup (p=0.153-1.0). Interrater agreement for objective image quality was excellent (ICC:0.833-0.930). Central CNRs were lower in the low CM dose group, but overall there was no significant difference between groups (p=0.11-0.86). Seven patients (17%) in the low CM and five patients (12%) in the standard CM dose group were diagnosed with PE. No patient suffered from subsequent PE or PE-associated death during follow-up.
Conclusion: With optimal CM bolus timing, CTPA with dual-energy and advanced monoenergetic reconstruction is feasible for safe exclusion and diagnosis of PE with 6g iodine.

PO38

Service Management in a Radiological Department with the ServiceBlueprint Model

M. Maurer; Bern/CH

Learning Objectives: To describe the ServiceBlueprint model as a suitable method of service management in the routine clinical setting of a radiological department.
Background: ServiceBlueprinting is a concept for the analysis, visualization, and optimization of service processes. To investigate whether the model will also provide a suitable representation of medical services, particularly the provision of radiological services, a ServiceBlueprint was created for the imaging modality of computed tomography.
Imaging Findings or Procedure Details: The ServiceBlueprint provided an analysis of the status quo of the service process in CT imaging. Weak points in the processes thus became immediately apparent. The model could also be used for personnel management in that it helped to define the roles of staff members from different categories in the value-added process. It served as a basis for the implementation of quality management systems according to Total Quality Management (TQM) and DIN-EN-ISO-9001:2000.
Conclusion: The ServiceBlueprint model is a service management concept that has a multifarious potential in process optimization, implementation of quality management systems, and human resources management. The use of the ServiceBlueprints model is benefical in the routine clinical setting of a radiological department to visualize and improve examination processes.

PO39

Does a Dose Monitoring Software in Computed Tomography Increase Technologists' Dose Awareness?

C. Heilmaier, N. Zuber, B. Bruijns, D. Weishaupt; Zurich/CH

Purpose: A reasonable dose management is increasingly important. The purpose of the study was to determine whether a dose monitoring software in computed tomography (CT) increases technologists' dose awareness.
Methods and Materials: Dose data of two CTs was collected from April 2014 to February 2015. (period 1: April to June 2014; period 2: July 2014 to February 2015). In period 1, the software ran in the background; in period 2, technologists were advised to read dose data after each scan and to answer dose alerts, indicating that dose exceeded predefined thresholds.
Results: A total of 13,217 scans were conducted (period 1, n=4,943; period 2, n=8883) and a total of 609 alerts occurred (period 1, n=293; period 2, n=316), leading to a mean alert quota of 5%. Comparison of both periods showed a significant decrease of mean alert quota in period 2 (4%; period 1,6%; p<0.001). Decline was mainly caused by a reduced number of notifications due to patient miscentering (period 1, n=129; period 2, n=77; p<0.001), which means patient was not positioned properly in the isocenter of the scanner. Contrary to that, number of overweight alerts (BMI≥25 kg/m^2) significantly grew in period 2 (51%, n=160; period 1,36%. n=106; p<0.001). All other alert causes (e.g. scan repetition due to motion artifacts) were comparable in both periods (p>0.05).
Conclusion: A dose monitoring software in CT increases technologists' dose awareness and leads to a reduced number of alerts due to human error.

PO40

The Diagnosis "Iodine Allergy" is a Risk Factor for Adverse Events under Clinical Routine Conditions

I. Böhm, P. Silva Hasembank Keller, K. Nairz, J. T. Heverhagen; Bern/CH

Purpose: To test the hypothesis that the diagnosis "iodine-allergy" is a risk factor for the acquisition of adverse events (AEs) under radiological routine conditions.
Methods and Materials: We retrospectively screened the RIS-database of 300 patients for a history of "iodine-allergy". We tried to identify the meaning, the clinical AE-symptoms, the radiological consequences, and analyzed potential risks/AEs that probably followed the prophylactic actions. We compared the "iodine-allergy" group with two age- and sex-matched groups: firstly, 230 patients with unspecific "iodine-contrast-medium-(ICM)-allergy", and secondly, 70 patients with a clearly stated culprit ICM-allergy. The study was done in accordance with IRB-policy.
Results: The term "iodine-allergy" remained unexplained in 84%. In this group the clinical symptoms of previous AEs were not documented in most cases. This was in contrast to the other groups (p<0.0001), where the reports were detailed. AEs/adverse drug reactions (ADR) after special management tasks occurred in 9 patients with "iodine-allergy", in only one patient with an ICM-diagnosis, and in none of the exactly diagnosed group. There was a clear correlation between the quality of diagnosis and the occurrence of AEs/ADRs: r=0.982 (p<0.001).
Conclusion: The data confirmed the hypothesis that the diagnosis "iodine-allergy" is dangerous, fuzzy, leads to uncertainty in the clinical management, and sometimes to ineffective prophylactic measurements. Therefore, we recommend to replace it by exact terms such as ICM-allergy or, even better, naming the exact allergen. This is not an academic sophistry, but essential in every-day-radiological-routine practice to better understand the reaction, to adequately manage the patient, and thereby to facilitate a safe ICM-application.

PO41

Swiss Survey on Imaging Algorithms in Polytrauma Patients

R. M. M. Hinzpeter[1], T. Böhm[2], D. T. Boll[3], C. Constantin[4], F. Del Grande[5], M. D. M. V. Fretz[6], S. Leschka[7], T. Ohletz[8], D. Ott[9], S. Schmidt[10], T. Treumann[11], P.-A. Poletti[12], H. Alkadhi[1]; [1]Zurich/CH, [2]Chur/CH, [3]Basel/CH, [4]Sion/CH, [5]Lugano/CH, [6]Winterthur/CH, [7]St. Gallen/CH, [8]Aarau/CH, [9]Bern/CH, [10]Lausanne/CH, [11]Luzern/CH, [12]Geneva/CH

Purpose: To identify the imaging algorithms, indications for imaging, whole body computed tomography (WBCT) protocols and associated radiation doses in Switzerland.
Methods and Materials: An online survey with 25 multiple choice questions or free text responses was sent to the 12 authorized centers for polytrauma patients (according to the HSM directive) in Switzerland.
Results: Responding hospitals indicated that they have internal standardized imaging algorithms regarding the radiologic work-up of polytrauma patients. WBCT was used in each trauma center, with more centers performing WBCT after focused assessment with sonography in trauma (FAST) and/or conventional radiography. A minority of trauma centers perform WBCT as initial imaging test without foregoing FAST and/or conventional radiography. The most common indications for WBCT were based upon mechanism of trauma, abnormal vital signs, and presence of multiple injuries. Regarding the variety of scanning protocols, the majority of trauma centers performed arterial and venous phase in split-bolus technique. Position of the arms was basically either on the patient`s body during the whole scan or down when scanning the head and up when scanning the torso. Associated radiation doses (dose length product) ranged between 1268 and 3988 mGy x cm per WBCT examination.
Conclusion: Imaging algorithms in polytrauma patients are standardized within but vary across trauma centers in Switzerland, similar to the individual WBCT protocols and associated radiation doses.

PO42

Vascular Closure Devices: When, How and Which One?

L. Crivelli, P. Douek, S. D. Hajdu, C. Sotiriadis, F. Doenz, S. D. Qanadli; Lausanne/CH

Learning Objectives: Explore and compare the different vascular closure devices (VCD) in routine interventional radiology.
Background: Patients treated with anticoagulation and antiplatelet therapy, which benefit from routine endovascular procedures, have a high risk of hematoma and pseudo-aneurysm when using manual compression following intra-arterial procedures. VCDs have proven to be effective in decreasing complications. However, their use in routine practice among low risk patients remains controversial.
Imaging Findings or Procedure Details: In the past decade, VCDs have decreased the time of hemostasis and complication rate when compared to manual compression of access sites after percutaneous vascular interventions when using large caliber sheaths. Currently, VCDs have similar complication rates ranging from 1.5-9% and can be classified into compression assisted, topical hemostasis and active closure devices. Active VCDs are further categorized into three major groups: suture-based, collagen-based and non-collagen-based bioabsorbable. The myriad of VCDs currently available, their risks and benefits will be presented.
Conclusion: On average, 30%-50% of all catheter based procedures performed use a VCD to establish hemostasis. These devices are all safe, effective, and have been demonstrated to significantly decrease the time to hemostasis and complications. Emerging techniques continue to reduce the risks of related complications and it enables the use of VCDs routinely for interventional radiology. The choice of device depends on their availability, operator preferences, puncture size and the possibility of repeat arterial access.

PO43

Endovascular Treatment of Glomus Tumors

S. R. Stojanović, P. D. D. Stojanov, M. S. D. S. Ristić; Niš/RS

Learning Objectives: Paragangiomas (glomus tumors) are benign neoplasms richly vascularised, contain neurosecretory granules that are the part of the symphetic nervous system, the autonomic nervous system.
Objective present the importance of endovascular treatment as acceptable safe and effective method for the treatment of paragangliomas in the preoperative course.
Background: Three patients with symptoms, painless sweeling in the neck, retromandibular, sensorineural hearing loss, vertigo disorders and problems with speech were initially reffered for neck and head MDCT (Toshiba Aquilion 64s) and MRI (Siemens Avanto 1,5T).
Imaging Findings or Procedure Details: Changes in the level of the left temporal bone pyramid, jugular foramen and CCA bifurcation were observed by MDCT/MRI characteristic correspond paraganglioma. All patients underwent bilateral carotid angiography. Cerebral angiography and selective catheterization detected a distinct and very rich pathological vascularization within the lesions, of primarily by type glomus tumor. In the same act supraselective catheterization and embolization of tumor feeder (BeadBlock sizes 500 - 700µm) was performed. Control angiography after embolization shows that are extensively tumor masses war excluded from circulation, with minimal "blush" (expected further thrombosis), no complications. The surgical operation was performed at an interval of 72 hours after. Histologically proven glomus jugular, glomus jugulotimpanicum and glomus caroticum.
Conclusion: This paper presents the significance of preoperative angiography and embolization of glomus tumor of different localization and benefits of these procedures in order to reduce intraoperative bleeding and with consequent reduction in the duration of the surgical procedure.

PO44

Radiological Diagnostic Imaging Diabetic Angiopathy

S. R. Stojanović, P. D. D. Stojanov, M. S. D. S. Ristić; Niš/RS

Learning Objectives: Diabetes mellitus as the "epidemic of the XXI century" that leads to acute and to chronic complications, of which the primary site occupies diabetic angiopathy associated with atherosclerosis and infections.
Background: Patients with advanced diabetic angiopathy and determination of the same type on the basis of CDFI and MDCT examination and confirm DSA.
Imaging Findings or Procedure Details: Patient (DM type 2) with pain in the legs to CDFI (Siemens Acuson X 300) and MDCT (Toshiba Aquilion 64s): SFA dex. 2 significant stenosis, SFA sin. occluded from the origin. POPLA and arteries of the lower limb without hemodynamically significant stenosis.
Patient (DM type 2): cramps in the lower legs and trophic changes of the right foot to CDFI and MDCT:POPLA, ATA and PTA dex. occluded, without connecting the foot. POPLA sin. with a few critical stenosis, ATA and PTA dex. occluded in the proximal third.
Patient (DM type 1): severe pain in the gluteal region to CDFI left leg CFA and SFA with monophasic and "parvus tardus" flows, without registration flow in distal arteries.
An overview DSA patients fully correlates with the previously well realized CDFI and MDCT findings and shows the "pelvic type of atherosclerosis" (SFA) in the first and third, and "popliteal type of atherosclerosis" (POPLA) in the second and third patient.
Conclusion: The paper presents the significance of diagnostic procedures (CDFI and MDCT) in the testing of blood vessel damage in patients with diabetes mellitus, which correlates with the finding of the DSA, the "gold standard" for the diagnosis of diabetic angiopathy.

PO45

Clinical Signs, Imaging Findings and Endovascular Treatment of Arterio-Ureteral Fistulas

L. Steinert, M. Randazzo, R. Pfiffner, T. Pfammatter; Zurich/CH

Purpose: To present clinical presentation, imaging findings and endovascular therapy of arterio-ureteral fistulas (AUF).
Methods and Materials: Between 01/2004 and 11/2015, an index term search in our radiologic information system revealed 5 patients (3 male and 2 female patients) with AUF's. Clinical data were retrieved from our hospital clinical information system and supplemented by phone calls to the patient's family physician or the patients themselves. All CT-scans and catheter angiographies were available for reviewing.
Results: The patients were aged from 59 to 80 years. Mean follow-up duration was 20 months (range 2 to 63 months). 4 patients presented with hemorrhagic shock. 4 patients had gross hematuria. 1 patient with an iliaco-uretero-enteral fistula suffered from massive lower GI-hemorrhage. 3 out of 5 patients had a history of pelvic cancer and surgery (2 out of 5 patients with additional external beam radiotherapy), whereas 2 out of 5 patients had a history of open vascular surgery (bifurcated grafts). The interval between the primary oncologic or vascular treatment and symptoms ranged between 20 months and 10 years. Diagnosis was missed on initial CT scans in 2 cases. Endovascular embolization / stent-grafting were clinically successful in all cases. None of the patients died of AUF specific causes.
Conclusion: Although being a rarity, AUF's are a potentially life-threatening emergency. In the light of the current successful interventional treatments, awareness of this differential diagnosis in patients with unexplained hematuria and history of pelvic cancer or vascular surgery is crucial.

PO46

A Comparative Study Between the Clinical Outcome of Untrasound Injection vs Palpation Guided Injection for Carpal Tunnel Syndrome Patients

A. Sobieh, A. Tohami, A. Omar, A. Gad; Ismailia/EG

Purpose: To determine the efficacy of ultrasound guided injection compared to palpation guided injection in treatment of Carpal tunnel syndrome. Comparison of complications of both techniques
Methods and Materials: 76 patients suffering from different degrees of carpal tunnel syndrome confirmed by nerve conduction studies were selected .They were assigned randomly to either of two groups,Group (A) were injected with ultrasonography guidance while group (B) were injected by palpation guided injection depending on anatomical landmarks. Both groups will receive local injection composed of a solution consisting of a cocktail formed of 0.5 ml of plain mepivacaine hydrochloride 3% and 0.5 ml of 40mg triamcinolone is injected using a 3 ml 25 gauge 1.5 inch needle syringe.Pre-injection pain, post-injection pain at 2 weeks and 12 weeks will be determined using visual analogue scale.Technical difficulties and complications will be assessed for both techniques including: number of punctures, failure of technique, duration of injection, difficulty of technique, patient satisfaction.
Results: At (P≤0.01), there is : Significant improvement of pain in group (A) compared to group (B) injection at 2,12 weeks. Positive significant correlation between patient age and duration of injection. Positive correlation between degree of CTS, degree of baseline pain and duration of injection. No correlation between mean improvement after injection on 2,12 w and age of patient and duration of injection.
Conclusion: Steroid injection under ultrasound guidance offers: visualizing carpal tunnel. proper injection around the nerve, peeling the nerve from surrounding adhesions. Less complications. less injection duration. Better patient satisfaction.

PO47

Possibilities in Supraaortic Viabahn Prosthesis, a Technical Note

D. Graf, L. Hechelhammer, J. Weber; St.Gallen/CH

Purpose: In this article we report on the possibilities of the Viabahn endograft in supraaortic endovascular treatment.
Methods and Materials: In 7 cases this endograft was used in 3 different locations: internal and common carotid artery, and vertebral artery. The pathologies were either aneurysm (cervical vertebral artery), blow out rupture due to tumor infiltration or prophylactic vessel protection prior to neck dissection.
Results: Viabahn endograft is a reinforced biocompatible polytetrafluoroethylene liner attached to an external nitinol stent structure with a heparin bioactive surface. The flexibility of the endoprosthesis enables it to traverse tortuous areas. These abilities make it a well known and often used endoprosthesis in peripheral interventions, in locations like iliac artery, superficial femoral artery and popliteal artery. The supraaortic use of the Viabahn endograft are largerly unknown although due to its characteristics.
Conclusion: Due to its chracteristics the Viabahn endoprosthesis was used in our IR department in 7 cases in a supraaortic location for different pathologies with good results.

PO48

"Virtual autopsy" of Living Trauma Victims: The Role of Forensic Radiology in Clinical Medico-Legal Expertise

P. Baumann, J.-B. Zerlauth, P. Mangin, S. Grabherr; Lausanne/CH

Purpose: The examination of victims having sustained aggressions is daily routine for forensic pathologists. The medico-legal exam is done to respond to specific questions and allows editing a medico-legal expertise. If available, clinical radiological images are analyzed. As forensic questions differ from clinical ones, image reading differs considerably from the clinical approach.
Methods and Materials: In our centre the analyses of radiological images by a forensic pathologist together with a forensically trained radiologist is a routine. More than 100 cases of living patients have been investigated during the last 3 years. The assessment of soft-tissue lesions is crucial. Beside the easy-understandable description of the lesions, editing of specific imaging catalogues for medical lay-persons is practiced. Images can be made understandable by adding orientation aids, arrows and other indications explaining the anatomy and specific findings.
Results: In cases of sharp trauma and gunshots, 2D-reconstructions allow determining length and angle of a wound channel, the involvement of vital structures or their distance to the wound channel. In cases of blunt trauma, such reconstructions together with 3D VR-images permit to visualize small fracture lines and give important information about the used weapon and their impacts.
Conclusion: Well described 2D- and 3D-reconstructions give the possibility to visualize the consequences of trauma in living patients in an understandable way for judges. The images allow performing a "virtual autopsy" in living victims. This presentation shall give an overview about today's state of the art in clinical forensic expertise and underline the differences between clinical and forensic approach.

PO49

Task-Based Evaluation of Image Quality with a Wide-Volume CT Scanner Using both Helical and Axial Acquisition Modes

D. Racine, J. Ott, F. Becce, D. Rotzinger, F. R. Verdun; Lausanne/CH

Purpose: To assess the change in low-contrast detectability as a function of radiation dose when switching from the helical to axial acquisition modes using a wide-volume CT scanner.
Methods and Materials: An abdominal phantom containing various spheres (8 and 5 mm diameters; 20 and 10 HU contrast levels) was scanned at decreasing CTDIvol of 15, 10, and 5 mGy using the helical and axial acquisition modes. CT images were reconstructed at a slice thickness of 2.5 mm, with varying ASiR-V strengths (0, 30, 50, and 70%). The objective image quality was subsequently evaluated using a mathematical model observer (Channelized Hotelling Observer (CHO)).
Results: Low-contrast detectability was systematically and statistically significantly improved when switching from the helical to axial acquisition modes. For the 5 mm/20 HU targets at 15 mGy, ASiR-V 50% yielded a detectability index of 3.6 using the axial mode compared to 2.8 using the helical mode. For the same spheres at 5 mGy, detectability indices were 2.3 and 2.1, respectively. At 5 mGy, 8 mm/10 HU targets yielded a detectability index of 3.7 using the axial mode compared to 3.2 using the helical mode. Moreover, regardless of the acquisition mode, an improvement in low contrast detectability is observed when switching from a 0% to 50%.
Conclusion: Thus the low contrast detectability was systematically and significantly improved when switching from helical to axial mode.

PO50

Evaluation of Image Performance of a Novel 3D X-Ray System with a 3D Image Quality Phantom and Comparison with Standard CT

R. M. Benz[1], M. Garcia[1], F. Amsler[2], B. Stieltjes[1], A. Hirschmann[1]; [1]Basel/CH, [2]Biel-Benken/CH

Purpose: Phantom-based performance assessment of a novel 3D X-ray system and comparison with standard CT.
Methods and Materials: A 3D image quality phantom (ConeBeam Phantom, QRM, Germany) was scanned with a 3D X-ray system (Siemens Multitom Rax) using three dedicated trajectories (163°/188°/200° scanning angle, 160 projections). Acquisition parameters were varied with different tube voltage (60/70/81/90/100/121kV) and detector surface dose (DSD) per projection (0.348/0.696/1.74/3.48µGy). Scans with 320 projections for each trajectory were performed with 80kV and 121 kV at 0.696 µGy DSD. Images were evaluated by two independent readers. Spatial resolution was assessed by visual distinction of line pairs per cm (lp/cm) (sharp reconstruction kernel). Low contrast resolution was assessed by detection of the smallest visible disc diameters and contrast values (soft kernel). SNR and CNR were calculated.
Results: With the 3D X-ray system and the investigated protocols a maximum of 16lp/cm were visible and best low contrast resolution was 2 mm at 30 HU, 16lp/cm and 4mm at 25 HU for 320 projections respectively. With CT a maximum of 12lp/cm were visible and best low contrast resolution was 2mm at 20HU. SNR and CNR are currently under evaluation.
Conclusion: With the investigated protocols the 3D X-ray system has a higher spatial resolution but a lower soft tissue contrast compared with standard CT. Additional projections do not have a significant influence. Further investigations are needed to evaluate image performance in patients for clinlical use.

PO51

Top 5 Lumbosacral Spine Pain Clinical Diagnoses: Evidence-Based Interventional Management.

H. Brat[1], T. Bouziane[2], D. Fournier[1]; [1]Sion/CH, [2]Tournai/BE

Learning Objectives: Evidence-based spine pain teaching file aiming at: Understanding management algorithms based on clinical diagnoses Learning current evidence and recommendations of diagnostic and therapeutic interventions Clarifying existing controversies in the decision making process of specific treatments Updating major references.
Background: Spine pain treatments and level of evidence have not matched very well the last decades, due to a lack of well conducted randomized comparative studies with sufficient patient numbers. Publication of lethal accidents have led to prohibition of particulate steroids and a number of controversies have arisen regarding the usefulness of pain treatments such as epidural steroid infiltrations, ...
Material & Methods: Comprehensive systematic literature review (Pubmed, Cochrane Database) using adapted USPSTF (United States Preventive Services Task Force) criteria Data published by ASIPP (American Society of Pain Physicians), NASS (North American Pain Society) and ISIS (International Spine Intervention Society) Reference Books edited from 2012.
Imaging Findings or Procedure Details: Each lumbosacral spine pain clinical diagnosis is illustrated by: Management algorithms Current diagnostic interventions evidence and guidelines Current therapeutic interventions evidence and guidelines Controversies (when adequate) Major references.
Top 5 lumbosacral spine pain clinical diagnoses:
1. Lumbosacral radicular pain
2. Discogenic low back pain
3. Lumbar facet joint pain
4. Sacroiliac joint pain
5. Coccygodynia

Conclusion: Based on a comprehensive review of the literature using the USPSTF (United States Preventive Service Task Force) analysis criteria, this educational poster presents an update of evidence based management algorithms, interventional procedures and recommendations for the top 5 lumbosacral spine pain diagnoses.

PO52

Top 5 Craniocervical Pain Clinical Diagnoses: Evidence-Based Interventional Management.

H. Brat[1], T. Bouziane[2], D. Fournier[1]; [1]Sion/CH, [2]Tournai/BE

Learning Objectives: Evidence-based spine pain teaching file aiming at: Understanding management algorithms based on clinical diagnoses Learning current evidence and recommendations of diagnostic and therapeutic interventions Clarifying existing controversies in the decision making process of specific treatments Updating major references.
Background: Spine pain treatments and level of evidence have not matched very well the last decades, due to a lack of well conducted randomized comparative studies with sufficient patient numbers. Publication of lethal accidents have led to prohibition of particulate steroids and a number of controversies have arisen regarding the usefulness of pain treatments such as epidural steroid infiltrations, ...
Material & Methods: Comprehensive systematic literature review (Pubmed, Cochrane Database) using adapted USPSTF (United States Preventive Services Task Force) criteria Data published by ASIPP (American Society of Pain Physicians), NASS (North American Pain Society) and ISIS (International Spine Intervention Society) Reference Books edited from 2012.
Imaging Findings or Procedure Details: Each craniocervical spine pain clinical diagnosis is illustrated by: Management algorithms Current diagnostic interventions evidence and guidelines Current therapeutic interventions evidence and guidelines Controversies (when adequate) Major references.
Top 5 craniocervical spine pain clinical diagnoses:
1. Cluster headache
2. Occipital neuralgia
3. Whiplash-associated disorders
4. Cervical radicular pain
5. Cervical facet joint pain.

Conclusion: Based on a comprehensive review of the literature using the USPSTF (United States Preventive Service Task Force) analysis criteria, this educational poster presents an update of evidence based management algorithms, interventional procedures and recommendations for the top 5 craniocervical spine pain diagnoses.

PO53

The Added Value of Dynamic Contrast Enhanced Magnetic Resonance Imaging in the Follow-Up of Soft Tissue Malignant Tumours. A Pictorial Essay

E. Astrinakis, A. Neroladaki, I. Bagetakos, C. D. Becker, S. Boudabbous; Geneva/CH

Learning Objectives: The purpose of this pictorial essay is to illustrate the added value of dynamic contrast enhanced magnetic resonance imaging (DCE-MRI) to conventional MRI as well as diffusion weighted imaging (DWI) for the assessment of treated soft tissue tumours.
Background: This retrospective study includes analysis of 47 MRI performed in our institution from 2013 to 2015, for a total of 34 patients (age range 19-86 years, average 56 years) with histology proven soft tissue malignant tumours and follow-up after surgical treatment, chemotherapy or radiotherapy.
Functional imaging analysis is based on the presence of arterial enhancement and the type of time intensity curve type on DCE-MRI with associated perfusion parametric maps, as well as DWI analysis with apparent diffusion coefficient maps (ADC).
Imaging Findings or Procedure Details: While the presence of mass effect and T2 hyperintensity is a sensitive criterion for tumour recurrence, it lacks specificity, as benign post-treatment nodular inflammatory or fibrotic changes; correlation with DCE-MRI as well as DWI increases diagnostic accuracy. Moreover, post radiation oedema versus tumoral infiltration is a common problem well addressed by DCE-MRI and DWI. In the presence of complications in the surgical bed, morphologic parameters and DWI are problematic, while DCE-MRI can be extremely helpful. Finally, DCE-MRI plays a crucial role in the presence of orthopaedic hardware, where DWI is non-applicable.
Conclusion: This educational presentation illustrates the added value of DCE-MRI, in the daily clinical practice assessment of treated soft tissue malignancies. An optimal interpretation requires a combined analysis of morphologic and functional imaging parameters.

PO54

Value of Fat-Suppressed Fluid-Sensitive MRI Sequences for the Detection and Characterization of Modic I End-Plate Changes of the Lumbar Spine

T. Finkenstaedt[1], F. Del Grande[2], N. Bolog[3], N. H. Ulrich[1], S. Tok[1], O. Kolokythas[4], J. Steurer[1], G. Andreisek[1], S. Winklhofer[1]; [1]Zurich/CH, [2]Lugano/CH, [3]Bucharest/RO, [4]Winterthur/CH

Purpose: To assess the value of fat-suppressed fluid-sensitive sequences for the assessment of Modic I end-plate changes on magnetic resonance imaging (MRI) of the lumbar spine.
Methods and Materials: Institutional review board–approved multi-center study with written informed consent. Sagittal T1-weighted (T1w), T2w, and fat-suppressed fluid-sensitive MRI images of 100 consecutive patients (consequently 500 vertebral segments; 52 female, mean age 74±7.4 years; 48 male, mean age 71±6.3 years) with suspected lumbar spinal canal stenosis were retrospectively evaluated. We recorded the presence (yes/no) and extension (i.e. Likert-scale of height, volume, and end-plate extension) of M1 end-plate changes in T1w/T2w sequences and compared the results to fat-suppressed fluid-sensitive sequences using the McNemar and Wilcoxon signed-rank test.
Results: Fat-suppressed fluid-sensitive sequences revealed significantly more Modic I changes compared to T1w/T2w sequences (156 vs. 93 segments, respectively; p<0.001). The extension of Modic I changes in fat-suppressed fluid-sensitive sequences was significantly larger compared to T1w/T2w sequences (height: 2.27±0.79 vs. 2.53±0.82, volume: 2.1±0.65 vs. 2.35±0.76, end-plate: 2.19±0.81 vs. 2.46±0.76), (p<0.05). Modic I changes which were only visible in fat-suppressed fluid-sensitive sequences but not in T1w/T2w sequences were significantly smaller compared to Modic I changes which were visible in T1w/T2w sequences (height: 1.8±0.8 vs. 2.54±0.8, volume: 1.72±0.7 vs. 2.34±0.8, end-plate: 1.97±0.9 vs. 2.46±0.8), (p<0.05).
Conclusion: In conclusion, fat-suppressed fluid-sensitive MRI sequences of the lumbar spine revealed significantly more Modic I end-plate changes and demonstrated a greater extent compared to standard T1w/T2w imaging.

PO55

Nontraumatic Incidental Findings in Patients undergoing Whole-Body Computed Tomography at Initial Emergency Admission

E. Krozcek[1], G. Wieners[2], I. Steffen[2], T. Lindner[2], F. Streitparth[2], B. Hamm[2], M. Maurer[3]; [1]Göttingen/DE, [2]Berlin/DE, [3]Bern/CH

Purpose: To evaluate the number, localization and importance of nontraumatic incidental findings in patients undergoing whole-body computed tomography (wbCT) for suspected multiple trauma or unclear unconsciousness.
Methods and Materials: The radiologic reports of all patients undergoing wbCT at admission to a level-1 trauma center between January 2009 and December 2013 were analyzed with regard to non-trauma-associated incidental imaging findings. Four severity categories of incidental findings were distinguished (category 1: urgent treatment or further clarification needed, category 2: further examination and follow-up within 3-6 months, category 3: findings likely asymptomatic but potentially symptomatic in the future, category 4: harmless findings).
Results: Altogether, there were 6053 reported incidental findings in the 2571 patients (1823 male, 748 female; mean age 45.7 years) included in the study. 245 patients (9.5%) had 343 urgent category 1 findings, 840 patients (32.7%) 1418 category 2 findings, 1333 patients (51.9%) 2153 category 3 findings and another 1257 patients (48.9%) 2139 category 4 findings. Most incidental findings (42.2%) were detected in the abdomen and pelvis, and about one fifth each were seen in the head (1188, 19.6%) and in the chest (1276, 21.1%).
Conclusion: A high number of nontraumatic incidental findings are present in patients undergoing whole-body CT. More than 40% of all patients have at least one finding needing urgent therapy, direct workup or at least a follow-up, which is a significant challenge for the trauma center whose primary responsibility is to provide trauma care.

PO56

Incidence and Clinical Importance of Extraspinal Findings at Lumbar Spine CT: A Retrospective Study of 810 Patients

K. Yalçin-Şafak, Ö. Elibol, A. Akça; İstanbul/TR

Purpose: To determine the incidence and clinical importance of extraspinal findings in outpatients undergoing CT of the lumbar spine when the full FOV images are evaluated.
Methods and Materials: 810 patients who referred to our clinic for lumbar spine CT were evaluated.Extraspinal findings were classified according to C-RADS.Patients with C-RADS E3 and E4 were correlated with medical records to determine how many of these findings were previously unknown.
Results: Extraspinal findings were detected in 370 of the 810 lumbar spine CT examinations.118 patients had intermediate or clinically significiant findings(who were classified as C-RADS E3 and E4) requiring clinical correlation or further evaluation.According to the medical records of the patients, C-RADS E3 and E4 findings were respectively undocumented in 76 of 92 patients and in 19 of 26 patients.The most common finding classified as C-RADS E4 was an abdominal aortic aneurysm in 16 patients, and in 10 patients, this finding had not been previously documented.The other extraspinal findings classified as C-RADS E4 included: aort aneursym with iliac artery aneursym, iliac artery stenosis, iliac artery aneursym, aort stenosis with iliac artery stenosis, renal cell carcinoma, over carcinoma, iliac giant cell tumor and two patients with solid renal mass and solid liver mass.
Conclusion: Extraspinal findings are common in patients undergoing lumbar spine CT. Clinically significant or potentially significant findings can be expected in 14.5% of patients, and these will require further evaluation and follow-up.Given the benefit of diagnosing clinicallly significant findings, full FOV reconstructions should be routinely provided for reporting.

PO57

Osteophytes of the Fovea Capitis Femoris – A Finding in Asymptomatic Volunteers

S. Bensler, C. A. Agten, C. W. Pfirrmann, R. Sutter; Zurich/CH

Purpose: To investigate the spectrum of osteophytes at the borders of the fovea capitis femoris and to assess different morphological types of the fovea capitis femoris in asymptomatic individuals and patients with hip osteoarthritis.
Methods and Materials: 59 asymptomatic volunteers and 65 patients with radiologically confirmed osteoarthritis of the hip underwent dedicated hip MRI. Two radiologists independently assessed fovea morphology (standard type, diamond type, flat type, triangular type), as well as frequency, location, and size of osteophytes at the border of the fovea. Descriptive and inferential statistics were applied.
Results: Distribution of fovea morphology was similar for volunteers and patients: 47%/51% (standard type), 9%/6% (diamond type), 20 %/25% (flat type), 24%/18% (triangular type), without a statistically significant difference (p=0.76). Osteophytes at the fovea were detected in 71% of volunteers and 97% of patients, but patients had significantly larger osteophytes (mean size 1.9mm±0.7) than volunteers (1.6mm±0.3) at all locations (p=0.004).
Osteophytes were most frequently located at the anterior border of the fovea capitis femoris both in the volunteers (42%) and in the patient group (80%).
Conclusion: Osteophyte-like structures of the fovea capitis femoris were found in 71% of healthy individuals, but were smaller in size and less commonly seen than in patients with hip osteoarthritis. Small osteophytes may be physiologically seen at the fovea and do not necessarily indicate that hip osteoarthritis is present.

PO58

Lumbar Spinal Canal Stenosis: Intra- and Inter-Reader Agreement for Magnetic Resonance Imaging Parameters

S. Winklhofer[1], U. Held[1], J. Burgstaller[1], T. Finkenstaedt[1], N. Bolog[2], N. H. Ulrich[1], J. Steurer[1], G. Andreisek[1], F. Del Grande[3]; [1]Zurich/CH, [2]Bucharest/RO, [3]Lugano/CH

Purpose: To assess the inter- and intra-reader agreement of commonly used quantitative and qualitative image parameters for the assessment of lumbar spinal canal stenosis (LSS) by magnetic resonance imaging (MRI).
Methods and Materials: In this ethical board approved prospective multicenter study, MRI of 100 randomly selected patients (median age 72.5 years, 48% female) of the Lumbar Stenosis Outcome Study (LSOS) were evaluated by two independent readers. A set of five previously published core imaging parameters as well as nine qualitative and five quantitative additional parameters were assessed in order to calculate k and intraclass correlation coefficients (ICC) for the inter-reader agreement. Additional repeated image evaluations were performed by one reader to calculate the intra-reader agreement.
Results: k values for the core image parameters ranged between 0.42 and 0.77 for inter-reader agreement and between 0.59 and 0.8 for intra-reader agreement. The inter-reader agreement for the non-core parameters showed k values of 0.27-0.69 and ICC values of 0.46-0.85. The intra-reader agreement showed k values of 0.53-0.69 and ICC values of 0.81-0.88.
Conclusion: The inter- and intra-reader agreement of commonly used quantitative and qualitative image parameters for the assessment of LSS showed quite a variability with previously defined core parameters having good to excellent inter- and intrareader agreements.

PO59

Value of Tomosynthesis for Lesion Evaluation in Osteoarthritic Hands Using the OARSI Score

K. Martini, A. Becker, R. Guggenberger, G. Andreisek, T. T. Frauenfelder; Zurich/CH

Purpose: To investigate the value of Tomosynthesis in depicting osteoarthritic lesions in comparison to conv. X-ray, with use of computed tomography (CT) as standard-of-reference.
Methods and Materials: Imaging of 12 cadaver wrists was performed with Tomosynthesis in anteriorposterior (ap) projection (50 kV at 40 mA; tube angle: 40°), conventional X-ray and multi-detector CT (70kV at 16mAs ref). Distal interphalangeal joint (DIP) II, DIP III, proximal interphalangeal joint (PIP) II, PIP III, first carpometacarpal (CMC) and scaphotrapezotrapezoidal joint (STT) were individually graded using the Osteoarthritis Research Society International (OARSI) score by two independent readers for the presence of osteophytes (0-3), joint space narrowing (0-3), subchondral sclerosis (0-1), lateral deformity (0-1), subchondral cysts (0-1) and erosion (0-1). Total scores range from 0-60. Inter-reader agreement (Cohen's k) was calculated. CT served as standard of reference.
Results: Comparing Tomosynthesis and conventional X-ray to CT, the agreement was of 69.64% vs. 63.89% for the presence of osteophytes; 80.56% vs. 56.94% for joint space narrowing; 69.44% vs. 68.1% for subchondral sclerosis; 94.44% vs. 91.67% for lateral deformity; 97.22% vs. 80.56% for subchondral cysts; and 100% vs. 97.22% for erosion. While Tomosynthesis showed no significant difference (p=0.846) in OARSI score grading to CT (mean OARSI-score CT: 16.8, SD=10.64 vs. mean OARSI-score Tomosynthesis: 16.25, SD=9.56), conventional X-ray had significant lower mean OASIS scores (mean OARSI-score X-ray: 11, SD=8.33; p=0.037). Inter-reader agreement for OARSI scoring was excellent (k= 0.83).
Conclusion: Tomosynthesis depicts more lesions than conventional X-ray compared to CT.

PO60

Metal Artifact Suppression at 3T MRI: Comparison of MAVRIC-SL with Conventional Fast Spin Echo Sequences in Patients with Hip Joint ArthroplastyMetal Artifact Suppression at 3T MRI: Comparison of MAVRIC-SL with Conventional Fast Spin Echo Sequences i

M. Kretzschmar[1], L. Nardo[2], M. Han[2], G. Joseph[2], U. Heilmeier[2], R. Krug[2], T. Link[2]; [1]Basel/CH, [2]San Francisco/US

Purpose: The purpose of our study was to evaluate the clinical feasibility and diagnostic value of a new MRI metal artifact reduction pulse sequence called MAVRIC-SL in a 3T MRI environment.
Methods and Materials: Two MAVRIC-SL sequences obtained in 61 patients with symptomatic total hip replacement were compared with standard FSE-STIR sequences optimized for imaging around metal. Artifact size was measured on the slice of greatest extent. Image quality, fat saturation, image distortion, visibility of anatomical structures and detectability of joint abnormalities were visually assessed and graded on qualitative scales. Differences between MAVRIC-SL and FSE sequences were tested with the Wilcoxon-signed-rank test.
Results: MAVRIC-SL sequences at 3T showed significantly smaller metal artifacts compared to FSE-STIR sequences (p<0.0001). The general image quality of MAVRIC-SL sequences was reduced with regard to spatial resolution, noise and contrast (p=0.001) and fat saturation (p<0.0001). The reduction of artifact size and image distortion significantly improved visualization of joint anatomy (p<0.0001) and diagnostic confidence regarding implant-associated abnormalities (p=0.0075 to <0.0001).
Conclusion: Although the image quality of MAVRIC-SL sequences is limited at 3T, its clinical application is feasible and provides important additional diagnostic information for the work-up of patients with symptomatic hip replacement through substantially reduced metal artifacts.

PO61

Central Osteophytes Develop in Cartilage with Abnormal Structure and Composition: Data from the OAI Cohort.

M. Kretzschmar[1], U. Heilmeier[2], C. McCulloch[2], M. Nevitt[2], T. Link[2]; [1]Basel/CH, [2]San Francisco/US

Purpose: To investigate the evolution of central osteophytes (CO) by analyzing the local structure and matrix composition of the overlying cartilage using 3T-MRI three to one year prior to the onset of COs.
Methods and Materials: Baseline, four and six year follow up MRIs of the right knee of 400 subjects of the Osteoarthritis Initiative were screened for the appearance of new COs. Twenty-eight subjects developed 31 COs. Cartilage T2 relaxation times of the local cartilage overlaying COs and the surrounding cartilage and morphological cartilage lesions and bone marrow edema pattern (BMEP) graded with whole organ MRI scores (WORMS) were analyzed in yearly MRIs from three year prior to the year of onset of the CO. Knee symptoms including pain, stiffness and function were recorded during this period.
Results: All subjects showed local cartilage abnormalities prior to the development of COs. Mean cartilage WORMS increased from 1.33±0.57 three years prior to 2.38±0.48 with onset of COs (p=0.003). Mean T2-values of the focal cartilage increased non-significantly from 36.9+/-6.9ms, to 37.7±5.8ms (p=0.229). Surrounding cartilage T2 increased from 34.0+/-4.9ms to 35.8ms±3.8ms (p=0.036). Focal T2-values were higher compared to T2-values in the surrounding cartilage at all time points reaching significance 3 and 2 years prior and at the year of CO onset (p=0.025). No significant increase of symptoms was found with the onset of COs.
Conclusion: This study provides evidence that focal cartilage structural and compositional degeneration precedes CO. No significant aggravation of knee symptoms could be found during the evolution of CO.

PO62

Iterative Reconstruction (IR) in MDCT: Which Type Ensures Diagnostic Image Quality when Considerably Reducing the Doses Delivered to Young Oncological Patients?

B. Pauchard, K. Higashigaito, A. Lamri, R. A. Meuli, H. Alkadhi, F. R. Verdun, S. Schmidt; Lausanne/CH

Purpose: To compare diagnostic image quality of low-dose thoraco-abdominal MDCT, reconstructed with two IR-algorithms (ASIRTM versus VEOTM, GE Healthcare)
Methods and Materials: Forty-four young patients (2 women, mean age 30 ±9) with stable oncological disease were prospectively included. After a routine intravenously contrast-enhanced thoraco-abdominal MDCT, defined as reference acquisition (dose 100%), the follow-up MDCT was performed with 50% (n=44) and, additionally, 20% of the dose (n=29). Low-dose MDCT was reconstructed with both, ASIR and VEO algorithm. Four radiologists (2 juniors, 2 seniors), blinded to dose and technique, read each set of MDCT-images (100%, ASIR-50%, VEO-50%, ASIR-20%, VEO-20%) concerning objective and subjective image quality (high-/low contrast structures), subjective image noise (ASIR) and pixilated blotchy appearance (VEO), diagnostic confidence and focal lesions detection.
Results: At all dose levels, the objective image noise was significantly higher on ASIR- than VEO-images (p<0.001). Despite the blotchy pixilated appearance of structures, inherent in VEO-images, the latter were read with significantly higher diagnostic confidence, especially by the juniors.
VEO-images significantly better demonstrated low-contrast structures (portal/hepatic veins) than the correpondant ASIR-images, regardless of the percentage of dose reduction.
Abdominal low-dose MDCT-images of patients with higher body-mass index (BMI>24.7) were read with significantly higher diagnostic confidence than these of slim patients, with better evaluation of both, low- and high-contrast structures, regardless of dose and technique
Conclusion: When acquiring low-dose thoraco-abdominal MDCT in young oncological patients the VEO-algorithm should be used for image reconstruction in order to ensure diagnostic quality. Elevated BMI does not hamper the quality of low-dose MDCT

PO63

Multimodality Imaging of Pediatric Tumors and Tumor-Like Conditions of the Maxillofacial Skeleton

S. S. Stefanelli, L. Merlini, A.-L. Rougemont, A. Ailianou, P. Scolozzi, A. Terzic, M. Becker; Geneva/CH

Learning Objectives: To understand key imaging features of pediatric lesions of the maxillofacial skeleton based on radiologic-pathologic correlation. To illustrate the importance of multimodality imaging for treatment planning and outcome. To recognize potential pitfalls of image interpretation.
Background: Tumors and tumor-like lesions originating in the pediatric maxillofacial skeleton represent a major challenge in clinical practice due to the complex anatomy of the face and their long-term effects on facial growth. Although very rare, they constitute a broad spectrum of lesions with a varying degree of malignant potential.
Imaging Findings or Procedure Details: The current exhibit is based on the retrospective analysis of a series of 40 children seen in our institution during the past 15 years. Primary intraosseous neoplasms included benign lesions (osteoma, Langerhans cell histiocytosis, desmoplastic fibroma, inflammatory myofibroblastic tumor, juvenile psammomatoid ossifying fibroma) and malignant tumors (Ewing sarcoma, primary intraosseous lymphoma and neuroblastoma). Common congenital intraosseous lesions comprised fibrous dysplasia, torus palatinus or mandibularis, and dermoids. Inflammatory lesions were mainly osteomyelitis with or without osteopetrosis. We illustrate typical findings and discuss the added value of multimodality imaging with US, CT, MRI, diffusion weighted imaging and PET CT. We provide radiologic-pathologic correlation for the understanding of characteristic features, and address pitfalls of image interpretation.
Conclusion: Multimodality imaging increases the diagnostic confidence and provides complementary information. This exhibit is a learning tool for imaging and interpretation of radiologic findings in these rare tumors.

PO64

Ovarian Cancer Staging and Treatment Planning: How Can the Radiologist Help the Multidisciplinary Team?

A. M. Kalovidouri[1], M. Picarra[1], I. Bagetakos[2], D. A. Djema[1], C. D. Becker[1], X. Montet[1], P. Petignat[1], D. Botsikas[1]; [1]Geneva/CH, [2]Thônex/CH

Learning Objectives: To illustrate the guidelines for staging and follow up of ovarian cancer, to provide the radiologist with a framework for use in interpretation of radiologic examinations and to convey what the multidisciplinary team needs to know in order to plan the best treatment strategy.
Background: Ovarian cancer is the most common cause of death due to gynaecologic malignancy in the western world. Staging depends mainly upon extension of peritoneal involvement, lymph nodes invasion and presence of distant metastases. The role of the radiologist is important in staging of ovarian cancer, determining of respectability and planning of surgery, but also in selection of patients who may benefit from neoadjuvant chemotherapy.
Imaging Findings or Procedure Details: Pelvic MRI is the examination of choice for local staging while abdominal and pelvic CT is indicated for staging. In advanced local disease and in cases of suspected recurrence, 18-fluorodeoxyglucose(FDG) positron emission tomography(PET)/CT is also appropriate.
Signs of intraperitoneal involvement are nodular soft-tissue thickening and enhancement of the peritoneum. Accurate knowledge of the complex peritoneal anatomy, directionality of the flow of peritoneal fluid and specific disease sites which may present particular difficulties to surgical access are necessary for detection of peritoneal involvement and correct staging. Lymph nodes involvement is mainly retroperitoneal and extensive lymph node disease may be associated with thoracic disease.
Conclusion: Imaging plays a crucial role in planning the appropriate treatment strategy for patients with ovarian cancer. Good knowledge of peritoneal anatomy and modes of tumour spread are necessary for accurate assessment of peritoneal involvement.

PO65

Gynaecologic Emergencies in the Spotlight: What Radiologists Need to Know!

M. W. Wagner[1], T. Bosemani[2], T. Huisman[2], R. A. Kubik-Huch[3]; [1]Zurich/CH, [2]Baltimore/US, [3]Baden/CH

Learning Objectives: To highlight frequently encountered acute gynaecologic emergencies and to sharpen the radiologist's mind for the imaging appearance of gynaecologic pathology on US, CT and MRI.
Background: Gynaecologic emergencies are a group of disorders mostly characterized by acute pelvic pain related to the genital organs and related or unrelated to pregnancy. Gastrointestinal diseases have considerable clinical overlap. Imaging plays an important role in the emergency setting by 1) assisting clinicians to diagnose acute gynaecological diseases and 2) helping to guide medical and surgical treatment. Diagnoses implicate potentially profound consequences for the female patient, consequently, it is important to accurately interpret the imaging findings in the context of the clinical signs.
Imaging Findings or Procedure Details: Recent literature was searched for publications on gynaecologic emergencies and their appearances on US, CT and MRI. Imaging findings of typical pathologies, e.g. extra-uterine gravidity, fibroid complications, adnexal torsion, and septic ovarian vein thrombosis will be illustrated based on the prevalence of diseases and the significance of the respective imaging modalities. Moreover, a compendium is provided on indications of CT and MRI during pregnancy and the current guidelines of the use of contrast agents during pregnancy and breast-feeding.
Conclusion: Acute gynaecologic conditions must be separated from gastrointestinal diseases. Cross-sectional imaging aids in the diagnosis of acute gynaecologic emergencies. We aim to illustrate US, CT and MRI findings of acute gynaecologic diseases to ensure adequate patient care and to increase sensitive and specific interpretation of findings among radiologists.

PO66

Haematometrocolpos: Aetiologies and Differential Diagnoses; What Radiologists Should Know!

M. W. Wagner[1], T. Bosemani[2], T. A. Huisman[2], R. A. Kubik-Huch[3]; [1]Zurich/CH, [2]Baltimore/US, [3]Baden/CH

Learning Objectives: To illustrate different aetiologies of haematometrocolpos (HMC) and to spotlight differential diagnoses of imaging appearances of HMC on US, CT and MRI in pediatric and adolescent females in order to increase perception among radiologists.
Background: HMC has an estimated incidence of 1 in 1000-2000 female teenagers. It is characterized by the accumulation of blood in the uterus and vagina and can be secondary to an imperforate hymen, transverse vaginal septum and vaginal stenosis or atresia. Differential diagnoses of haemato(-metro)colpos include hydro(-metro)colpos, pelvic abscess, rhabdomyosarcoma and ovarian tumours. Clinical presentation of patients with HMC is nonspecific (vague abdominal pain, lower abdominal mass or amenorrhoea). Cross-sectional imaging plays an important role in 1) assisting clinicians to diagnose HMC and narrowing down the differential diagnoses and 2) helping to guide medical and surgical treatment. Consequently, it is important to accurately interpret the imaging findings in the context of the clinical signs.
Imaging Findings or Procedure Details: Imaging findings of HMC and associated Mullerian anomalies (i.e. uterus didelphys) will be highlighted based on the significance of the respective imaging modalities. Moreover, we draw attention to the imaging appearances of essential differential diagnoses with emphasis on the additional diagnostic value of MRI.
Conclusion: HMC is a frequent condition in pediatric and adolescent females and must be separated from a number of differential diagnoses including pelvic abscesses und tumours. US and CT aid in the diagnosis of these conditions. In equivocal cases MRI is helpful as 2nd line imaging modality.

PO67

Standardization of Image Quality Assessment in PET and SPECT.

G. Di Domenicantonio[1], S. Gnesin[2], T. V. M. Lima[3]; [1]Geneva/CH, [2]Lausanne/CH, [3]Aarau/CH

Purpose: Quantification in nuclear medicine imaging is affected by numerous parameters including acquisition and reconstruction methods and scanner technology. Standardization of image quality assessment enables the reduction of such variability.
We present the implementation of a protocol that can be combined to the current Swiss stability tests routine (Directive L-09-04 of FOPH, 11.9.2007) and aims to standardize quality assessment for quantification, harmonization and dose optimization in PET and SPECT imaging. The inter-comparison of values obtained for different scanners allows for the definition of a reference level and of the corresponding acceptance window.
Methods and Materials: Standard phantoms (NEMA-NU2 and Jaszczak) filled with typical clinical activity concentration (5MBq/ml for PET, 10MBq/ml for SPECT) were scanned with different acquisition times. Image quality descriptors were extracted for detectability and signal recovery evaluation as a function of spheres' size, lesion contrast and background noise
Results: The performances of 12 PET and 12 SPECT scanners across Switzerland were evaluated with the proposed protocol. Standard metrics, such as recovery coefficient, coefficient of variability and contrast to noise ratio have been measured under typical clinical conditions and their acceptance window has been determined between the 25th and 75th percentile. The same analysis has been performed for different acquisition times in order to test the possibility of dose reduction.
Conclusion: The proposed protocol could be adopted as part of standard stability test of PET and SPECT scanners, facilitating the harmonization of quality assessment procedures at a national level and allowing for inter-center data-sharing. It is furthermore a useful tool in dose optimization.

PO68

Major Discrepancies Between Official Quality Control Methods of the Radiopharmaceutical Preparation of Nanocoll

M. Straub, J. Caputo, M. Leresche, J. Delage; Lausanne/CH

Purpose: Methods for the quality control (QC) of radiopharmaceutical preparations have to be easy and fast in their application to guarantee a smooth work flow within a clinical center. For this reason most QC methods are based on simple paper chromatography if possible. It occurs that different methods exist for the same product within different countries and regulatory instances. One example is the radiopharmaceutical kit preparation of Nanocoll, used for bone marrow or inflammation scanning and lymphoscintigraphy. We present a comparison of the efficiency and reliability of 7 different methods applied in different clinical centers.
Methods and Materials: The radiopharmaceutical kit was prepared respecting the instructions of the summary of product characteristics (SPC) from the producer (GE healthcare). Quality control was performed immediately after the preparation and after two additional time steps within the 6 hours of validity of the product. The results show major discrepancies between the individual methods.
Results: Only three out of the seven QC methods allow a release of the product after the indicated incubation time of 30 minutes, one with 4.7% impurity being at the upper limit of the total impurities allowed (5%). Two other methods allow release only after additional 60 minutes, whereas after 1.5 hours all 7 quality controls allow the release within the criteria of the SPC.
Conclusion: Our results illustrate the complexity of having a reliable QC. Small changes in the production of the starting materials, minor changes in the solvent composition or the kit formulation itself may cause these discrepancies leading to false negative results.

PO69

The Role of Fluorodeoxyglucose–Positron-Emission Tomography in the Staging and Follow-Up of Head and Neck Squamous Cell Carcinoma (HNSCC)

M. Jreige[1], N. Mechleb[2], T. Ibrahim[2], M. Haddad[2], F. Chehadeh[2], A. Tfayli[2], M. Haidar[2]; [1]Lausanne/CH, [2]Beirut/LB

Purpose: To expose the role of Fluorodeoxyglucose–Positron-Emission Tomography in the staging and follow-up of HNSCC in a single site in Lebanon.
Methods and Materials: This retrospective study was conducted on 81 patients with HNSCC referred for initial staging or follow-up between June 2008 and June 2014. PET/CT analysis focused on the following variables: hyperactivity in primary, presence of loco-regional adenopathy and distant metastasis thus categorizing the cases into local, loco-regional and metastatic. Complete/partial response, stable/progressive disease and remission were indicated for different follow-up exams. SUVmax (standardized uptake value maximal) was measured.
Results: *In staging:* PET/CT was realized in 30 patients with a median age of 64 years. The median SUVmax of primary HNSCC tumors was 10.5 with a SD of 4.1 (3.8-20.7). Primary HNSCC localization was larynx and nasopharynx. Three (10%), 6 (20%), 8 (26.7%) and 13 (43.3%) subjects had respectively stage I, II, III and IV. Sites of distant spread were mainly the lungs and bones. *In follow-up:* PET/CT defined the response type to treatment for the 51 patients, independently of the degree of excision (complete/incomplete). High SUVmax helped certifying malignant nature of lesions (lowest at 6.1 in progressive disease and 6.6 in partial response).
Conclusion: Our data in correlation with the literature shows that18-FDG-PET/CT detects primary malignant lesions, allows an accurate staging especially N and M, and can precisely monitor recurrence and metastasis. The main pitfalls remain its low PPV in the setting of inflammatory radiation changes which can be overcome with PET/MRI and new PET/CT tracers.

PO70

Pilot Study of Head and Neck Tumors Angiogenesis Imaging αvβ3 Integrins with Ga-68 NODAGA-RGD in Comparison to F-18-FDG PET/CT.

S. Durante[1], P. Mitsakis[1], A. Pomoni[1], V. Dunet[1], M. Nicod Lalonde[1], J. Delage[1], J. Prior[1], N. Schäfer[2]; [1]Lausanne/CH, [2]Zurich/CH

Purpose: Pilot study presenting the first imaging of patients with head and neck (H&N) tumors evaluated with Ga-68 NODAGA-RGD targeting $\alpha_v\beta_3$ integrins involved in angiogenesis in comparison to F-18-FDG PET/CT.
Methods and Materials: Prospective study of 4 patients with proven H&N squamous cell carcinoma (SSC) who underwent PET/CT with the new radiotracer Ga-68 NODAGA-RGD in comparison to F-18-FDG
Results: Patients aged 52–62y (55.5±6y; 3 males, 1 female) with proven ENT SCC underwent Ga-68-NODAGA-RGD and with 1–8 days a F-18 FDG PET-CT (mean: 5±3). SUVmax (g/mL) from both studies were measured on primary tumor. Our results show a significant linear correlation between the two tracers, with FDG SUVmax (14±SD4.5) and Ga-68 NODAGA-RGD (3.6±SD1.1) (p=0.01). There was no correlation between these two SUVmax (rho_Spearman = 0.4, p=0.6).
Qualitative analysis showed different mapping of the tumor activity, demonstrating that in some cases the angiogenesis is localized in one part of the tumor. Correlation with grade, HPV and p16 showed no correlation (p=0.22).
Conclusion: This preliminary study shows that PET/CT with Ga-68 NODAGA-RGD brings different information than F-18-FDG that might help to plan therapy of H&N SSC regarding the peritumoural activity, which could indicate a propensity to metastasize. It may also help to choose antiangiogenic therapy if RGD are well expressed.

PO71

Evaluation of Spleen Uptake of Ga-68-NODAGA-Arginine-Glycine–Aspartic Acid (RGD) Peptide in Positron Emission Tomographic (PET) Imaging

M. Jreige[1], P. N. Schaefer[1], P. Mitsakis[1], J. Delage[1], M. Straub[1], C. Soares Sobral[1], M. Pappon[1], A. A. van der Gucht[2], J. Prior[1]; [1]Lausanne/CH, [2]Strasbourg/FR

Purpose: To investigate the variable uptake of spleen in Ga-68-NODAGA-RGD in PET/CT imaging.
Methods and Materials: In a different study, RGD- and FDG-PET/CT in 14 oncologic patients were performed (aged 61±7, range 49–74y). Spleen maximal standardized uptake values SUV_{max}, spleen-to-liver and spleen-to-mediastinum SUV_{max} ratios were calculated for both tracers. Spearman correlation to age, sex, BMI, spleen size, spleen volume, white blood cell counts, hemoglobin, LDH, platelets count and presence of prior chemotherapy were computed.
Results: RGD/FDG SUV_{max} were 5.0±1.3/3.5±1.3g/mL for spleen; 3.5±1.2/4.0±0.7g/mL for liver; and 2.1±0.6/2.9±0.5g/mL for mediastinum. The spleen-to-liver SUV_{max} ratio was significantly greater for RGD than FDG (1.58±0.44 vs. 0.86±0.23g/mL, p<0.001) contributing to the general appearance of "hot spleen". Interestingly the variability (SD) of spleen SUV_{max} was greater for RGD than FDG (p=0.032). There was no significant correlation between RGD spleen SUV_{max} and any other variable, except an inverse correlation with platelets count (r=−0.55, p=0.043).
Conclusion: Contrariwise to FDG, spleen SUV_{max} of RGD PET/CT was higher than liver (+58%) and more variable. The inverse correlation of spleen RGD SUV_{max} with platelets might be related to hematopoiesis stimulation, but this would explain only 30% of the observed variability. Thus, the exact significance of increased spleen uptake on RGD PET/CT remains to be found.

PO72

Cardiac Computed Tomography Angiography and Positron Emission Tomography Myocardial Perfusion Hybrid Imaging in Complex Coronary Artery Anomalies – Case Series

C. Gräni, D. Benz, B. Hirt Moch, F. Mikulicic, J. Vontobel, A. P. Pazhenkottil, O. Gaemperli, P. A. Kaufmann, R. Buechel; Zurich/CH

Purpose: There is no data available about the value of computed tomography angiography (CCTA) and positron emission tomography myocardial perfusion (PET-MPI) hybrid imaging in patients with complex coronary artery anomalies (CCAA).
Methods and Materials: We retrospectively identified 7 patients with CCAA (mean 57±7 years, 86% were male) who underwent clinically indicated hybrid CCTA/PET-MPI between 2005 and 2015 in our clinic. The findings from both modalities and hybrid imaging were evaluated in these patients.
Results: Out of the 7 CCAA, 2 were Bland-White-Garland anomalies, 2 showed a coronary artery fistula, 2 showed a "single right" coronary artery and one patient showed a "single left" coronary artery. Semiquantitative PET-MPI revealed a fixed lateral and reversible inferior perfusion defect matching the territory of a non-anomalous vessel with significant concomitant coronary artery disease (CAD) in the patient with "single left" coronary artery. By contrast, analysis of quantitative myocardial blood flow (MBF) as assessed by PET-MPI showed abnormally reduced flow capacities in the territories subtended by the anomalous vessels in 4 patients.
Conclusion: In this case series of middle-aged patients with CCAA, perfusion defects as assessed by semiquantitative PET-MPI were rare and attributable to concomitant CAD rather than to the anomalous vessel itself. By contrast, impaired MBF as assessed by quantitative PET-MPI was commonly found in the vessel territories subtended by an anomalous coronary artery. Hybrid imaging incorporating morphological information from CCTA constitutes a tool to discriminate territories subtended by an anomalous vessel from those subtended by vessels with concomitant CAD and may, thus provide valuable information for further patient management.

PO73

How-To: Split-Bolus Protocol for Optimal CT Contrast in Post-Radioiodine SPECT/CT Scans in Thyroid Cancer Patients

M. K. Werner, M. de Bloeme, S. Metzger, G. Giovacchini, D. Weishaupt, A. Haldemann; Zurich/CH

Learning Objectives:
- learn about CT contrast agent (CA) administration in a split-bolus protocol to reach optimal contrast in SPECT/CT of the neck
- learn to design split-bolus contrast protocols specifically adapted to head & neck SPECT/CT without increasing the total amount of CA administered or hampering workflow

Background: Optimal CT contrast in SPECT/CT after radioiodine therapy in thyroid cancer patients is desirable for an adequate delineation of cervical anatomy and detection of residual disease.
Traditionally, a single bolus of CA is timed to contrast either neck parenchyma or vessels. We implemented a split-bolus protocol where CA is subsequently injected as two volumes to optimally contrast parenchymal neck tissue and arterial and venous vessels simultaneously.
Imaging Findings or Procedure Details: The Triemli split-bolus protocol was established as follows: 40ml CA (Bayer Ultravist® 370) at 2.5ml/s (duration of injection 16s), 20ml saline at 2.5ml/s (8s), 16s delay, 20ml CA at 2.5ml/s (8s), 30ml saline at 2.5ml/s (12s), total 60s with immediate subsequent CT scan (120 kV, 100-300 mAs with dose modulation, GE NM/CT 670 Pro).
In all studied patients, the split-bolus protocol allowed an adequate parenchymal enhancement of the neck as well as excellent delineation of arterial and venous vessels simultaneously, enabling easy detection and characterization of lymph nodes and/or residual tumor.
Conclusion: Our split-bolus protocol for contrast-enhanced SPECT/CT of the neck has proven to provide optimal contrast of parenchyma, arterial and venous vessels (triple-contrast) in only one CT scan. Reliable diagnostic performance is possible without the need for multiple CT scans reducing patient radiation exposure.

PO74

Bone and Muscular Viability Assessment Before Amputation: Usefulness of Bone Scan and 99mTc Sestamibi Dual-Phase Scintigraphy

S. Durante, M.-H. Perez, D. Longchamp, A. de Buys Roessingh, S. Di Bernardo, O. El Ezzi, A. Boubaker; Lausanne/CH

Learning Objectives: ^{99m}Tc-sestamibi before surgery of extremity amputation: a simple method to assess muscle viability.
Background: For 25 years, ^{99m}Tc-sestamibi has been used to evaluate metabolic muscle abnormalities. Uptake and retention in myocytes correlate with mitochondrial content and have been used to evaluate muscle functionality and viability.
Imaging Findings or Procedure Details: A one-year old boy presented musculoskeletal necrosis due to Streptococcus septicaemia. Level of amputation of the right arm was modified during surgery, necrosis being far more extensive than predicted by a preoperative MRI. Therefore, a bone scan was undertaken to assess perfusion and bone viability before amputation of both legs. Bone viability was demonstrated for both femurs and proximal left tibia. Muscle viability being essential for functionality, a 2-phase ^{99m}Tc sestamibi was done 2 days after. Early and delayed uptake allowed to assess muscle viability in both thighs and level of amputation was modified accordingly aiming at preserving functionality of the pelvic girdle and proximal limbs. Clinical outcome was favorable with preserved functionality of both thighs enabling sitting position of the child and future prosthetic limb.
Fig 1: Bone scan (A). Soft tissue uptake in anterior left thigh suggested inflammation. Delayed views confirmed bone viability of femurs and proximal left tibia (B). Subcutaneous activity corresponded to necrosis.
Fig 2: Early (C) and delayed (D) anterior projections after ^{99m}Tc sestamibi injection demonstrated muscle viability in medial thighs and pelvis. Lack of delayed activity was consistent with necrosis/inflammation.
Conclusion: ^{99m}Tc-sestamibi muscle scintigraphy is a simple and useful method to help assessing the level of limb amputation in young children.

PO75

Branchial Cleft Cysts – Diagnostic Pitfalls

T. Baumann, J. Lieb, M. Kretzschmar, J. Jakscha, D. Wild; Basel/CH

Learning Objectives:
- Clinical and imaging presentations of branchial cleft cysts (BCC).
- Reasons for possible diagnostic pitfalls.
- Review cases with unexpected findings complicating further work-up.

Background: Lateral cervical cysts are considered remnants of the branchial clefts. They are usually located between the mandibular angle and the middle part of the sternocleidomastoid muscle. Patients commonly present in the second to fourth decade with cervical swelling and sometimes tenderness. Diagnosis is achieved by ultrasound and fine needle aspiration (FNA) in unequivocal cases.

Imaging Findings or Procedure Details: BCC usually present as bland, unilocular cystic lesions on all imaging modalities and do not exhibit any significant uptake of molecular imaging tracers commonly applied for head and neck imaging (18F-FDG, thyroid tracers).
Inflammatory changes, cystic degeneration of other cervical masses or collision lesions represent possible diagnostic pitfalls.

Case 1: 18F-FDG-PET/CT and cytology suggested cervical CUP-syndrome with muscular infiltration in a 54-year-old patient. Histology after radical neck dissection revealed BCC with intense inflammatory changes, but no signs of malignancy.

Case 2: Ultrasound and cytology suggested BCC in a young patient with cervical swelling. Histology showed metastatic squamous cell carcinoma. Further work-up including 18F-FDG-PET/CT revealed tonsillary cancer.

Case 3: Patient was correctly diagnosed with BCC, but histology revealed population of the cyst by papillary thyroid cancer.

Conclusion: Although BCC usually represent a straightforward diagnosis, imaging and cytology alike are prone to diagnostic pitfalls. These unusual presentations should be kept in mind, when reporting the differential diagnosis for cervical cystic lesions. Nuclear medicine modalities can aid in the work-up and follow-up of complicated cases.

Richtlinien für die interdisziplinäre Zusammenarbeit im Bereich der Teleradiologie

Y. Jaermann, Vevey/CH, M. Mordasini, Bern/CH, E. Rezzonico, Lugano/CH, L. Strebel, Sursee/CH, N. Hänsli, Sursee/CH

Purpose: Das Thema „E-Health" hat im Rahmen der Digitalisierung zunehmend an Bedeutung gewon-nen und führt immer wieder zu Diskussionen. Unter dieses Themengebiet fällt ebenfalls die Teleradiologie, die zunehmend auch in Schweizer Spitälern angewandt wird.
Die Schweizerische Vereinigung der Fachleute für medizinisch technische Radiologie SVM-TRA hat eine Projektgruppe gegründet um Richtlinien für die interdisziplinäre Zusammenarbeit im Bereich der Teleradiologie zu erarbeiten.
Methods and Materials: Die rechtlichen Rahmenbedingungen der Telemedizin sind noch immer Gegenstand von Diskussionen. Basierend auf der Analyse der rechtlichen Grundlagen wurde eine Direktive verfasst, welche die Aufgaben und Kompetenzen der Fachleute für medizinisch-technische Radiologie (MTRA) festhält.
Results: Von Bedeutung ist die rechtliche Diskussion um die Verantwortungsdiffusion und die Sorgfaltspflicht des Arztes bzw. Radiologen. Diese beinhaltet u.a. folgende Fragen: „Was darf der Radiologe an wen delegieren? Was gehört zu seinen Kernaufgaben und ist nicht an Fachleute für medizinisch-technische Radiologie (MTRA) übertragbar?"
Conclusion: Die Richtlinie für die interdisziplinäre Zusammenarbeit im Bereich der Teleradiologie zeigt die Voraussetzungen für eine gesetzeskonforme Teleradiologie auf. Es werden die daraus resultierenden Kompetenzen und Verantwortungen der beteiligten Personen definiert. Es handelt sich bei diesen Darstellungen um Richtlinien, welche den betroffenen Personen und Institutionen im Sinne einer Empfehlung im Hinblick auf die Betriebsorganisation und Aufgabenverteilung behilflich sein sollen.

Promotion du Métier de TRM

S. E. de Labouchere[1], S. Sergio[1], J. Rossier[1], N. Correia[1], P. Vorlet[2], F. Descombes[1], F. Bouamine[1], M. Champendal[1]; [1]Lausanne /CH, [2]Savigny/CH

Purpose: La promotion du métier de Technicien en Radiologie Médicale (TRM) est une des préoccupations actuelle. Contrairement à d'autres professionnels de la santé pour lesquels les rôles, les activités et les compétences sont bien compris par le public, ceux des TRM ne semblent pas clairs. Nous avons pu observer que souvent les TRM sont faussement identifiés en tant que médecin ou infirmier aussi bien de la part des professionnels de la santé que de la part du public.
Selon la littérature, ce manque de reconnaissance du métier serait l'une des raisons d'une pénurie de personnel qualifié.
L'objectif de notre travail, dans le contexte de cette problématique, était de promouvoir les différentes disciplines et les compétences du TRM.
Methods and Materials: Lors de la formation Bachelor of Science en Technique en Radiologie Médicale à la Haute Ecole de Santé Vaud (HESAV), un module sur la thématique de gestion de projet est proposé. Au travers de ce module, nous avons pu construire un projet de promotion du métier de TRM en partenariat avec la section romande de l'ASTRM.
Results: Cette formation et cette collaboration nous ont permis de réaliser globalement un processus allant d'une problématique à la création d'un livrable sous forme d'affiches et flyers explicatifs.
Conclusion: Avec le soutien d'HESAV et le partenariat avec l'ASTRM, nous avons encouragé la promotion du métier de TRM en diffusant ces supports dans tous les centres de radiologie de suisse romande. Ceux-ci ont eu le choix de les mettre à disposition des patients, du public et des professionnels de la santé.

Le Réseau de Veille Métier TRM, un instrument innovant au service du développement de la profession. Résultats du projet pilote.

P. Vorlet, X. Realini; Lausanne/CH

Purpose: Le projet pilote « Réseau de Veille Métier TRM » s'est déroulé du mois d'avril 2015 au mois d'avril 2016. Il a poursuivi les objectifs suivants :
- Identifier les tendances d'évolution de l'environnement du métier de TRM sur les axes suivants : la technique, l'organisation, le cadre normatif, le marché et la médecine.
- Analyser les impacts de ces tendances d'évolution sur le métier de TRM en termes d'activités, de responsabilités et de compétences professionnelles.
- Fournir des bases de décisions relatives à la politique professionnelle (ASTRM), au management du métier (institutions sanitaires) et à la formation au métier (HESAV et HEdS).

Methods and Materials: Le projet pilote « Réseau de Veille Métier TRM » s'est appuyé sur un modèle d'organisation de la profession, le Réseau de Veille Métier et sur une démarche méthodologique de Veille Métier innovants.
Le Réseau de Veille Métier a réuni les acteurs clés du développement de la profession en Suisse occidentale : l'association professionnelle (SR-AS-TRM), des institutions sanitaires représentatives du champ professionnel (CHUV, HUG, etc.) et les hautes écoles de santé (HESAV et HEdS).
La démarche de veille métier a compris 5 phases : la mise en place du Réseau de Veille Métier, la définition des axes de la veille, l'identification et la mobilisation des sources d'information humaines et électroniques, la réalisation des séances et du forum de veille métier et l'élaboration du rapport final.
Results: La veille métier a permis d'identifier les tendances lourdes d'évolution de l'environnement (24) du métier de TRM et d'expliciter leurs impacts (18) actuels et à venir sur son évolution. Ce résultat a permis de définir des mesures concrètes de développement de la profession (19) à tous les niveaux : politique professionnelle, management des institutions, formation de base, formation continue et recherche et développement. Un plan de développement intégré comprenant 7 projets a été validé pour 2016-2017. Le projet pilote a rassemblé les parties prenantes autour de la nécessité d'anticiper les évolutions du métier par une veille permanente et de renforcer la coopération entre l'association et les terrains de pratique ainsi que la coopération entre la profession et les hautes écoles de santé au niveau régional.
Conclusion: Plateforme indispensable au développement de la profession, le Réseau de Veille Métier TRM sera élargi dès cette année à d'autres institutions partenaires et verra son organisation renforcée (leading house).

Contrôle de Qualité en Echographie

J. Künzli, G. Gullo, P. Frossard; Lausanne/CH

Purpose: Le contrôle de qualité des appareils de radiologie est un thème récurrent.
Dans le domaine des radiations ionisantes ces contrôles sont régulés et formalisés. A l'inverse dans le domaine de l'échographie ces contrôles restent à ce jour informels et autorégulés.
Le but est de présenter les bénéfices d'un contrôle de qualité structuré réalisé par les TRM
Methods and Materials: Depuis une quinzaine d'année nos différents appareils sont contrôlés bi-annuellement selon diverses recommandations à l'aide d'un fantôme spécifique (CIRS 040 GSE)
Des rapports de suivi sont établis, ils servent à identifier différents écarts en rapport aux valeurs de base.
Results: La résolution, précision, pénétration et homogénéité restent relativement stables.
Des actions préventives peuvent être entreprises lorsque des dommages sont constatés sur les membranes ou les câblages de même qu'en cas de cristaux défectueux. Ces altérations sont généralement en dessous du seuil d'identification clinique
Conclusion: Même recommandés les contrôles qualité des appareils d'ultrason sont rares, il y a là un facteur de risque objectif d'avoir une qualité d'image et un niveau de performance de l'appareil qui n'est pas celui attendu.
Un programme structuré de contrôle des appareils a le potentiel d'identifier des anomalies avant que celles-ci ne soient cliniquement perceptibles. Les actions préventives ainsi réalisées permettent un fonctionnement idéal des appareils et assurent de ce fait une imagerie optimale pour l'opérateur ainsi que pour le patient.

Ex-Vivo MRI; The Role of the Radiographer in the Multidisciplinary Research – Preliminary results

E. Maturana, S. Decker; Thônex/CH

Purpose: In the aging brain different pathologies often co-exist, including cerebrovascular lesions and neurodegenerative changes. To shed light on the pathophysiology and relevance of MRI-defined lesions and their clinical implications we have designed a multidisciplinary portfolio of related projects focussing on post-mortem neuroimaging and its histopathological validation. This multidisciplinary team includes radiographers. Their role was to evaluate, propose and optimise the MRI sequences, to find the most pertinent solution for examination and performed the acquisitions.
Methods and Materials: Perform post-mortem MRI on a series of 10-20 brains on 3-Tesla MRI. The following 3-D sequences has been proposed by radiographers and validated by the radiologist: T1-MPRAGE, T2-SPACE; T2-FLAIR, SWI. After 1month in formalin and before scanning the brain was immersed in a saline and air aspirated. Arachnoid was separeted with fenestration on the base of the third ventricle to evacuated the residual air.
Results: Evaluate the feasibility of such an examination; to improve the quality of MRI sequences (reduction of the susceptibility artefacts). This project will provide data on the possible optimised sequence protocol for MRI diagnosis of cortical microinfarcts and cerebrovascular lesions in normal brain aging and dementia.
Conclusion: Our protocol offers a very high spatial resolution and allows analyses of smalls cerebral vessel diseases as microbleeds.We could aspirate a majority of air and reduce potential susceptibility artefacts. Increasing bandwidth in SWI sequence we also reduce this kind of artefact but without losing its sensibility thanks to a high spatial resolution. The analyses and correlation in between MRI and histological validation is still in progress.

Konventionelle Röntgendiagnostik: Multifunktionsröntgengerät 3D-Tomographie im Stehen

L. Rizzo; Basel/CH

Purpose: Hintergrund/Ausgangslage
Die konventionellen Röntgendiagnostik, wie auch andere Modalitäten der Radiologie, konnten in den letzten Jahren technische Fortschritte verzeichnen.
Seit Oktober 2015 haben wir im Universitätsspital Basel weltweit das erste Multifunktionsröntgengerät (Multitom RAX) mit einer konventionellen Röntgenröhre und einem Flachdetektor, welches 3D-Tomographien unter Belastung erlaubt.
Mit dem 3D-Datensatz können wir axiale, coronare sowie sagittale Schnittbilder rekonstruieren. Diese neue Technologie ermöglicht eine exakte, physiologische Gelenkanalyse in stehender, gewichtsbelasteter Position in dreidimensionalen Bildern. Dies kann für Gelenkfehlstellungen, unklare biomechanisch bedingte Gelenkschmerzen der unteren Extremität aber auch der Wirbelsäule hilfreich sein.
Zweck/Ziel
Im CT oder im MR werden fortlaufend neue Innovationen entwickelt.
Aber was passiert mit den konventionellen Röntgengeräten? Gibt es neue Innovationen?
Mit dieser neuen 3D-Technik wurde nun etwas Neues in der konventionellen diagnostischen Radiologie entwickelt.
Ziel des Referats ist, den Teilnehmerinnen und Teilnehmer diese neue Technologie im konventionellen Bereich aus dem Blickwinkel einer MTRA vorzustellen.
Ich werde über das Gerät, über die Technik, über die Vorteile aber auch über die Nachteile dieses Gerätes/Technologie bzw. über nötige Entwicklungen referieren.
Diese neue Technologie bietet nun für die MTRAs im Bereich der konventionellen diagnostischen Radiologie neue Möglichkeiten z.B. Gelenkrekonstruktionen ähnlich einem CT-Arbeitsplatz.
Methods and Materials: Inhalt des Referats:
Kurze Apparatekunde:
- Komponenten des neuen Gerätes
- Flexibilität des Gerätes? Was bietet das Gerät für den Alltagsgebrauch?

3D –Bildgebung:
- Technik – Ablauf der 3D-Aufnahmen mit einer konventionellen Röntgenanlage

Vorteile und Nachteile dieser neu entwickelten 3D-Technik
Results: Siehe oben
Conclusion: Siehe oben

CT vs IRM: Le Clash des Grands Esprits dans le Monde de l'Imagerie de l'Hypertension Pulmonaire

J. Lanitis-Handschin, M. Bontean; Geneva/CH

Purpose: L'hypertension pulmonaire (HTP) est une maladie grave et mortelle, entrainant des modifications pulmonaires et cardiaques. Le diagnostic précis est primordial pour la prise en charge. Il existe de nombreuses causes à l'HP notamment pulmonaire, cardiaque, médicamenteuse ou idiopathique. Chez l'enfant et le nouveau né, elle s'associe fréquemment avec des cardiopathies complexes.
Au niveau physiopathologique, le HTP est responsable d'une augmentation progressive des pressions artérielles pulmonaires entrainant à terme la défaillance du cœur droit.
Les symptômes sont peu spécifiques, et les différentes modalités d'imagerie jouent un rôle primordial dans la caractérisation précise des anomalies cardio-thoraciques.
Grâce à l'avancement technologique, l'IRM concourt avec le CT dans l'exploration du réseau vasculaire cardio-thoracique. Les innovations en IRM arriveront-t-elles à faire oublier la précision qu'apporte le CT en double énergie dans l'analyse des artères pulmonaires et systémique combinée à l'étude de la perfusion pulmonaire? Et le CT cardiaque ECG-gated remplacera-t il l'IRM dans l'imagerie du cœur?
Methods and Materials: Ce travail propose de démontrer par une approche ludique de juxtapositions, les mérites et les limites des deux modalités en termes de résolution, performance diagnostique et risque aux patients.
Results: Les considérations actuelles seront traitées afin de présenter le progrès et les ambitions de ces deux modalités dans le domaine de l'HTP. Les séquences IRM Twist thoraciques et les séquences sensibles à la vélocité seront notamment développées en parallèle des techniques CT en double-énergie, high pitch et ECG-Gated.
Conclusion: Notre présentation veut démontrer que tout en gardant leurs spécificités, le CT et l'IRM sont complémentaires et non concurrentes.

Optimierung des Arbeitsplatzes Computertomographie – ein Puzzle mit vielen Einzelteilen

G. Stadelmann; Basel/CH

Purpose: Hintergrund/Ausgangslage
Die Computertomographie hat sich aufgrund der technischen Entwicklung und der permanenten Verfügbarkeit in den letzten Jahrzehnten zu einer der wichtigsten bildgebenden Verfahren in der Radiologie entwickelt.
Die Komplexität der Organisation einer funktionierenden CT-Einheit ist eine sehr grosse sowie auch spannende Herausforderung.
Beispiel aus der Praxis: Modalität CT, Radiologie Universitätsspital Basel
Methods and Materials: Erfahrungsbericht aus der Praxis
Eine CT-Einheit bildet ein komlexes Gebilde, welches von direkten oder übergeordneten Komponenten beeinflusst wird. Diverse Personen und Themen beeinflussen den Arbeitsplatz CT, wie z.B. Radiologen, MTRA`s, Physiker, Zuweiser, Patienten, Arbeitgeber, der Gesundheitsmarkt und die Gesetzgebung, Technik, Fachwissen, Qualität, Strahlendosis und Zeit.
Es gilt das Fachwissen, die Interessen und Ansprüche der einzelnen Berufsgruppen innerhalb der Radiologie zu vereinen, um möglichst den Radiologie-internen und übergeordneten Anforderungen gerecht werden zu können. Diverse Faktoren sind dafür massgeblich entscheidend wie z.B. klar definierte Strukturen und Kompetenzen, berufsübergreifende gute offene Kommunikation, Zusammentragen von Fachwissen, Definition und Festlegung von Zuständigkeiten, gemeinsame Ziele festlegen und motivierte engagierte, flexible sowie kompromissbereite Mitarbeiter und Kollegen.
Conclusion: Der Erfahrungsbericht soll aufzeigen, dass es Dank einer gut strukturierten berufsübergreifenden Einheit gelingen kann, vielseitige Herausforderungen, Ansprüche und Schwierigkeiten gemeinsam anzunehmen und lösungsorientiert zu bewältigen.

Comparaison des Différents Types de Contrôles Dosimétriques Effectués en IMRT Statique et Dynamique

A. Guney; Geneva/CH

Purpose: Ce travail de recherche s'inscrit dans le cadre de la formation post-graduée, CAS HES-SO en Dosimétrie en radio-oncologie.
L'objectif de cette étude, est de documenter, d'analyser les caractéristiques physiques et de mettre en évidence les avantages et inconvénients des contrôles dosimétriques EPID, PTW et PinPoint effectués au sein du service de radio-oncologie des HUG.
Methods and Materials: Des données scientifiques (thèse, articles scientifiques, recommandations SSRPM), ainsi que mon expérience dans ce domaine ont contribués à élaboration de cette étude.
La description des caractéristiques physiques, l'explication du déroulement du contrôle ainsi qu'une synthèse sur les avantages et inconvénients pour chacun de ces contrôles dosimétriques ont été étudiés.
Results: Bien que certains contrôles fournissent une information sur la distribution de dose globale du plan de traitement, on se rend compte qu'ils ne renseignent pas tous sur la dose absolue, tel que le contrôle par imageur portal EPID. D'autre système de contrôle dosimétrique engageant une installation plus complexe, PTW et PinPoint, renseignent sur la dose absolue. L'étude de la répartition de la dose sur une coupe frontale à l'isocentre est garantie par la matrice PTW, et la dose en un point pour la sonde PinPoint. L'influence du maniement du gamma index selon les circonstances ont également été élucidés.
Conclusion: Les caractéristiques propres de chacun de ces contrôles dosimétriques étudiés, ne permettent pas indépendamment de garantir la validation du plan de traitement. Chacun d'entre eux, présente des avantages comme des inconvénients. Ces contrôles sont complémentaires, et au moins deux de ces contrôles doivent être effectué par plan de traitement.

Comparison of Palliative Irradiation with the Criteria of a Successful Treatment According to the Swiss Association for Quality in Palliative Medicine.

N. Mamboury; Lausanne/CH

Purpose: The purpose of this work is to compare the modern irradiation techniques (irradiation, positioning, reduction of acute side effects, etc.) for palliative irradiation with the qualitative criteria of a successful palliative treatment according to the recommendations of the Swiss Association for Quality in Palliative Medicine.
Methods and Materials: Comparison of the benefits of the modern irradiation techniques (tomotherapy, cyberknife, IGRT, etc.) with the recommendations for succesfull quality care by the SAQPM (absence of nocturnal pains, no pains when being at rest, when eating, when urinating, when defeacating, etc.) while enabling the patient to remain lucid for communication.
Results: Nowadays palliative care should offer symptom reliefs such as pains, digestive troubles (nausea, diarrhea, constipation), dyspnea or mental confusion. The modern irradiation techniques for palliative diseases (bone metastasis, brain metastasis, medullar compression, vena cava syndrome) allow for accurate targetting of the tumor by avoiding the organ at risk and by reducing dramatically the side effects, although it may also cause side effects such as nausea, diarrhea, mental confusion (cerebral oedema) or acute inflammation.
Even if an accurate palliative irradiation is offered to a patient, the treatment may also provocate unpleasant side effects and reduce the quality of life. This is why the benefits should be seriously balanced with the side effects and why an alternative treatment should be proposed in case of risk of major side effects.
Conclusion: A palliative irradiation should be discussed and proposed to the patient in the light of preserving his dignity, autonomy and autodetermination.

Untersuchungen des Myokards

E. Müller, Chur/CH

Purpose: Moderne koronare Bildgebungsverfahren sind in der Lage Verdachtsdiagnosen zu präzisieren und Therapientscheidungen entscheidend zu beeinflussen.
Methods and Materials: Die Sterberate durch den akuten Myokardinfarkt konnte in den letzten 10 Jahren in den Industriestaaten kontinuierlich gesenkt werden. Dies begründet sich zum Einen mit der gesteigerten Sensibilisierung gegenüber dieser Krankheit, zum Anderen haben sich neben der klassischen Koronarangiographie in den letzten Jahren vermehrt modernste Schnittbildverfahren (CT,MRT) zur diagnostischen Abklärung etabliert. Die Fragestellung der hämodynamischen Relevanz einer Koronarverengung lässt sich zusätzlich mit Nuklearmedizinischen Untersuchungsverfahren (SPECT , PET) abklären. Die Berücksichtigung aller Untersuchungsergebnisse ermöglicht es eine mögliche Myokarderkrankung genauer zu präzisieren.
Results: Für die Behandlung einer koronaren Herzkrankheit stehen unterschiedlichste Therapieverfahren zur Verfügung. Moderne diagnostische Untersuchungsmethoden können, aufgrund ihrer Sensitivität und Spezifität, die Wahl der geplanten Therapien signifikant beeinflussen und verändern.
Conclusion: Die frühe Erkennung eines Myokardproblems gewährleistet, durch rechtzeitig einleitbare Therapiemassnahmen die Erhaltung der Lebensqualität der betroffenen Patienten und kann den akuten Myokardinfarkt verhindern.

Réceptivité des Étudiants TRM à l'Interprofessionalité, un Enjeu à Venir pour la Profession

F. Bouamine, L. Franco, C. Becherraz; Lausanne/CH

Purpose: Depuis 2010, HESAV a implémenté un programme d'Education Interprofessionnel l'EIP dans les 4 programmes de formation existants à l'école : sages-femmes, physiothérapie, technique en radiologie médicale et soins infirmiers. Cette implémentation est la réponse aux développements en matière de santé publique, de l'augmentation de la multimorbidité et de la complexité de soins qui en résulte. Un rapport du groupe thématique interprofessionnalité (OFSP) cite une étude réalisée aux Etats-Unis, selon laquelle jusqu'à 98 000 personnes par an décèdent des suites d'erreurs médicales évitables, dont une partie serait due à une communication déficiente entre différents groupes professionnels (Kohn, 2000). Le but est de mettre en évidence l'influence de l'enseignement EIP sur la réceptivité aux pratiques collaboratives des étudiants TRM de Bachelor 1ère année à HESAV en comparant les résultats pré-test avec ceux du post-test.
Methods and Materials: Le questionnaire utilisé est le RIPLS (Readiness for interprofessional Learning Scale) mesurant la réceptivité à l'apprentissage interprofessionnel. Il comprend une échelle de Likert avec 19 items et 4 sous échelles.
Results: En 2015, 58 étudiants TRM parmi 225 étudiants ont participé à la semaine EIP. Au total 71 données toutes filières ont été incluses dans l'analyse. Globalement, les réponses des étudiants TRM (N=15) soit 21.1% des étudiants HESAV démontrent une attitude favorable à l'apprentissage interprofessionnel.
Conclusion: Suite à leur participation à la semaine EIP, les étudiants TRM de 1ère année construisent leur rôle professionnel. L'EIP constitue un axe prioritaire afin de promouvoir la qualité des soins qui reste dépendante de tous les acteurs potentiels de l'amélioration des soins.

Der MTRA bei Kriegseinsätzen im Feldlazarett

A. Pedergnana; Winterthur/CH

Purpose:
- Eigenerfahrungen aus aktuellen Kriegsgebieten und Katastrophensituationen
- soll zeigen, wie Arbeitserfahrung, Flexibilität, Fantasie und psychologische Belastbarkeit eine wichtige Rolle spielen
- Gibt Überblick, wie solche «harten» Erfahrungen trotzdem auch sehr lehrreich sind

Ziel: ein «Lichtlein» in eine noch unbekannte Welt zu bringen
Methods and Materials: Frontale Präsentation mittels Powerpoint; Dauer: ca 30-45 min.
Results: Einteilung:
- Einsatz der ersten Röntgenapparate im Krieg, kurz nach der Entdeckung der X-Strahlen
- heut. Kriegslazarette (nach Klassifikation)
- Datenübertragung
- Irak: Operation “Altes Babylon”
- Sri Lanka: Einsatz in Südostasien
- eigene Projekterfahrungen
- Katastrophenpsychologie

Conclusion: Der MTRA ist heutzutage immer mehr ein wichtiger Teil eines Systems, welches nicht nur Technologie und Fachkenntnisse verlangt, sondern auch Erfahrung, Flexibilität und Fantasie. Die eigenen Fähigkeiten werden täglich überprüft. In den Auslandsmissionen sind die oben genannten Punkte, noch wichtiger, denn die Umstände sind sehr unterschiedlich. Man lernt die eigenen Limits kennen, und man reagiert dementsprechend.

PO76

Image Guided Radiation Therapy of Liver Using a New Contrast Agent

K. Sprengers, L.-V. Tran, S. Ding, M.-C. Vozenin, B. Petit; Lausanne/CH

Purpose: Liver cancer is one of the most aggressive digestive cancer against which SBRT is nowadays an attractive therapeutic strategy. During treatment planning, tomodensitometry is used for the delineation of tumor volumes and organs at risk like the bowels or the stomach as well as for dosimetry. Accordingly, these images need to be highly contrasted. The use of iodinated contrast agents can be problematic because of fast body elimination, nephrotoxicity and possible allergic reactions. Furthermore, high iodine concentration does affect radiodensity measurement, *i.e.* Hounsfield Units (HU), preventing the use of the contrast-enhanced images for dosimetric purposes. Therefore, non-iodinated contrast agents (e.g. nanoparticulate) have been developed for micro-CT.
Our objective was to optimize imaging of liver using nanoparticulate based contrast agents and to determine optimal schedule.
Methods and Materials: Six 8-10 weeks old C57BL/6 female mice were retro-orbitally injected with 100µL/25g of ExiTron Nano 6000 (Miltenyi Biotec) contrast agent. They were scanned with X-Rad 225Cx-CB-CT (40kV/3mAs and 80kV/1.5mAs) before injection, at 0mn, 30mn, 1h, 2h, 4h, 8h, 4d, 9d and 40d post-injection (p.i.).
Results: A maximum density of 700HU at 80kV/1.5mAs was measured in the liver 8 hours p.i. that progressively decreased to 500HU at 9 days p.i and remained stable until the 40th day p.i. Yet, strong liver and splenic contrast enhancements were still observed. No complication related to the contrast agent was noticed. A maximal enhancement ratio of 350% was calculated.
Conclusion: This study shows the feasibility of contrast enhancement in CBCT to optimize liver visualization.

PO77

Image Guided Radiation Therapy of Lung Using New Contrast Agent

L.-V. Tran, K. Sprengers, S. Ding, M.-C. Vozenin, B. Petit; Lausanne/CH

Purpose: SBRT is today an attractive strategy for the treatment of lung cancer. During treatment planning, tomodensitometry is used for the delineation of tumor volumes and organs at risk such as the heart, the esophagus or the spinal cord as well as for dosimetry. Accordingly these images need to be highly contrasted. The use of iodinated contrast agents can be problematic because of fast passage through blood pool, nephrotoxicity and possible allergic reactions. Furthermore, high iodine concentration does affect radiodensity measurement, *i.e.* Hounsfield Units (HU), preventing the use of contrast-enhanced images for dosimetric purposes. Therefore, non-iodinated contrast agents (e.g. nanoparticulate) have been developed for micro-CT.
Our objective was to optimize imaging of lung using nanoparticulate based contrast agents and to determine optimal schedule.
Methods and Materials: Two 22-24 weeks old C57BL/6 female mice were retro-orbitally injected with 100µL/25g of ExiTron Nano 12000 (Miltenyi Biotec) contrast agent. They were scanned with X-Rad 225Cx-CB-CT (80kV/1.5mAs) before injection, at 0mn, 15mn, 1h, 2h, 4h and 24h post injection (p.i).
Results: A maximum density of 1100HU was measured in the left cardiac ventricle immediately after injection that decreased to reach a plateau at about 900HU the following hours generating a strong lung vessels enhancement. Enhancement of the left ventricle then decreased to a nearly native level 24h p.i. No complication related to the contrast agent was noticed. A maximal enhancement ratio of 550% was calculated.
Conclusion: This study shows the feasibility of contrast enhancement in CBCT to optimize lung vessels visualization.Abdominal and Pelvic Imaging

PO78

Nuklearmedizinische Nierenuntersuchungen

S. Lukic; Chur/CH

Learning Objectives: Das Ziel des Posters ist es die nuklearmedizinischen Nierenuntersuchungen mit den verschiedenen Radiopharmaka darzustellen und miteinander zu vergleichen. Die Radiopharmaka MAG3, DTPA und DMSA haben alle verschiedene Eigenschaften, die man je nach Fragestellung nutzen kann. Während sich sich das DMSA an die vitalen Zellen der Tubuli fixiert, wird das MAG3 zum grössten Teil tubulär sezeniert und zum kleineren Teil glomerulär filtriert. Das DTPA wird ebenfalls glomerulär filtriert und eignet sich dadurch sehr gut zur Bestimmung der glomerulären Filtrationsrate.
Background: Kurze Darstellung der Anatomie und Physiologie der Niere Indikationen für Nierenuntersuchungen mit MAG3, DTPA und DMSA Pharmakokinetik der Tracer
Imaging Findings or Procedure Details: Auch der Untersuchungsablauf ist je nach verwendetem Tracer unterschiedlich. Durch die Fixation des DMSA im Tubulus, eignet sich dieser Tracer sehr gut für statische Bilder. Beim MAG3 und DTPA hingegen, kann man auf die dynamischen Serien nicht verzichten.
Conclusion: Ich möchte aufzeigen, auf was die MTRA bei den Untersuchungen der Niere achten muss, um eine möglichst gute Auswertung der Bilder zu gewährleisten.

PO79

La Simulation comme Outil dans l'Interprofessionnalité pour les TRM

O. Sautier, L. Franco; Lausanne/CH

Learning Objectives: La formation des étudiants en silo ne leur permet pas d'exercer une pratique collaborative avant les stages. Ceux-ci ne leur offrent ni une formation interprofessionnelle adéquate ni le temps nécessaire pour une analyse réflexive.
La simulation est utilisée comme outil d'apprentissage socio-constructiviste en vue d'une collaboration renforcée entre les soignants et le patient. Une cible commune doit être construite dans laquelle le patient retrouve un statut d'acteur-auteur.
Par cette approche, les étudiants TRM de HESAV, Lausanne, doivent être acteur, réfléchir à leur rôle, à leurs responsabilités dans l'interaction avec les autres professionnels dont le patient. Pour Kant, « ce que l'on apprend le plus solidement, c'est ce que l'on expérimente soi-même », principe repris par Dewey, avec son leitmotif « learning by doing ».
Background: Aux Etats-Unis, le rapport « to ERR is Human », met en lumière l'importance du facteur humain dans les erreurs médicales. Il propose l'utilisation de la simulation pour en réduire la fréquence ou les conséquences. En Suisse, dans la cadre de la réforme santé 2020, l'OFSP a mandaté un groupe thématique « Interprofessionnalité ».Celui-ci recommande l'introduction d'une formation interprofessionnelle initiale comportant de la simulation, démarche déjà initiée dans les HES romandes.
Imaging Findings or Procedure Details: A Hesav, 3 modules interprofessionnels d'une semaine chacun sont implémentés de la 1ère à la 3ème année de formation bachelor avec comme focus une simulation qui permettra aux étudiants de mettre en pratique leurs acquis théoriques.
Conclusion: La simulation permet aux étudiants TRM d'être acteurs de leurs prestations et de développer des compétences interprofessionnelles.

PO80

Ex-Vivo MRI; The Role of the Radiographer in the Multidisciplinary Research – Preliminary results

E. Maturana, S. Decker; Thônex/CH

Purpose: In the aging brain different pathologies often co-exist, including cerebrovascular lesions and neurodegenerative changes. To shed light on the pathophysiology and relevance of MRI-defined lesions and their clinical implications we have designed a multidisciplinary portfolio of related projects focussing on post-mortem neuroimaging and its histopathological validation. This multidisciplinary team includes radiographers. Their role was to evaluate, propose and optimise the MRI sequences, to find the most pertinent solution for examination and performed the acquisitions.
Methods and Materials: Perform post-mortem MRI on a series of 10-20 brains on 3-Tesla MRI. The following 3-D sequences has been proposed by radiographers and validated by the radiologist: T1-MPRAGE, T2-SPACE; T2-FLAIR, SWI. After 1month in formalin and before scanning the brain was immersed in a saline and air aspirated. Arachnoid was separeted with fenestration on the base of the third ventricle to evacuated the residual air.
Results: Evaluate the feasibility of such an examination; to improve the quality of MRI sequences (reduction of the susceptibility artefacts). This project will provide data on the possible optimised sequence protocol for MRI diagnosis of cortical microinfarcts and cerebrovascular lesions in normal brain aging and dementia.
Conclusion: Our protocol offers a very high spatial resolution and allows analyses of smalls cerebral vessel diseases as microbleeds.We could aspirate a majority of air and reduce potential susceptibility artefacts. Increasing bandwidth in SWI sequence we also reduce this kind of artefact but without losing its sensibility thanks to a high spatial resolution. The analyses and correlation in between MRI and histological validation is still in progress.